12-2014

Thermal Analysis and Dielectric Spectral Characteristics of Poly(ionic Liquids): Towards exploration of their utility in capacitive electrochemical devices

Meng Zhao

THERMAL ANALYSIS AND DIELECTRIC SPECTRAL CHARACTERISTICS OF POLY(IONIC LIQUIDS): Towards exploration of their utility in capacitive electrochemical devices

by

Meng Zhao

A dissertation submitted in partial fulfillment of the requirements
for the degree of Doctor of Philosophy in Microsystems Engineering

Microsystem Engineering
Kate Gleason College of Engineering

Rochester Institute of Technology
Rochester, NY
December 2014

THERMAL ANALYSIS AND DIELECTRIC SPECTRAL CHARACTERISTICS OF POLY(IONIC LIQUIDS): Towards exploration of their utility in capacitive electrochemical devices

By

Meng Zhao

Committee Approval

We, the undersigned members of the Faculty of the Rochester Institute of Technology, certify that we have advised and/or supervised the candidate on the work described in this dissertation. We further certify that we have reviewed the dissertation manuscript and approve it in partial fulfillment of the requirements of the degree of Doctor of Philosophy in Microsystems Engineering.

Dr. Thomas W. Smith Date

(Committee Chair and Dissertation Advisor)

Dr. Christopher J Collison Date

Dr. Seth M Hubbard Date

Dr. Karl Hirschman Date

Dr. Brian Landi Date

Certified by

Dr. David Borkholder Date

Dr. Harvey J. Palmer Date

ABSTRACT

Kate Gleason College of Engineering

Rochester Institute of Technology

Degree Doctor of Philosophy **Program** Microsystems Engineering

Name of Candidate Meng Zhao

Title: THERMAL ANALYSIS AND DIELECTRIC SPECTRAL CHARACTERISTICS OF POLY(IONIC LIQUIDS): Towards exploration of their utility in capacitive electrochemical devices

It has been proposed that the function of lithium ion batteries, fuel cells, capacitors, solar cells and actuators might be improved if membranes impregnated with organic salt solutions or conventional ionic liquids were replaced by film-forming ionic liquid polymers like those derived from 4-vinylimidazolium (4-VIm^+) salts. 4-VIm^+ polymers with a methyl substituent at the 2-position of the imidazole ring may have greater chemical and electrochemical stability than poly(ionic liquids), PILs, derived from 1-vinyl- and 4-VIm^+ polymers with a hydrogen at the 2-position of the imidazole ring. The utility of PILs, in capacitive devices, however, is limited by poor ion mobility caused by incorporation of anionic and/or cationic components in the polymer chain. The ionic conductivity of PILs can be improved by lowering the glass transition temperature and/or reducing the dimensions of the ion-conductive phase. In the present research, 4-VIm^+-based PILs were designed and synthesized with six different anions. The effect of anions of differing kind on the thermal properties of these polymers was evaluated and dielectric characteristics of 4-vinyl- and 1-vinylimidazolium polymer salts were compared. The glass transition temperature of the PF_6^- and trifluoromethylsulfonylimide, $TFSI^-$, salts of polymers derived from1-butyl-2,3-dimethyl-4-vinylimidazolium (23D4VIm^+) triflate polymers were found to be anomalous (substantially invariant) as compared to those of PF_6^-, $TFSI^-$, and triflate salts of 4-vinyl- and 1-vinylimidazolium polymers. The invariance in the glass transition of poly(23D4VIm^+) with different anions was attributed to increased separation between ion pairs, enforced by having substituents on the 1, 2, 3,and 4 positions of the imidazolium ring.

ACKNOWLEDGMENTS

First I would like to thank Dr. Thomas Smith for being my thesis advisor. He inspired my curiosity about polymer science and open the door for me to become a polymer engineer. With his encouragement, I have enjoyed my life in my graduate school and kept moving forward for this dissertation. None of my research success would have been possible without his guidance. Dr. Thomas Smith will always be my mentor and my friend.

I am also grateful to Dr. Bruce Smith, who is not only the department head of Microsystem Engineering, but also my thesis advisor for my master degree. He has been very supportive and gave me a lot of advice in both research and career. He provided me great help when I first came to RIT several years ago. Without his help, I won't be able to accomplish this dissertation.

I also would like to thank Dr. Brian Landi, Dr. Christopher J Collison, Dr. Karl Hirschman and Dr. Seth Hubbard for their time serving in my dissertation advisory committee. Their experience in various areas makes this dissertation possible. I appreciate this discussions I have had with them. Their invaluable experiences will benefit me for a life time. I would also like to thank Dr. Peggy Cebe in Tuffs University. She and her research group provided me the tools and techniques to make the dielectric measurements. They also provided me the software (DFit) they made to analyze the data. Their effort and their time in training me and supporting me is highly appreciated.

I would also thank the department of Microsystem Engineering and Chemistry in RIT for supporting me financially and academically. All the staff and faculties' hard work has made it to be very enjoyable to work in these years. I want to also thank the department of Chemistry to hire

me as a teaching assistant so I can support myself through graduate school. I also thank National Science Foundation to provide the funding.

The support from our group members is highly appreciated. I thank Fan Yang for her effort in making polymers for me and her constant companion in my personal life. I also thank Mr. Darren Smith for his help in training me many valuable skills and preparing many materials for me to finish this dissertation. I also want to thank Ran Yin for his help when I first joined this research group and his valuable advice

Table of Contents

List of Figures

Chapter 1 Introduction

Optimal capacitive electronic devices would employ thin-film polymer electrolytes. Unfortunately, with ion motion generally being correlated with segmental motion in the polymer, covalent incorporation of an ionic moiety (cation or anion) in a polymer composition invariably results in dramatically reduced ion mobility and conductivity. [1] This limitation can be addressed to some degree by lowering the glass transition temperature of the polymer and reducing the dimensions of the ion-conductive phase. [2], [3], [4], [5] It has also been suggested that ionic and segmental dynamics in solid polymer electrolytes can be decoupled. [6] There have been a number of reports detailing the synthesis, glass transition properties, and ion conduction in poly(ionic liquids, specifically N-vinyl- and 1-acryloyloxyethylimidazolium polymers. [3], [4] **The goal of the present research is to better understand how the relative degree of freedom and the accentricity of the imidazolium moiety tethered to the polymer backbone influences the glass transition and molecular relaxations in poly(ionic liquids) derived from 4-vinylimidazolium polymers**. The size and character of the counterion in these polymers, which can also have a dramatic impact on the glass transition of the polymer and the accentricity of imidazolium salt, has also been studied.

This dissertation is comprised of six chapters.

The first chapter provides context for, and briefly presents the objectives of this research. Chapter 2 provides background on three types of capacitive electrochemical devices, batteries, fuel cells and capacitors.

Chapter 3 provides relevant history on solid polymer electrolytes. It contains three sections introducing the topics of ion transport in polymer, solid-phase electrolytes and ion conductivity of solid-phase electrolytes, respectively

The Chapter 4 is the experimental section. It contains information on materials and methods used in this project and detailed procedures for synthesis of the monomers and polymers utilized in this research.

In Chapter 5, the results of thermal analysis, including the glass transition temperatures of the two families of polymers synthesized in this project, are presented. In section 2 of Chapter 5, comparative thermal characteristics of poly(1-ethyl-3-vinylimidazolium) and poly(1-ethyl-3-methyl-4-vinylimidazolium) salts, and poly(1-butyl-2,3dimethyl-4-vinylimidazolium) and poly(1-ethyl-3-methyl-4-vinylimidazolium) salts are presented.

Chapter 6 provides the results of dielectric measurements on the two families of polymers. The first section in Chapter 6 gives a brief introduction on dielectric relaxation. The second section provides information on models for understanding dielectric relaxation phenomena in polymer systems. The third section of Chapter 6 gives the results of dielectric measurements for poly(ionic liquids) derived from 4-vinyl- and N-vinylimidazolium polymers with no substituent at the 2-position of the imidazolium ring and dielectric properties of imidazolium polymers derived from 1-butyl-2,3-dimethyl-4-vinylimidazolium triflate.

The appendix contains the DSC thermograms of N-vinylimidazolium polymers, poly(1-ethyl-3-methyl-4-vinyl imidazolium salts) and poly(1-butyl-2,3-dimethyl-4-vinylimidazolium) salts. It also contains some theoretical information of dielectric relaxation.

Chapter 2 Background

2.1 Overview

Energy production that relies on the combustion of fossil fuels is forecast to have a severe impact on global economics and ecology [7]. Electrochemical energy storage and production is a key element in managing energy consumption in a more sustainable and more environmentally friendly way. Systems for electrochemical energy storage and conversion include batteries, fuel cells, and electrochemical capacitors (ECs). Common features are that the energy-storage or generation processes take place at the phase boundary of the electrode/electrolyte interface and that electron and ion conduction are separated [7], [8]. **Figure 1 (a ,b,** and **c)** shows the basic structure of the three systems. They all consist of two electrodes separated by an ion-conductive electrolyte. The anode and cathode in these devices must be electronically conductive and may be ion-conductive. The electrolytes must be ion-conductive but not electronically conductive [9].

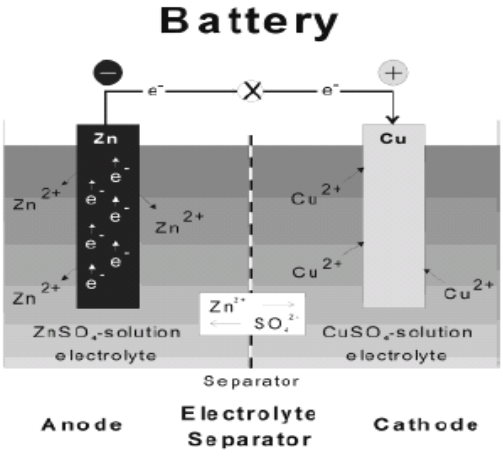

(a)

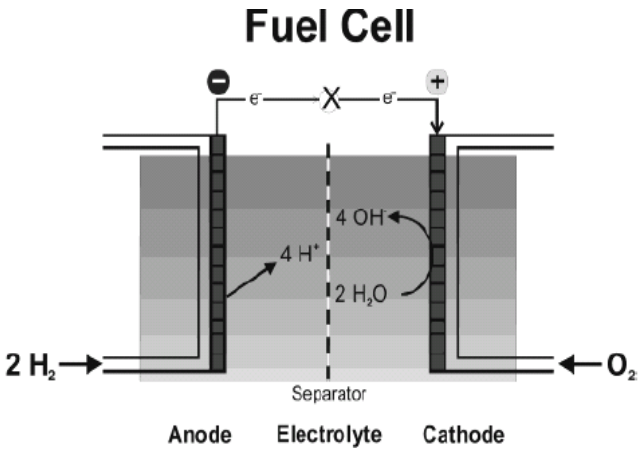

(b)

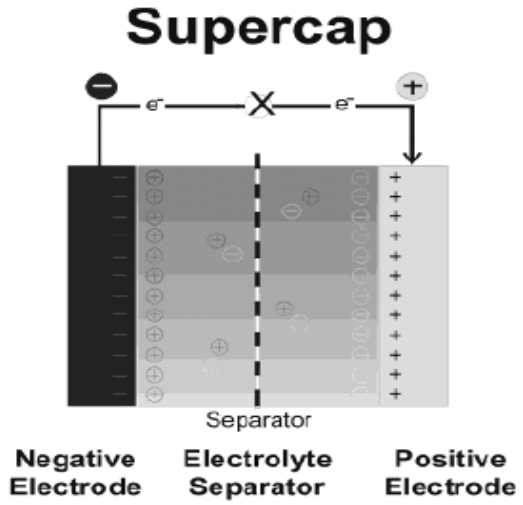

(c)

Figure 1 Three electrochemical systems: (a) battery (b) fuel cell (c) supercapacitor [1] (Figures reprinted from reference 1 with permission of M. Winter)

2.2 Introduction

Electrochemical energy production entails reactions which convert chemical energy to electrical energy. These reactions, which take place at the interface of an ion-conductive material and electron conductors, often involve electron transfer between an anode (negative electrode of a cell associated with oxidative chemical reactions that release electrons into the external circuit) and a cathode (positive electrode of a cell associated with reductive chemical reactions that gain

electrons from the external circuit). Batteries and supercapacitors are capacitive electrochemical devices that produce and store energy.

In batteries electrical energy is generated by conversion of chemical energy *via* redox reactions at the anode and cathode. Batteries are closed systems, where the anode and cathode are the charge-transfer medium and take an active role in the redox reaction as "active masses."[7], [10], [11] In other words, energy storage and conversion occur in the same compartment.

2.2.1 Supercapacitors

In supercapacitors (or electrochemical capacitors), redox reactions may not be involved in the energy generation process; and, thus the common practice of using the terms anode and cathode may not strictly be appropriate. By polarization of electrolyte ions at the electrode/electrolyte interface, so-called electrical double layers (EDLs) are formed. When charge stored in these electrical double layers is released, parallel movement of electrons in the external occurs, and stored electrical energy is delivered. [7], [12] Supercapacitors differ from conventional capacitors primarily in the mechanism of energy storage. Supercapacitors store electrical charges in electric double-layers that form at the interface between each electrode and a common electrolyte. Therefore they are also called electrochemical double layer capacitors, or EDLCs. [7], [13-16] EDLCs typically have energy densities 300 times that of the conventional capacitors and one tenth that of batteries. However, their power density is typically 10 times that of the most batteries. [16] By offering high power and energy density, the supercapacitors are a suitable intermediate power source between batteries and conventional capacitors. [15], [16] A typical structure of an EDLC is shown in **Figure 2**. [13]

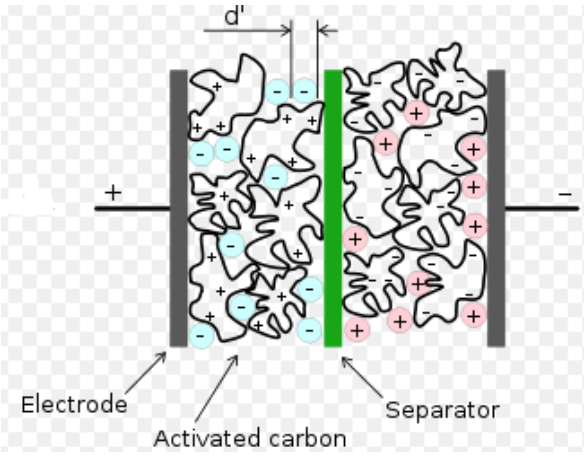

Figure 2 Electrochemical double layer capacitor: The activated carbon granules are in electrical contact with each other to constitute a "plate" with a huge surface area. The separator is permeable to the electrolyte [13].

It has been demonstrated that the performance of supercapacitors is determined by the composition of electrodes and the electrolyte. [17], [18] The predominant electrode materials are activated carbon [13] and graphene. [14] The properties of electrode materials that affect the EDLC's performance are porosity, pore size distribution, wettability and specific surface area (a measurement of the total surface area per unit of mass). [14]-[19]

Electrolyte materials that have been described in the literature include aqueous salt solutions, organic salt solutions, ionic liquids and polyelectrolyte materials. [20-25] Given that energy density is proportional to the square of the operation voltage; because of their greater electrical stability window (ESW), (4V *versus* 1V), which enables higher operation voltage, organic salt solutions, have proven to be better electrolytes than aqueous salt solutions. [20] Because of safety concerns, ionic liquids are being explored in EDLCs as "solvent-free" electrolytes. [21-23] Polymeric materials have long been of interest as film-forming electrolytes. [22], [24], [25] These solid-phase electrolytes can improve the power density of EDLCs by lowering the mass of

devices. Additionally, thermally stable polymeric materials can have a higher temperature-use range. [22], [24]

2.2.2 Batteries

Lithium-ion batteries are a class of rechargeable batteries in which lithium ions move from the negative electrode to the positive electrode during discharge, and back when charging. [7], [26] As compared to other types of batteries, they provide significantly higher energy density and lighter weight. During discharge, lithium ions carry the current from the negative to the positive electrode, through the non-aqueous electrolyte and separator diaphragm. During charging, an external electrical power source (the charging circuit) applies a higher voltage (but of the same polarity) than that produced by the battery, forcing the current to pass in the reverse direction. The lithium ions then migrate from the positive to the negative electrode, where they become embedded in the porous electrode material by a process known as intercalation. [7], [26-28] The structure of a lithium ion battery is illustrated in **Figure 3**.

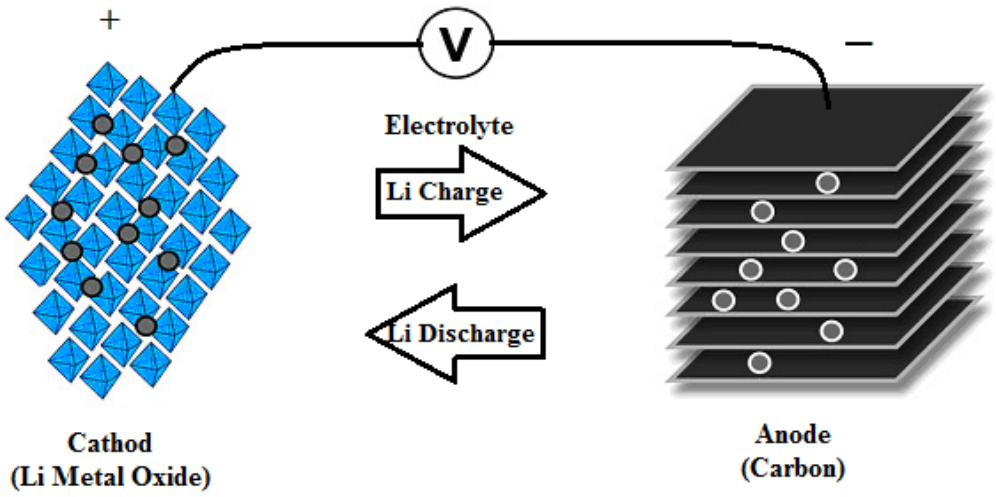

Figure 3 Rechargeable Li-ion battery with porous cathode and anode as a lithium-ion source

The choices of materials for cathodes, anodes and electrolyte are particularly important in lithium-ion batteries. A major concern regarding performance of lithium-ion batteries is safety, specifically the reactivity of electrodes in organic solvent electrolytes. [26-28] Ionic liquids have been widely investigated as solvent-free electrolytes for lithium ion batteries with a large electrochemical stability window. [29-31] Plasticized polymer films are also an option for safe, high-energy-density, and, environmental-friendly designs. [32-35] The so-called lithium-polymer battery (LPB) contains thin layers of laminated material that is flexible and may be shaped into non-planar geometries. [28], [33], [34] As mentioned in the previous section, the issue with the LPB is the low conductivity of solid-phase electrolytes and their reactivity with electrode in presence of plasticizer. [32-35]

2.2.3 Solar Cells

Because solar energy is essentially unlimited, photovoltaic devices are considered as an alternative to fossil fuels for energy-production. As shown in **Figure 4**, multi-junction solar cells based on semiconductor compounds give the highest efficiency, around 40%. However, because of the high cost of the materials and processing difficulties, these solar cells have, so far, only been employed in space applications. Solar cells based on polymers have been reported to give conversion efficiency as high as 12%. Compared to semiconductor-based devices, polymer solar cells are lightweight (which is important for small autonomous sensors), potentially disposable, and inexpensive to fabricate and have lower potential for negative environmental impact. They have been fabricated using printed electronics, are typically flexible, and their design can be customized. [36]

The Solar cell is an electrical device that converts the energy of light directly into electricity by the photovoltaic effect. It is a form of photoelectric cell (in that its electrical characteristics—e.g. current, voltage, or resistance—vary when light is incident upon it) which, when exposed to light, can generate and support an electric current without being attached to any external voltage source. [37] Polymer solar cells usually consist of an electron- or hole-blocking layer deposited on top of an indium tin oxide (ITO) conductive glass followed by electron donor and an electron acceptor (in the case of bulk heterojunction solar cells), a hole or electron blocking layer, and metal electrode on top. The nature and order of the blocking layers – as well as the nature of the metal electrode – depends on whether the cell follows a regular or inverted device architecture. [36]

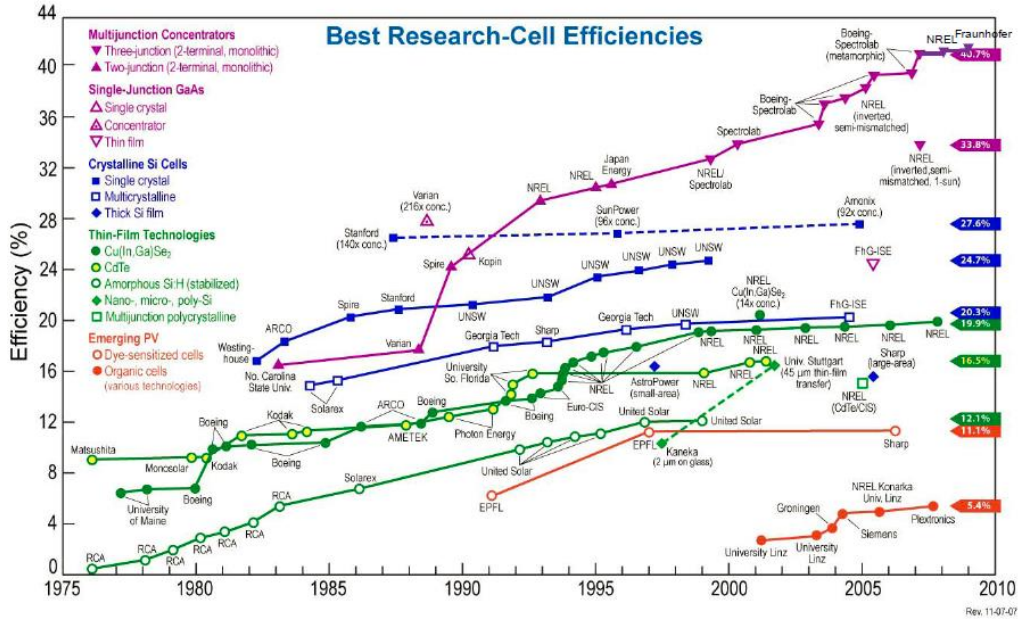

Figure 4 Chronological record energy-conversion efficiencies of solar cells. [38]
http://en.wikipedia.org/wiki/Solar_cell

Chapter 3 Solid Polymer Electrolytes – Relevant History

3.1 Ion Transport in Polymers

In 1973, Wright and co-workers [39] reported the complexation of alkali metal ions by poly(ethylene oxide), an important discovery that led to the development of new polymer/salt complexes known as solid polymer electrolytes [40]. Berthier and co-workers [41] demonstrated that in these semi-crystalline systems, ion transport occurs through the amorphous regions. Angell and co-workers [42] studied the conductivity of polymer electrolytes and observed an Arrhenius relationship between conductivity and temperature which suggested a similarity in behavior between the viscosity [43] and conductivity [44] of super-cooled molten salts.

Ion transport in glass-forming polymer electrolytes has been understood by fitting the data to the Vogel-Tammann-Fulcher (VTF) equation [45] where equivalent conductance, σ, is a function of temperature.

$$\sigma = \sigma_0 T^{-\frac{1}{2}} \exp\left(\frac{-K}{T - T_0}\right) \qquad \text{Equation 3.1}$$

In Equation 3.1, σ_0 is the constant term and K is a term analogous to activation energy in the Arrhenius behavior. T_0, also known as the Vogel temperature, corresponds to the absolute zero of the Arrhenius theory or the temperature at which ions cease to transport. Experimentally, T_0 is difficult to obtain and has been suggested to be 50K below the glass transition temperature, T_g, [46], [47] determined by differential scanning calorimetry (DSC). T_0 might also be obtained from the three parameter fit of Equation 3.1. But according to Angell, [42] accurate determination of T_0 by regression requires measurement of transport properties that span 1.5 orders of magnitude,

corresponding to a temperature range between T_0 and $2T_0$. Barreira and Barreira [43] noted that at temperatures much greater than T_0, the behavior becomes Arrhenius-like.

$$\sigma = \sigma_0 \exp\left(\frac{-E_a}{RT}\right) \qquad \text{Equation 3.2}$$

In Equation 3.2, R (=8.314 J/mol K) represents the gas constant and E_a (J/mol) is the activation energy in Arrhenius relationship. The activation energy can be rationalized as the resistance to diffusion jumps and for the Arrhenius equation this does not change with temperature. Bartholomew [48] proposed that an equivalent activation energy for Equation 3.2 might be obtained by taking its derivative with respect to temperature, yielding Equation 3.3.

$$E_{a,VTF} = -R\frac{\partial \ln\sigma}{\partial\left({}^{1}/_{T}\right)} = -{}^{1}/_{2}\,RT + KR\left(\frac{T}{T - T_0}\right)^2 \qquad \text{Equation 3.3}$$

Equation 3.3 shows the temperature dependence of activation energy in VTF equations. When the temperature, T, equals Vogel temperature, T_0, the activation energy goes to infinity; this is consistent with the definition of T_0 as being the temperature at which the ion transport ceases.

The VTF equation can also be used in understanding the plots of ion conductivity against temperature as shown in **Figure 5**. [4] This model has three fitting parameters instead of two in Arrhenius model, which gives better accuracy when being used in analyzing large, complicated systems like polymer electrolytes. The ability to extract physical meaning from the fitting constants provides a means of comparing the conductivity data from different samples.

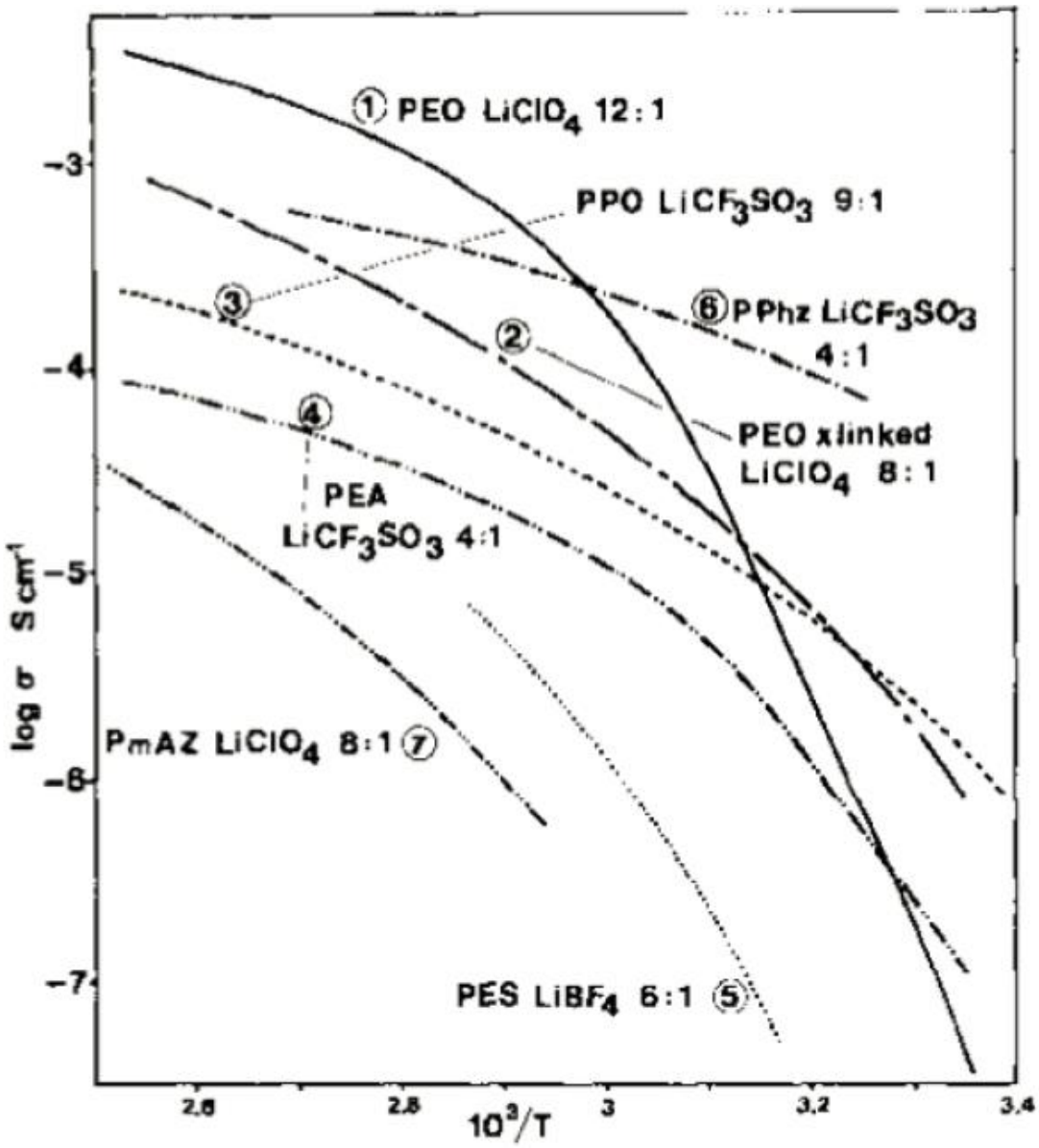

Figure 5 Arrhenius plot of the conductivity of various polymer/lithium salt[48] (Figures reprinted from reference 48 with permission of Armand, M. B.)

The difference between Arrhenius model and VTF models lies in the fitting parameter, T_0, which is also called Vogel temperature. This parameter may provide a clue on how the polymer chain dynamics influence the ion transport process. In both models σ_0 is related to the conductivity at infinite temperature (or when T is much greater the T_0) and K is the activation energy related to the diffusion jump in polymer electrolytes.

Another well-known protocol to describe the temperature dependence of mechanical and electrical properties of polymers is the Williams, Landel, and Ferry (WLF) model. [49] This model is shown in Equation 3.4. In Equation 3.4, a_T is the shift factor. As presented here, the shift factor is defined as the ratio of the temperature dependent viscosity, $\eta(T)$, and the viscosity measured at a chosen reference temperature, T_s, so that it is a ratio of relaxation times at the temperature of the measurement *versus* the relaxation time at the reference temperature.

$$\mathrm{Log}(a_T) = \mathrm{Log}\left[\frac{\eta(T)}{\eta(T_s)}\right] = \frac{-c_1(T - T_s)}{(c_2 + T - T_s)} \qquad \text{Equation 3.4}$$

Williams, Landel, and Ferry [49] made the observation that among seventeen different polymers, polymer solutions, and glass-forming liquids, plots of the shift factor, a_T, *versus* $T\text{-}T_s$ yielded plots which superimposed on each other. They found that the universal constants are C_1= -8.86 and C_2 = 101.6. In addition, T_s was often found to be equal to T_g + 50K. [60] Since the reference temperature, Ts, is arbitrary, the substitutions, $T_s = T_s + \delta$, $C_1 = C_1C_2/(C_1 + \delta)$ and $C_2 = C_2 + \delta$, where δ = 50K can be used to transform Equation 3.4 into a form, as shown in Equation 3.5, that is a function of T_g with C_1=17.44 and C_2=51.6.

$$\mathrm{Log}(a_T) = \frac{-c_1(T - T_g)}{(c_2 + T - T_g)} \qquad \text{Equation 3.5}$$

Equation 3.5 can be related to conductivity using Nernst-Einstein equation, shown below in Equation 3.6, where σ is the conductivity at temperature T, D is the diffusivity of ions, N is the number of charge carriers, and q is the charge constant. Since viscosity is inversely proportional to conductivity, Equation 3.6 can be converted to Equation 3.7 to describe conductivity.

$$\sigma = \frac{DNq^2}{kT} \qquad \text{Equation 3.6}$$

$$\mathrm{Log}(a_T) = \log\left[\frac{\eta(T)}{\eta(T_s)}\right] = \mathrm{Log}\left[\frac{\sigma(T_s)}{\sigma(T)}\right] \qquad \text{Equation 3.7}$$

Adam and Gibbs [50] proposed a molecular kinetic model explaining the temperature dependence of relaxation in glass-forming liquids based on thermodynamic arguments. This work is of particular interest because while based on theory, it predicts behavior that is described by the empirical WLF equation. The glass transition temperature is described by Adam and Gibbs [50] as a quasistatic temperature below which the time-scale related to establishment of equilibrium is beyond physical realization of most experiments. This was suggested to be due to an increase in relaxation times due to the small number of configurations available to the system, suggesting the smallness of equilibrium entropy as the glass transition temperature is approached. Extrapolation of equilibrium data collected above the glass transition temperature to temperatures below the T_g resulted in negative configurational entropies, a thermodynamic "catastrophe".

Besides the VFT and WLF behavior of polymer/salt systems described above, there are other cases in which ion transport in polymers is better described by the Arrhenius equation. An example is proton transport in sulfonated polymers (i.e., polymers containing sulfonic acid). The most popular example is a perfluorinated sulfonic acid polymer membranes referred to as Nafion (DuPont), which show high water-saturated proton conductivities of >10 mS/cm at room temperature. Nafion consists of a poly(tetrafluoroethylene) (PTFE) backbone with perfluoroether side chains terminated in sulfonic acid moieties. The backbone is hydrophobic, while the acid containing side chains are hydrophilic. This difference is a likely reason for the interesting co-continuous microphase separated morphology observed in these polymer membranes.

3.2 Ionic Liquids in solid polymer electrolytes

Batteries addressed to small and light-weight electronics require film-like electrolyte materials such as polymer electrolytes. The choice of solid electrolyte materials implies several advantages: (1) the absence of liquids or gases which may leach out, damaging the cell; (2) the possible realization of low-specific-capacity electrochemical devices; (3) a long lifetime due to the high mechanical resistance of the materials; and, (4) a utilization temperature range larger than that for liquid electrolyte systems. [51] ILs are an important option in this respect because their unique physical and chemical properties meet the requirements of plasticizing salts for polymers. Furthermore, ILs may expand the temperature range where flexible polymers can be used.

Ionic liquids (ILs) are are typically: (1) liquid over a wide temperature range - with low melting points, (2) nonvolatile, (3) thermally stable, (4) nonflammable, (3) high in ion content, (5) high in ionic conductivity, and (6) chemically and electrochemically stable. [52-54] Typical ionic liquids are comprised of tertiary or quaternary sulfonium, phosphonium, or ammonium (imidazolium, pyridinium, pyrrolidinium) cations in combination with anions that have low Lewis basicity, such as BF_4^-, PF_6^-, $CF_3SO_3^-$, $(CF_3SO_2)_2N^-$, etc. [52]

The modern era of ionic liquids stems from the work, in the late 1970's, on alkylpyridinium and dialkylimidazolium salts. [55] The discovery, in the early 1990's, of hydrolytically stable, liquid, 1,3-dialkylimidazolium tetrafluoroborate and hexafluorophosphate salts, led to an explosive growth in the number of publications relating to the synthesis, properties and applications of this unique class of materials that came to be known as room temperature ionic liquids (RTILs). [56] Because of frustration in packing, salts derived from large, irregularly shaped

cations and anions, have low melting points, typically less than 100°C and often below room temperature. Common cations in RTILs (shown in **Figure 6**) are quaternary ammonium salts, such as tetralkylammonium $[R_4N]^+$ or cyclic amines, both aromatic (pyridinium, imidazolium) and saturated (piperidinium, pyrrolidinium). [57], [58] Large inorganic or organic anions like BF_4^-, PF_6^-, AsF_6^- $N(CN)_2^-$ $C_4F_9SO_3^-$, $CF_3CO_2^-$, $CF_3SO_3^-$ etc. are also crucial to formation of salts with low-melting points.

The conductivity of RTILs, at ambient temperature, falls into a broad range of 0.1–14 mS/cm, which is lower than that for aqueous solution (500–700 mS/cm) or organic solvent solution (60 mS/cm) electrolytes. The conductivity of ionic liquids, however, may be comparable to that of lithium solution electrolytes (10 mS/cm). [52], [53], [54-57].

Cations:

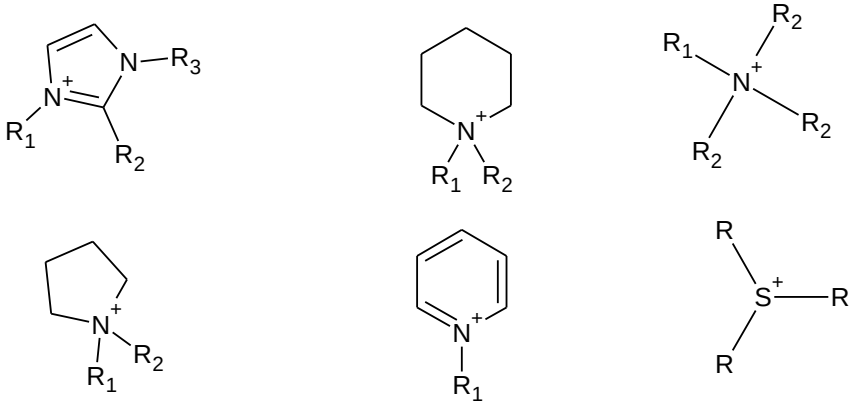

R_1 = Me-, Bu-
R_2 = Me-, H-
R_3 = Me-, Et-, Pr-, iPr-, Bu-

R_1 = Me-, Et-, Pr-, iPr-, Bu-
R_2 = Me-, Et-, Pr-, iPr-, Bu-

Anions:

F^- Cl^- I^- BF_4^- PF_6^- AsF_6^- $N(CN)_2^-$ $CF_3SO_3^-$ $CF_3CO_2^-$

$N(C_2F_5SO_2)_2^-$ $N(CF_3SO_2)_2^-$ $CF_3CONCF_3SO_3^-$ $C(CF_3SO_2)_3^-$

Figure 6 Common Cations and Anions for ionic liquid

Given the almost unlimited structural variation that can be realized with organic ions it is possible to engineer the structure of ionic liquids to get a wide range of physical and chemical properties. It has also been postulated that the function of capacitive electrochemical devices might be further improved if conventional ionic liquids were replaced by film-forming poly(ionic liquids) in which only the target ion is mobile. [51] However, covalent incorporation of an ionic liquid moiety in a polymer backbone invariably results in dramatically reduced ion mobility and conductivity. [1] This limitation can potentially be addressed by reduction in the dimensions of the ion transporting phase. [2], [3] Reduced dimensions can be realized by incorporating the poly(ionic liquid) in a polymer blend, [4] or precision block copolymer whose morphology can be rationally designed. [5]

There are two general methods to obtain an ILs-based polymer electrolyte. The first is the incorporation of the IL as a solvent or plasticizer for a nonionic polymer or by *in-situ* polymerization of a nonionic vinyl monomer in an IL solvent. [59-62] The resultant solid gel electrolytes provide the structural advantages of the nonionic polymer and thermal stability and ion conductivity of the IL salt. [60] Another way to make a film-forming ionic liquid electrolyte is synthesis of a homogeneous ionic liquid polymer. Such a polymer can be realized by introducing a polymerizable group into the cationic or anionic moieties of the ionic liquid. In such poly(ionic liquids), only the target ion is mobile. [63-65]

3.2.1 Polymer/Ionic Liquid Mixtures

The polymer electrolyte options introduced above may be broadly categorized as either solid polymer electrolytes (SPE) or gel polymer electrolytes (GPE). SPE's are based on high molecular weight polymers which perform the dual purpose of solvating the ions and providing mechanical

strength. GPE's are polymer gels in which the polymer is plasticized by a liquid electrolyte. Due to their higher conductivity GPE's, have received more attention and the literature reports numerous studies of polymer/IL gel electrolytes. [52-54], [51], [63] Poly[(vinylidene-fluoride)-*co*-hexafluoropropylene]/1-ethyl-3-methylimidazolium trifluoromethylsulfonate [52], [53] and poly(lithium-2-acrylamido-2-methyl-1-propanesulfonate-*co*-dimethylacrylamide)/1-ethyl-3-methylimidazolium dicyanamide [64] gel electrolytes were reported to exhibit high conductivities at room temperature (~1 mS/cm). The conductivity of these gels was found to decrease with increasing polymer content due to increasing viscosity and glass transition temperature of the mixture. [60] The stability of high-IL-content polymer/IL gels is improved by cross-linking. Susan et al. [66] reported that a lightly cross-linked polymer/IL gel prepared by *in-situ* polymerization produced materials having conductivity around 10 mS/cm at room temperature.

3.2.2 Polymerized Ionic Liquid/Ionic Liquid Mixtures

Poly(ionic liquids) synthesized by polymerization of ionic liquids with vinyl or acrylic groups incorporated in their molecular structure have also been investigated as candidates for solid-state electrolytes. [63-68] A schematic showing possible structures and architectures of poly(ionic liquids) (PILs) [1] is presented in **Figure 7**. Poly(ionic liquids) can have either the cation or anion tethered to the polymer chain with the counterion being bound by ionic attraction to the cation. One can also envision polycation/polyanion systems and zwitterionic- polymers in which both the cation and anion are covalently tethered to the polymer chain, either in zwitterionic copolymers or polymerizable zwitterionic moieties.

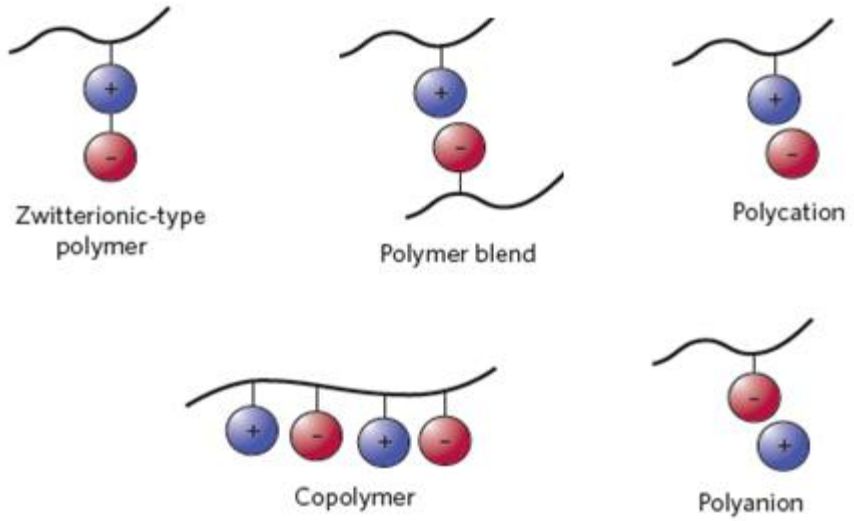

Figure 7 Options to make a solid-phase electrolyte based on PILs [1]

The ionic conductivity of polymerized ionic liquids has been studied by a number of researchers. [66-68] Ionic conductivity is reduced significantly after polymerization. The conductivity of a small molecular, monomeric, ionic liquid based on an imidazolium cation is on the order of 10 mS/cm. After polymerization the ionic conductivity is reduced to 10^{-2}mS/cm or less. [1]

3.3 Ion Conductivity of Solid-phase Electrolyte

As mentioned in previous sections, because of their film forming characteristics and higher temperature use range, polymerized ILs can be advantegeous in capactive electrochemical devices. It has been reported that the ionic conductivity of a poly(ionic liquid) is increased when doped with lithium salts. The conductivity of poly(1-vinylimidazolium tetrafluloroborate), P(VyImBF4), doped with LiCl, $LiBF_4$ or LiTFSI was increased substantially as the lithium salt content was increased, up to the solubility limit of the salt in the polymer (see **Figure 8**). [62] Above the solubility limit, ionic conductivity starts to decrease due to phase separation.

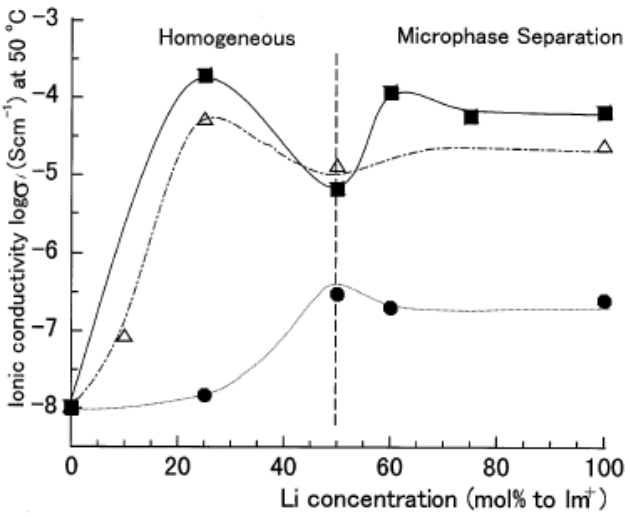

Figure 8 The ionic conductivity of P(VyImBF4) as a function of salt concentration ● LiCl; ∆ LiBF4; ■ LiTFSI [62] (Figures reprinted from reference 65 with permission of H. Ohno)

3.3.1 Glass Transition Temperature

As discussed in Section 3.1, the ionic conductivity of solid polymer electrolytes is a function of the glass transition and viscoelastic properties of the composition. The glass transition, T_g, is a key characteristic of an amorphous polymer. When the polymer is heated above T_g, there is a substantial increase in the free volume of the polymer (the space in polymer that is not occupied by polymer molecules) and, with the onset of large scale segmental motion in the polymer backbone, the polymer becomes soft and flexible. In this rubber-like state, the polymer molecules are able to move and ionic conductivity is higher.

Ohno *et al.* [72] have shown that the glass transition temperature and the ionic conductivity of poly(ionic liquids) can be linearly related. **Figure 9** displays the relationship between ionic conductivity and T_g for poly(ionic liquids) with imidazolium, piperidinium, and other onium cations. [72] This figure clearly demonstrates that PILs having lower glass transition temperatures exhibit higher ionic conductivity.

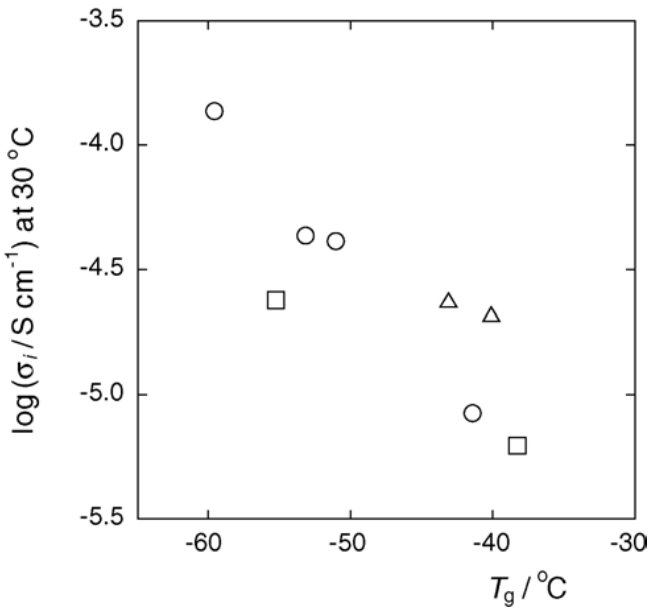

Figure 9 Relationship between ionic conductivity and Tg for PILs. Imidazolium cation (o), piperidinium cation (□), other onium cation (∆) [72] (Figures reprinted from reference 72 with permission of H. Ohno)

Ohno *et. al.* also sythesized and polymerized ionic liquid monomers with an alkyl spacer between a polymerizable acryloyl group and an imidazolium cation. [63], [72] The ionic conductivity of polymers with longer alkyl spacers was increased by two orders of magnitude.

The glass transition temperature of poly(ionic liquids) can also be lowered by making copolymers. The T_g of a copolymer is predicted by Flory-Fox equation (Equation 3.8), where W_1, and W_2 are the weight fractions of two components.

$$\frac{1}{T_g} = \frac{W_1}{T_{g,1}} + \frac{W_2}{T_{g,2}} \qquad \text{Equation 3.8}$$

From this equation, it can be seen that by copolymerizing an ionic liquid monomer with a non-ionic monomer that would yield a low-T_g homopolymer, one can obtain copolymers with lower glass transition temperatures. Even though the ion concentration is lower, in nonionic monomer/ionic liquid monomer copolymers, the conductivity is typically higher than that of a

homopolymerized ionic liquid. Elabd *et al.* [69] synthesized a random copolymer of hexyl methacrylate (HMA) with methacrylate-based imidazolium tetrafluoroborate (BF_4) or bis(trifluoromethane sulfonyl) imide (TFSI) monomers, shown in **Figure 10**. Up to 50 mol% HMA, copolymers showed increasing ionic conductivity with increasing HMA content.

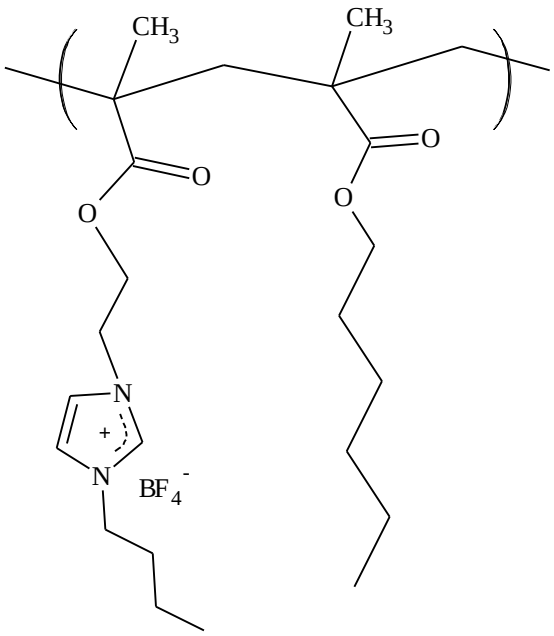

Figure 10 Poly(methacryloylethylbutylimidazolium tetrafluoroborate-co-hexylmethacrylate)

3.3.2 Anion effect

Few papers have been published relating to the effect of the counterion on ionic conductivity in poly(ionic liquids). [70], [71] Factors affecting ionic conductivity include the size and symmetry of the counterion and the dissociation energy of ion pairs. Elabd *et. al.* prepared the N-methacryloyloxyethyl imidazolium bromide homopolymer and ion exchanged the homopolymer with bis(trifluoromethanesulfonyl) imide (TFSI), tetrafluoroborate (BF_4), trifluoromethanesulfonate (CF_3SO_3), and hexafluorophosphate (PF_6) anions.[70] **Figure 11** shows the structure of the homopolymer, counterions and ionic conductivity data.

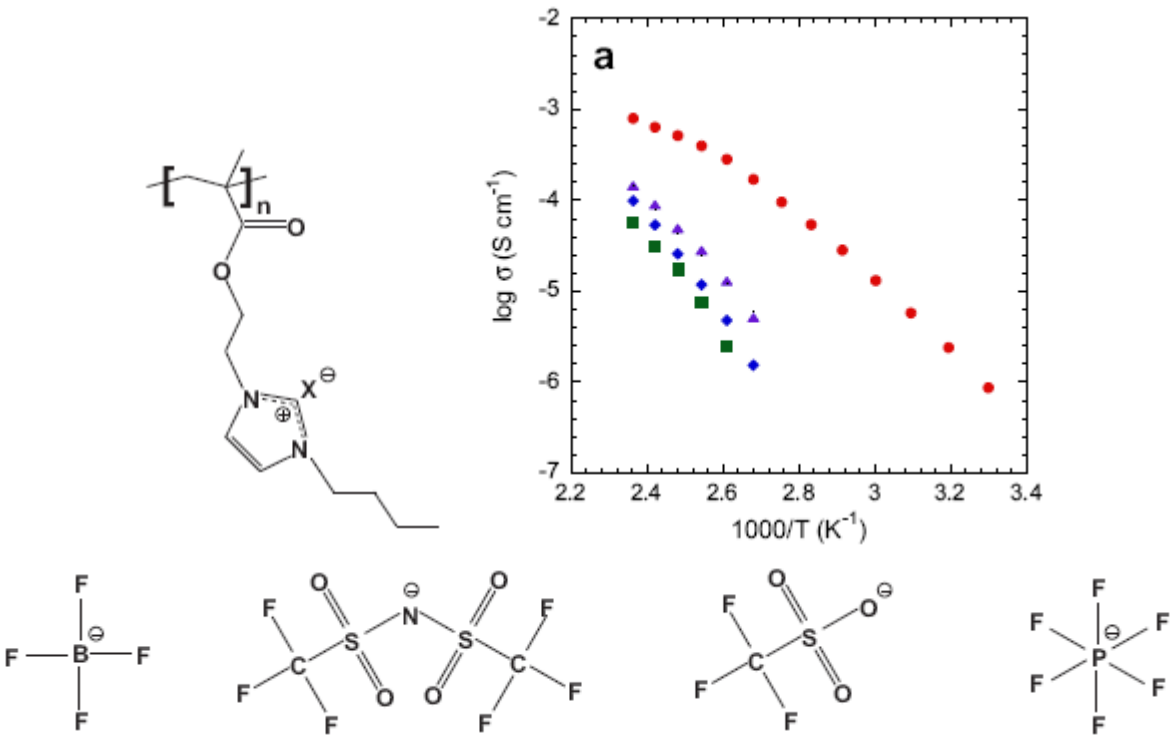

Figure 11 Ionic conductivity versus 1000/T (K-1) of PILs: poly(MEBImeBF4) (blue diamonds), poly(MEBImePF6) (green squares), poly(MEBImeTriflate) (magenta triangles), poly(MEBImeTFSI) (red circles)[70].(Reprinted from reference 70 with permission from Elsevier)

It can be seen from Figure 11 that the conductivity of PILs follows the order: TFSI>Triflate>BF_4>PF_6. This is opposite order of glass transition temperatures of the respective polymer salts, [72] poly(MEBImePF_6), 367K > poly(MEBImeBF_4, 358K > poly(MEBImeTriflate), 337K > poly(MEBImeTFSI), 280K.

3.3.3 Reduced Dimensions for Ion Conduction

Although the conductivity of polymerized ionic liquids can be improved by properly designing the structure of cations, making copolymers and choice of anion, it is the influence of these factors on T_g that effectively determines or limits ionic conductivity. Given the viscoelastic

character of polymers (or polymer gels) ionic conductivity is too low for utility in many electrochemical devices.

Recently, ion conduction has been found to be anisotropic in self-organized nanostructured compositions. [2], [3] The proposition that reduced dimensions will result in higher ion conductivity is supported by literature reports of two-dimensional ionic conductivity in a smectic liquid-crystalline structure containing a lithium salt complexed with tetraoxyethylene moieties. [2] Enhanced ionic conductivity has also been reported in one dimensional channels of a polymerized liquid crystal having a tethered 1,3-dialkylimidazolium functional group in the one-D channel. [3] The one-dimensional ion-conductive film was fabricated by photopolymerization of aligned columnar liquid crystals of a fan-shaped imidazolium salt. In the columnar structure, the ionic moiety self-assembles to the inner part of the column. The column was oriented macroscopically parallel to a glass surface by mechanical shearing. Anisotropic ionic conductivities were observed for the oriented films stabilized by photopolymerization. The data showed that ion conduction in the parallel direction was higher than that in the vertical direction by about two orders (**Figure 12**).

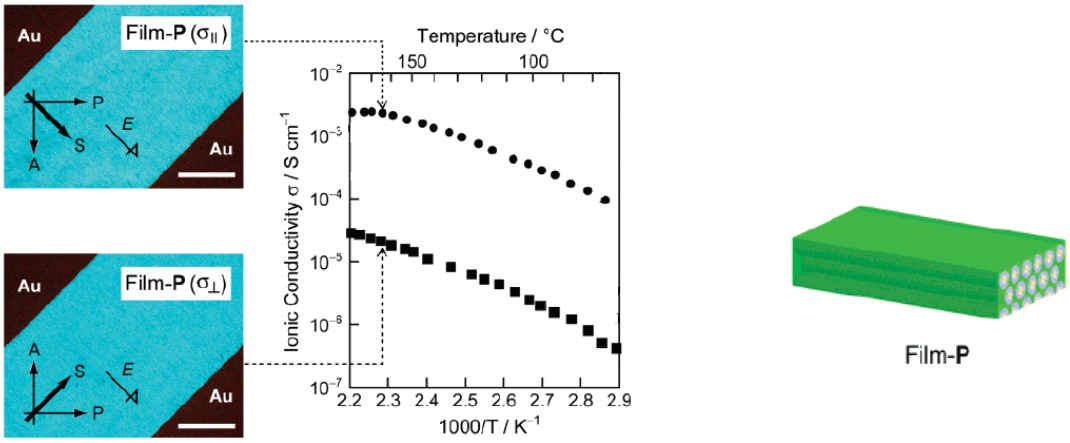

Figure 12 One-dimensional ion-conductive polymeric films: anisotropic ion conduction [3] (Figures reprinted from reference 3 with permission of H. Ohno)

Poly(ionic liquid) block copolymers, poly[styrene-b-4-vinylbenzylalkylimidazolium *bis*(trifluoromethanesulfonyl)imide] [PS-b-PVB-alkylIm^{+}TFSI]; alkyl = CH_3, n-C_4H_9, n-C_6H_{13}, were designed and synthesized by Yossef A. Elabd *et. al.* [73] The polymer structure is shown in **Figure 13(a)**. The morphology of the block copolymer was found to be a mix of cylindric and lamellar phases [see **Figure 13(b)**] which provide nanoscale channels for ion transport. The ionic conductivity for this block copolymer was measured to be 0.1 mS/cm^{-1} at 150 ºC, which is comparable with small-molecule ionic liquid. [1] Ionic conductivity was also found to increase with the increasing molar percent of the ionic component. [73]

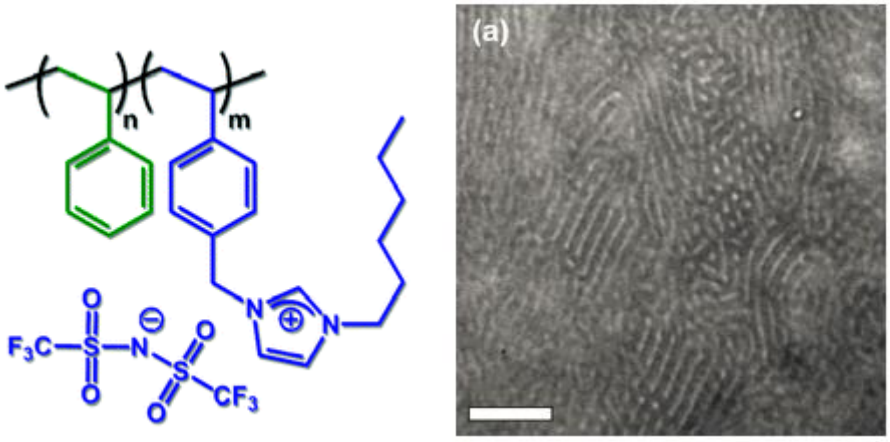

(a) **(b)**

Figure 13 (a) Chemical structure of [PS-b-PVB-alkylIm+TFSI] (b) TEM images of cylinders and lamellae phase coexistence exhibited by solvent-cast [PS-b-PVB-alkylIm+TFSI], scale bar is 200 nm [73]

Chapter 4 Experimental

4.1 Materials and Methods

4.1.1 Materials

Unless otherwise noted, all chemicals were used as received, without further purification. 1,1,1,3,3,3-hexamethyl disilazane (99.9%), 1-vinylimidazole (99+% distilled *in vacuo*), AIBN, (98%, recrystallized from methanol), 4-imidazoleacrylic acid (99%), calcium hydride (coarse granules, 95%), ethyl trifluoromethane sulfonate (99%), lithium hexafluorophosphate ($LiPF_6$, 98%), lithium trifluoromethanesulfonimide (LiTFSI, 99.95%), picric acid (99+%), and tetrafluoroboric acid (48 wt% solution in water) were purchased from Sigma-Aldrich. Ammonium chloride (99.5%, analysis ACS), ammonium sulfate (reagent ACS), iodomethane (stabilized, 99%), isopropanol (IPA, analysis), methyl alcohol (reagent ACS, 99.8%), potassium carbonate (reagent grade ACS, anhydrous), sodium bicarbonate (p.a.), and sodium dicyanamide (97% pure), were purchased from Acros Organics. Ethyl acetate (EA, AR ACS), hydrochloric acid (AR ACS), dichloromethane (AR ACS) were obtained from Mallinckrodt Chemicals. Sodium hydroxide (pellets), silica gel (40-140 Mesh), magnesium sulfate (Anhydrous Powder) were obtained from J.T. Baker. N,N-Dimethylformamide (Spectrograde), benzene (GR ACS), acetonitrile (GR ACS), hexanes (GR ACS) were obtained from EMD. Methanol (GR ACS), hexanes (GR ACS), Spectra/Por Membranes (MWCO 6-8,000) were purchased from VWR Inc.

4.1.2 Instruments

NMR

Proton NMR spectra were obtained using a Bruker, DRX-300 spectrometer. Unless noted, all samples were dissolved in chloroform-d (Aldrich, 99.8 atom % D, 0.05% v/v TMS).

Differential Scanning Calorimetry (DSC)

Glass transition thermograms were obtained under nitrogen using a TA Instruments DSC Q100 equipped with a liquid-nitrogen cooling system. All samples were prepared in an Ar-filled, Vacuum Atmospheres glove box. Polymer samples were placed in an open, hermetically-sealable, aluminum pan and heated to 100^{o}C for 15 minutes on the surface of a digital hot plate in the glove box. The aluminum pan was then capped and sealed. In the DSC, samples were ramped to 200^{o}C then cooled to -50^{o}C at a rate of 20^{o}C/min. Each sample was subjected to at least three heating and cooling cycles and held at -50^{o}C and 200^{o}C, respectively, for 1 minute in between each heating and cooling cycle. It was generally found that the DSC traces for the second and third heating cycles were identical and could be overlaid. Data recorded in the tables in this thesis were taken from the second of the three heating cycles. T_g values are reported as midpoint glass transition temperatures, T_g-mid. The analysis was a 7-step process: (1) heating from 22^{o}C to 200^{o}C at 20^{o}C/min; (2) holding for 1 minute at 200 °C; (3) cooling from 200 to-50^{o}C at 20^{o}C/min; (4) holding for 1 minute at -50^{o}C; (5) heating from -50^{o}C to 200^{o}C at 20^{o}C/min; (6) holding for 1 minute at 200°C, and; (7) cooling from 200^{o}C to -50^{o}C at 20^{o}C/min. It cannot be emphasized too strongly that obtaining accurate, repeatable measures of the glass transition in poly(ionic liquid) 1-vinyl- and 4-vinylimidazolium salts requires substantial diligence and care. In the present research, rough correspondence in heating cycle and cooling cycle heat capacity

changes was generally required to validate a heat capacity change as a glass transition. Additional validation was garnered by way of a final heating cycle from -50 to 200°C, heating at 40°C per minute. Under these conditions heating cycle heat capacity changes associated with the glass transition will be amplified and shifted to a somewhat higher temperature.

Size Exclusion Chromatography

Molecular weight and polydispersity were determined using an Agilent 1100 series gel permeation chromatograph with two Agilent Zorbax PSM 60-S columns (in series). The samples were eluted at 35°C, using *N,N'*-dimethylformamide as the solvent. Molecular weight values reported are styrene equivalent molecular weights based on hydrodynamic radius.

Dielectric Spectroscopy

Dielectric properties were measured with an ARES rheometer system from TA Instruments coupled with an Agilent LCR Meter 4284A. Polymer films whose thickness ranged from 250 μm to 1600 μm were prepared by solution casting from ethanol or DMF on Al foil substrates at ambient temperature. The films were dried in a fume hood at room temperature and cut to 22 mm by 24 mm before a final drying process in which they were further dried at 120 ˚C on the surface of a digital hot plate for at least 24 h. The dried films were then stored in a desiccator until use. The samples were placed between two stainless steel electrodes in the ARES and isothermally measured as a function of frequency, between 20 Hz and 10^6 Hz. The temperature was controlled by the ARES with liquid nitrogen and compressed air as the gas at low and high temperatures, respectively.

The Havriliak–Negami (HN) model [74] is used to analyze the dielectric relaxation measurements. The complex dielectric function, $\varepsilon^*(\omega) = \varepsilon' - i\varepsilon''$, is written as:

$$\varepsilon^*(\omega) = \varepsilon_\infty + \frac{\Delta\varepsilon}{\left(1+(i\omega\tau)^\beta\right)^\gamma} - i\frac{\sigma_0}{\omega^s\varepsilon_0} \qquad \text{Equation 4.1}$$

where $\omega = 2\pi f$ is the radian electric field oscillation frequency; ε_∞ is the high frequency limit of the dielectric constant; $\Delta\varepsilon$ is the relaxation strength, defined as $\Delta\varepsilon = \varepsilon_s - \varepsilon_\infty$. τ is the relaxation time which is the reciprocal of the radian frequency of maximal loss, $\omega_{max.}$ β and γ ($0 < \beta \leq 1$, $0 < \beta\gamma \leq 1$) are the shape parameters of the relaxation spectra. For a purely Debye relaxation process, both β and γ would be equal to unity. The added term, $-i(\sigma_0/\varepsilon_0\omega^s)$, refers to effects of conduction, where σ_0 is related to dc conductivity and ε_0 is the permittivity of vacuum. The exponential parameter, *s*, is equal to 1 for ohmic conductivity and less than 1 for non-ohmic effects in the conductivity [74]. The relationship between frequency at maximum loss, f_{max}, which is known as the relaxation rate, and the corresponding temperature can be described by an Arrhenius function. The frequency of maximum loss, f_{max}, was most often evaluated directly from plots of tan δ (= $\varepsilon''/\varepsilon'$) vs. frequency. In three instances [poly(1-ethyl-3-methyl-4-vinylimidazolium PF_6^-), poly(1-ethyl-3-vinylimidazolium PF_6^-) and poly(1-ethyl-3-methyl-4-vinylimidazolium BF_4^-)] additional data were obtained by fitting plots of ε'' vs. frequency, according to Equation 4.1, with $\Delta\varepsilon$, τ, β, γ, σ_0 and s as fitting parameters.

4.2 Synthesis of imidazole and imidazolium monomers

4.2.1 Synthesis of 4(5)-Vinylimidazole and 1-Methyl-5-vinylimidazole

4(5)-Vinylimidazole (1)

4(5)-vinylimidazole (1) was synthesized by decarboxylation of urocanic acid (4-imidazole acrylic acid (99%), Sigma-Aldrich). The procedure employed was analogous to that of

Overberger, *et al*. [75] Thus, in a typical procedure, urocanic acid (3.70 g, 26.8mmol) was decarboxylated *in vacuo* (10 µm Hg) at 230°C to yield 1.46g (58%) of crude 4(5)-vinylimidazole. The process was repeated as required to provide sufficient material for subsequent reactions.

1-Methyl-5-vinylimidazole (2)

The synthesis of **(2)** was carried out, as described in the M.S. Thesis of Darren Smith, using crude 4(5)-vinylimidazole. The 1-pot, regiospecific alkylation process was run in acetonitrile; a sub-stoichiometric (1:0.95 equivalent of 1-trimethylsilyl-4-vinylimidazole to methyl iodide) amount of methyl iodide was used. This process differs from those reported by Kawakami and Overberger [76] and Wang and Smith [77] in that an excess of methyl iodide was not employed. The process is outlined in **Reaction Scheme 1**.

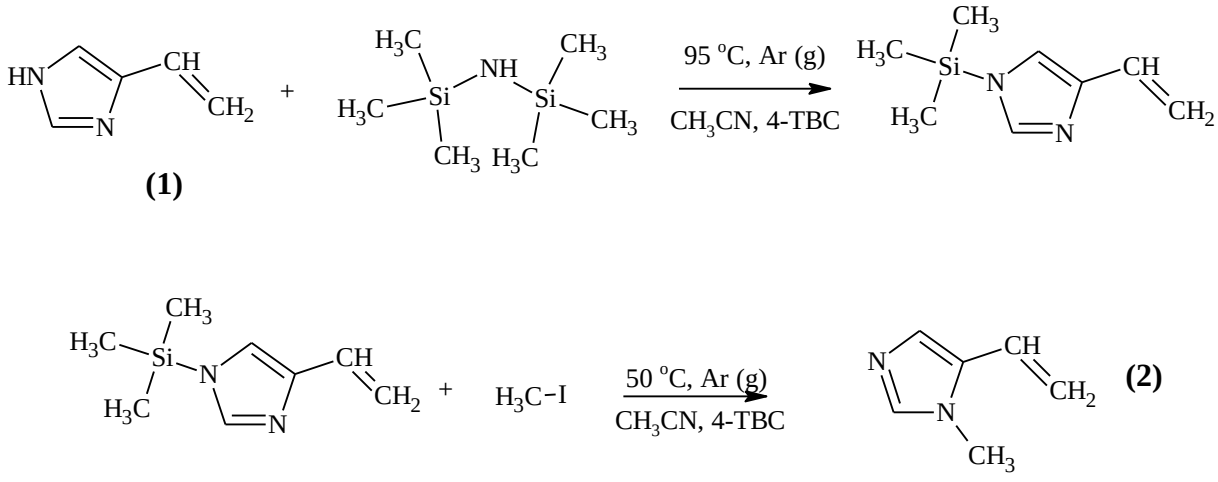

Reaction Scheme 1 Single pot synthesis of 1-methyl-5-vinylimidazole

***4.2.2 1-ethyl-3-methyl-4-vinylimidazolium trifluoromethane sulfonate* (3)**

The synthesis of **(3)** was also carried out, as described in the M.S. Thesis of Darren Smith. The process is outlined in **Reaction Scheme 2**. Thus, freshly distilled (1) (4.22g, 39.1mmol) and dichloromethane (50mL) were charged to a 250 mL three-neck round bottom flask, equipped

with gas inlet valve, Teflon adapter with thermometer, addition funnel, and magnetic stir bar. The solution was cooled to 0°C, by immersion into an ice-water bath, and stirred under an Argon blanket. Ethyl trifluoromethane sulfonate (28.38g, 0.16mol,) and dichloromethane (50 mL) were charged to the addition funnel. This solution was added to the reaction vessel drop-wise over a 30 minute period and the reaction mixture was stirred at 0°C for 2 hours. The addition funnel was then replaced by a short-path distillation head and the solvent was removed *in vacuo*, at 0°C, yielding 10.64g, 99%, 3-ethyl-1-methyl-5-vinylimidazolium trifluoromethane sulfonate as a white crystalline solid melting at 41°C. ^{1}H NMR (in THF-d_8) 1.47 (3H, t, N-CH2*CH3*), 3.81 (3H, s, N-CH3), 4.18 (2H, q, N-*CH2*CH3), 5.54 (1H, d, ^{3}J 11.31Hz, *cis*-vinyl H), 5.88 (1H, d, ^{3}J 17.46Hz, *trans*-vinyl H), 6.54 (1H, $^{3}J_{cis}$ 11.31, $^{3}J_{trans}$ 17.46, vinyl *H*-C), 7.75 (1H, s, C-4*H*), 8.92 (1H, s, C-2*H*), see **Figure 14**.

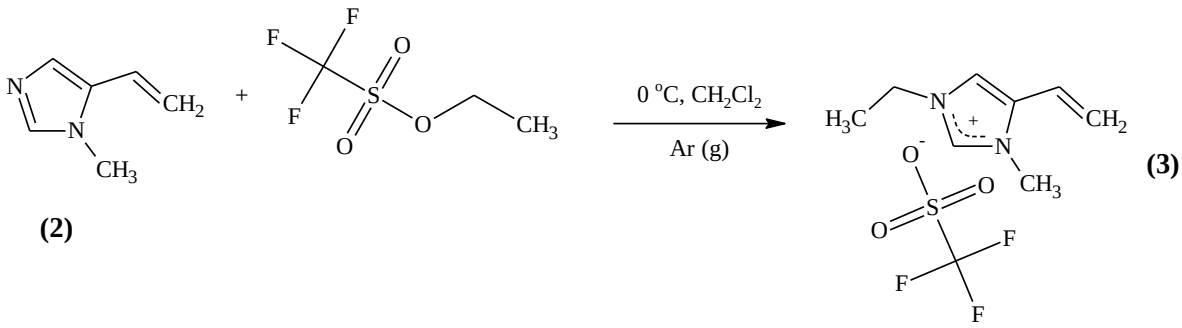

(2) **(3)**

Reaction Scheme 2 Synthesis of 1-ethyl-3-methyl-4-vinylimidazolium trifluoromethane sulfonate

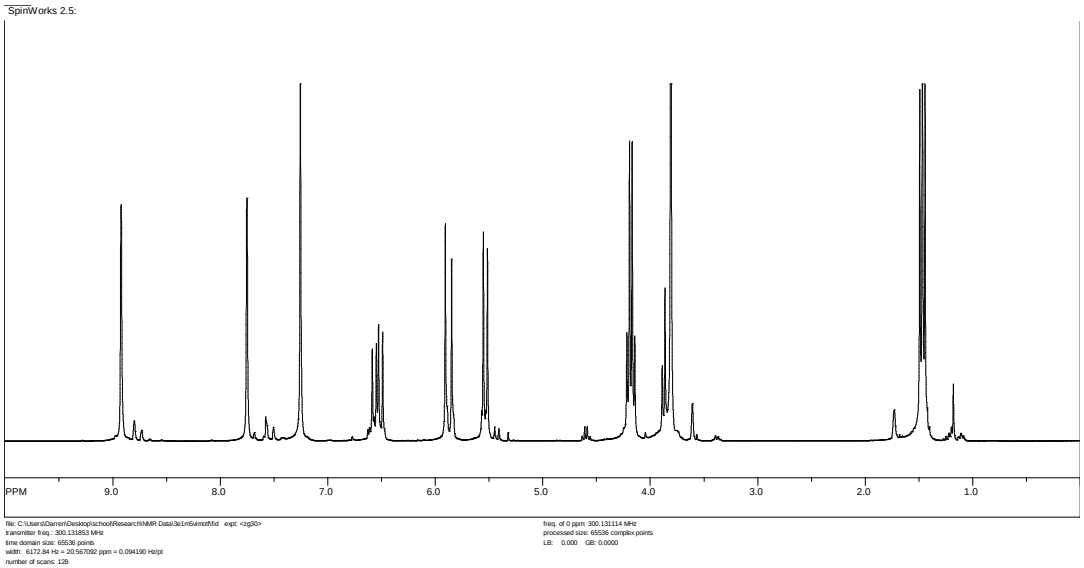

Figure 14 ^{1}H NMR of 1-ethyl-3-methyl-4-vinylimidazolium triflate

4.2.3 Poly(1-ethyl-3-methyl-4-vinylimidazolium trifluoromethane sulfonate)

1-ethyl-3-methyl-4-vinylimidazolium trifluoromethane sulfonate **(3)** was polymerized as outline in Reaction Scheme 3. Thus, monomer **(3)** (5.3g, 39mmol) was dissolved in ethyl acetate (30mL) and transferred to a polymerization tube at 0^{o}C, under an Argon blanket. One ml of a solution of AIBN (0.03g, 0.183mmol) dissolved in ethyl acetate (10mL) was added to the polymerization tube and mixed. The solution was then degassed in three freeze-thaw cycles. The tube was sealed *in vacuo* and immersed in a water bath at 65^{o}C for 20 hours. The resulting polymer was isolated by dissolution in methanol and precipitated in methyl-*tert*-butyl ether. The precipitate was air dried on a hot plate at 90^{o}C for 1 hour. Yield = 3.07g, 88%, M_n = 8730 g/mol, M_w = 14,722 g/mol, PD = 1.7. The ^{1}H-NMR spectrum of the polymer is shown in Figure 15.

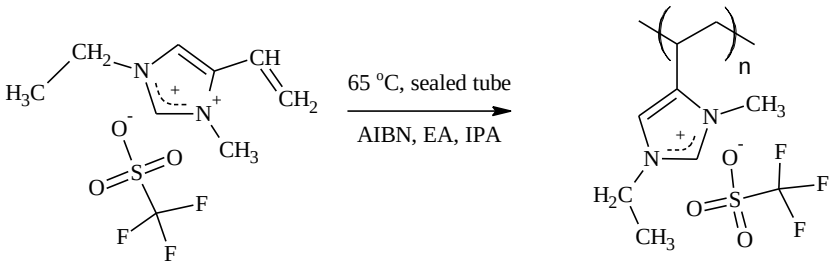

(3) **(4)**

Reaction Scheme 3 Polymerization of 1-ethyl-3-methyl-4-vinylimidazolium triflate

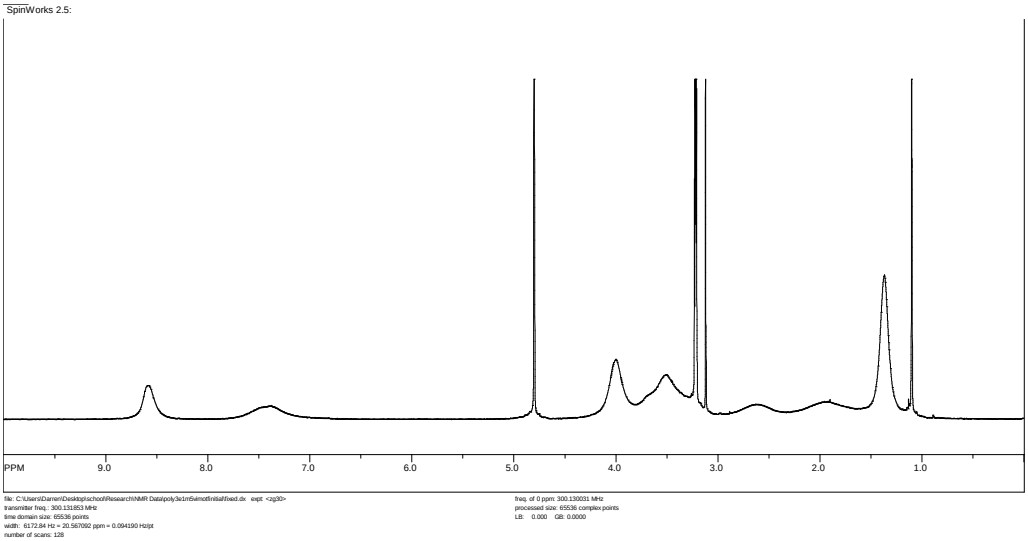

Figure 15 ^{1}H NMR of poly(1-ethyl-3-methyl-4-vinylimidazolium triflate)

4.2.4 Anion exchange of poly(1-ethyl-3-methyl-4-vinylimidazolium salts)

Poly(1-ethyl-3-methyl-4-vinylimidazolium triflate) **(4),** 3g, was dissolved in 30mL of methanol. 5mL aliquots of this solution were used in the ion-exchange processes detailed below.

Poly(1-ethyl-3-methyl-4-vinylimidazolium tetrafluoroborate) (5)

5mL (1.84mmol) of the stock solution of **(3)** was added to a centrifuge tube, to which 5mL of 48% tetrafluoroboric acid (79.5mmol) in water was added. The solution was shaken vigorously and a precipitate formed. The solution was centrifuged, decanted, and rinsed several

times with methanol to remove excess HBF_4, in order to prevent the decomposition of the polymer; the tube was transferred to a glove box with inert atmosphere for further drying. T_g onset: heating cycle = 178-186°C, cooling cycle = 198°C.

Poly(1-ethyl-3-methyl-4-vinylimidazolium hexafluorophosphate) (6)

5mL (1.84mmol) of that the stock solution of (3) was added to a centrifuge tube, to which a 25mL methanol solution containing $LiPF_6$ (1.39g, 9.14mmol) was added. The solution was shaken vigorously and a precipitate formed. The solution was centrifuged, decanted and the tube was transferred to a glove box with inert atmosphere for further drying. T_g onset: heating cycle = 187°C, cooling cycle = 200°C.

Poly(1-ethyl-3-methyl-4-vinylimidazolium hexafluoroarsenate) (7)

5mL (1.84mmol) of that the stock solution of (3) was added to a centrifuge tube, to which a 5mL methanol/water (50/50) solution containing $KAsF_6$ (2.1g, 9.18mmol) was added. The solution was shaken vigorously and a precipitate formed. The solution was centrifuged, decanted, and the tube was transferred to a glove box with inert atmosphere for further drying. T_g onset: heating cycle = 206°C, cooling cycle = 234°C.

Poly(1-ethyl-3-methyl-4-vinylimidazolium trifluoromethylsulfonylimide) (8)

5mL (1.84mmol) of that the stock solution of (3) was added to a centrifuge tube, to which a 25mL methanol solution containing LiTFSI (2.64g, 9.15mmol) was added. The solution was shaken vigorously and an oil separated out on the bottom. The top layer was removed and the tube was transferred to a glove box with inert atmosphere for further drying. The oil turned into a brittle film. T_g onset: heating cycle = 72°C, cooling cycle = 92°C.

Poly(1-ethyl-3-methyl-4-vinylimidazolium dicyanamide) (9)

5mL (1.84mmol) of that the stock solution of (3) was added to a centrifuge tube, to which a 25mL methanol solution containing sodium dicyanamide (0.82g, 9.2mmol) was added. The solution was shaken vigorously and a precipitate formed. The solution was centrifuged, decanted, and the tube was transferred to a glove box with inert atmosphere for further drying. T_g onset: heating cycle = 73^{o}C, cooling cycle = 114^{o}C.

4.2.5 1-Butyl-2,3-dimethyl-4vinylimidazolium triflate) **(14)**

1-Butyl-2,3-dimethyl-4-vinylimidazolium triflate) **(14)** was provided by Fan Yang and was prepared as described in her published M.S. Thesis [78], by alkylation of 1-butyl-2-methyl-4-vinylimidazole **(13)** with methyltriflate,. The 4-vinyl monomer **(13)** was prepared by butylation of 2-methyl-4(5)-vinylimidazole **(12)** which was prepared by hydrolysis of 1-trityl-2-methyl-4-vinylimidazole **(11)**. **(11)** was obtained by lithiation and methylation of 1-trityl-4-vinylimidazole **(10)** which was prepared from 4(5)-vinylimidazole **(1).** The process for tritylation of 4(5)-vinylimidazole was analogous to that published by Schiavone *et al*. [75] The entire process is outlined in **Reaction Scheme 4**. The ^{1}H-NMR spectrum of 1-butyl-2,3-dimethyl-4-vinylimidazolium triflate) **(14)** is shown **Figure 16**.

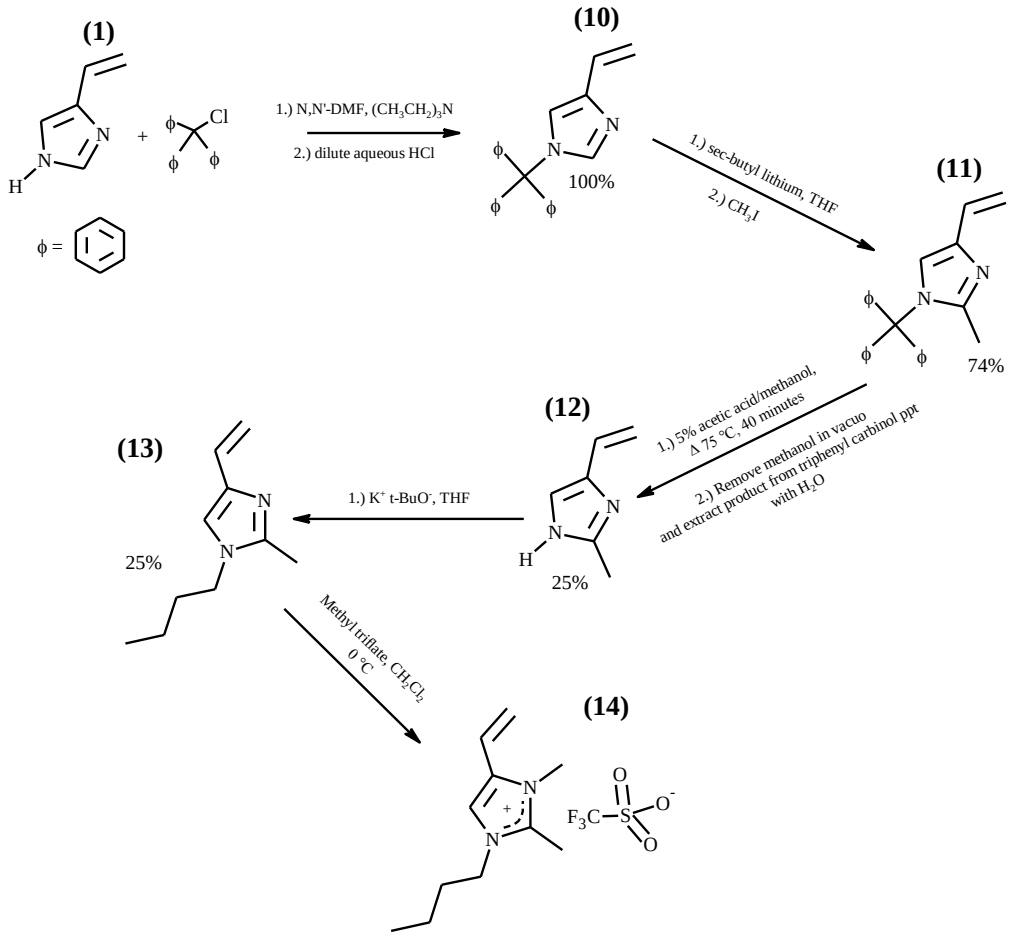

Reaction Scheme 4 Synthesis of 1-butyl-2,3-dimethyl-4-vinylimidazolium triflate

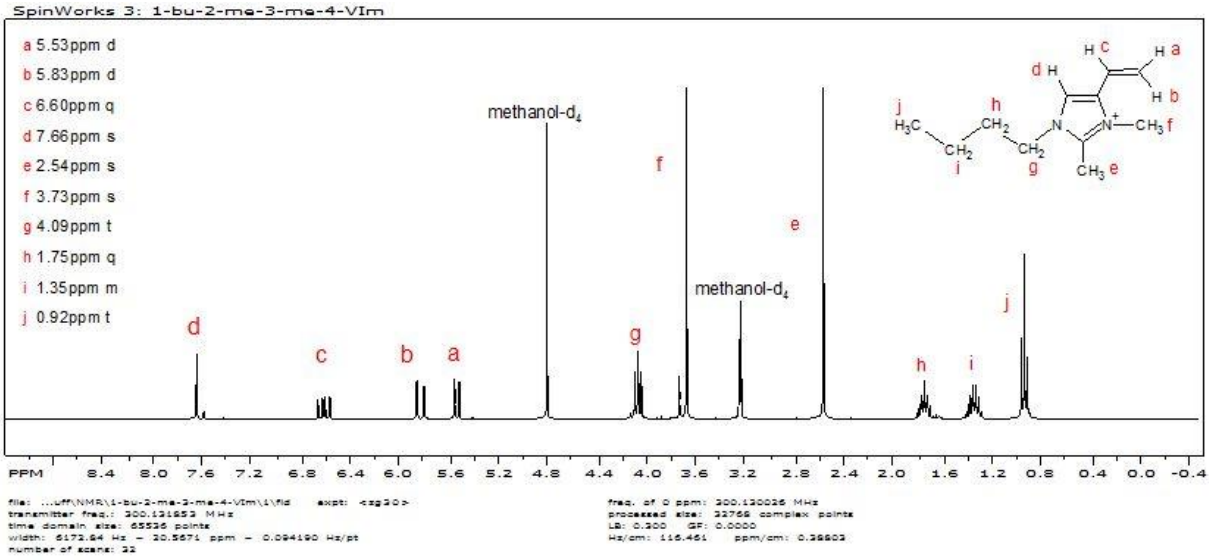

Figure 16 ^{1}H NMR of 1-butyl-2,3-dimethyl-4-vinylimidazolium triflate

Poly(1-butyl-2,3-dimethyl-4-vinylimidazolium triflate) (15)

1-butyl-2,3-dimethyl-4-vinylimidazolium trifluoromethane sulfonate **(14)** (1.68g, 5.80mmol) was dissolved in ethyl acetate (8mL) and ethanol (2mL) and charged to a polymerization tube at 0°C. A 0.012 molar solution of AIBN in ethyl acetate (1mL) was added to the polymerization tube; and the reaction mixture was degassed in three freeze-thaw cycles, flame sealed, and immersed in a water bath at 65°C for 20 hours. A viscous polymer solution was formed. The polymerization tube was opened and the reaction mixture was precipitated in 300ml of diethyl ether. The product was isolated by centrifugation and dried in an inert atmosphere to yield 1.68g, 100%, of a fluffy white polymer, M_n ~ 39,600 g/mol, polydispersity = 1.75. The ^{1}H-NMR spectrum of poly(1-butyl-2,3-dimethyl-4-vinylimidazolium triflate) is given in **Figure 17**.

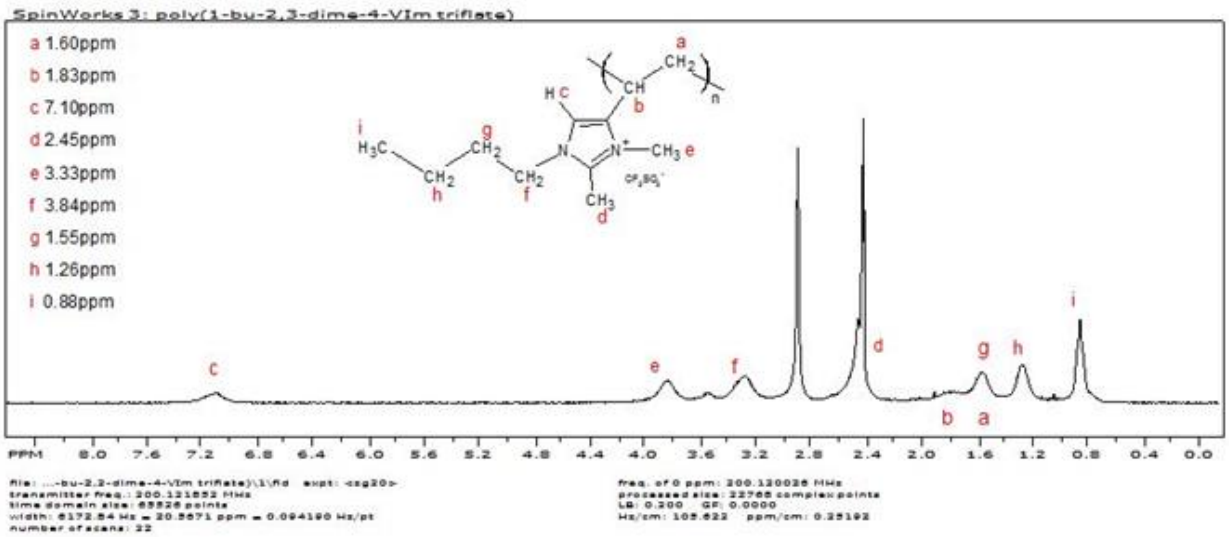

Figure 17 ^{1}H-NMR of poly(1-butyl-2,3-dimethyl-4-vinylimidazolium triflate)

Formation of poly(1-butyl-2,3-dimethyl-4-vinylimidazolium salts) by anion exchange

A "stock solution" with a concentration of 0.02 g/mL of poly(1-butyl-2,3-dimethyl-4-vinylimidazolium trifluoromethane sulfonate) **(15)** in methanol was prepared and 10 ml aliquots of this solution were used in the ion-exchange processes detailed below.

Poly(1-butyl-2,3-dimethyl-4-vinylimidazolium hexafluorophosphate) (16)

10 mL (0.70mmol) of the above stock solution was added to a centrifuge tube, to which 10 mL of ammonium hexafluorophosphate (0.90mmol) in methanol was added. The solution was shaken vigorously and a precipitate formed. The suspension was centrifuged, decanted, and rinsed twice with methanol to remove excess NH_4PF_6. The precipitated polymer was dried in the vacuum anti-chamber of a glove box. Elemental analysis (Galbraith Laboratories, Knoxville, TN – report Number 64747) indicated 77% ion exchange.

Poly(1-butyl-2,3-dimethyl-4-vinylimidazolium trifluoromethylsulfonylimide) (17)

10 mL (0.70mmol) of the above stock solution was added to a centrifuge tube, to which 10 mL of lithium trifluoromethylsulfonylimide (0.90mmol) in methanol was added. The solution was shaken vigorously and a precipitate formed. The suspension was centrifuged, decanted, and rinsed twice with methanol to remove excess LiTFSI. The precipitated polymer was dried in the vacuum anti-chamber of a glove box. Elemental analysis (Galbraith Laboratories, Knoxville, TN – report Number 64747) indicated 84% ion exchange.

4.2.6 Copolymerization

Copolymerization of 1-ethyl-3-methyl-4-vinylimidazolium with ethyl vinyl ether

A solution of monomer **(14)** in ethanol (7mL) at 0°C was charged to a polymerization tube. AIBN (0.04g) was dissolved in cold ethyl vinyl ether (0.66g, 9.11mmole, about 3.5mL) and this

solution was added to the ethanol solution of monomer (14). The resulting reaction mixture was degassed in three free-and-thaw cycles. The polymerization tube was sealed and. was immersed in water bath (65˚C) for overnight. The resulting polymer solution was only slightly viscous. A brittle brownish colored solid was isolated by precipitation in t-butyl methyl ether. Yield=0.35g

Copolymerization of 1-ethyl-3-methyl-4-vinylimidazolium with n-butyl acrylate

0.72g (2.5mmol) of monomer (14) and 0.64g (5mmol, 0.71mL) of n-butyl acrylate were dissolved into 7mL of ethyl acetate together with 0.013g of AIBN. The solution was charged into a polymerization tube and degassed in three freeze-and-thaw cycles. The tube was sealed and immersed in water bath (65˚C) for overnight. The polymer solution was precipitated in t-butyl methyl ether to yield a white solid. M_n = 37,000 g/mol, M_w = 80,000 g/mol, PD = 2.15.

Chapter 5 Thermal Properties of Imidazole Polymers Derived from Ionic Liquid 4-vinylimidazolium Monomers

5.1 The Glass Transition in Ionic Polymers

It is often said that the glass transition in polymeric liquids is a poorly understood phenomenon. This is particularly true for ionic polymers whose glass transition characteristics have received only limited attention since the early analysis by Eisenberg *et al*. [79] in which the glass transition of ionic polymers was found to be proportional to the ratio of the counter ion charge, *q*, to the distance between the centers of cations and anions, *a*. Following on the work of Eisenberg, Tsutsui and Tanaka [80] reported that the glass transition temperatures of ionic polymers could be correlated with cohesive energy density,

$$CED_{ionic} = N_A e^2 \left(\frac{\rho}{M} \frac{q_c}{a} \right) \qquad \text{Equation 5.1}$$

in accordance with Equation 5.1

$$T_g = K_1 \left(N_A e^2 \left(\frac{\rho}{M} \frac{q_c}{a} \right) \right)^n \qquad \text{Equation 5.2}$$

where N_A is Avogadro's number, e is the electronic charge, ρ is the polymer density, M is the molecular weight per skeletal ion, and a is the equilibrium distance between the center of the anion and the cation. Equation 5.2 shows that the glass transition temperature is approximately equal to the cohesive energy density multiplied by a coefficient, K_1. The coefficient varies from polymer to polymer; and, in keeping with the analysis by Eisenberg, the glass transition temperature is predicted to be inversely proportional to the distance between the anion and the cation. Upon approaching the glass transition temperature, segmental relaxation slows down by

many orders. To quantify the steepness of the temperature dependence of the segmental relaxation time, τ_α, close to T_g, Angell [81] introduced a fragility parameter, *m*, that characterizes the deviation of the temperature dependence of τ_α from Arrhenius behavior.

$$m = \left. \frac{d\log\tau_\alpha}{d\frac{T_g}{T}} \right|_{T=T_g} \qquad \text{Equation 5.3}$$

Systems that have highly non-Arrhenius temperature dependence of τ_α with steep variations close to T_g are called "fragile", and the systems that show nearly Arrhenius dependence of τ_α are called "strong". Agapov has studied the effect of polar interactions on the temperature dependence of structural (segmental) and chain dynamics in polymeric liquids [82]. The glass transition temperature, T_g, and fragility index, *m*, were found to depend on the monomer's polarity and the relative position of the polar group. The effect of polar interactions on T_g and *m* was discussed in terms of a balance between changes in the cohesive energy and conformational rigidity.

5.2 Thermal Properties of Imidazolium-based poly(ionic liquid)

In this research, the thermal and dielectric properties of the family of 4-vinyl- imidazolium polymers has been examined. As compared to the more widely studied 1-vinylimidazolium polymers [71-73], the pendant imidazolium group in 4-vinylimidazolium polymers exhibits additional degrees of freedom, increased free volume and enhanced lateral overlap between proximate imidazole residues that may be situated 1,3 or 1,5 with respect to each other on the carbon chain. Moreover, increased degrees of freedom and greater asymmetry may allow for greater free volume and greater ability for the

imidazolium moiety to interact cooperatively in the transport of target ions. **Figure 18** displays a pentad of a poly(1-ethyl-3-methyl-4-vinylimidazolium salt) in which the counterion is sandwiched between pendant functional moieties positioned 1,3 on the polymer backbone.

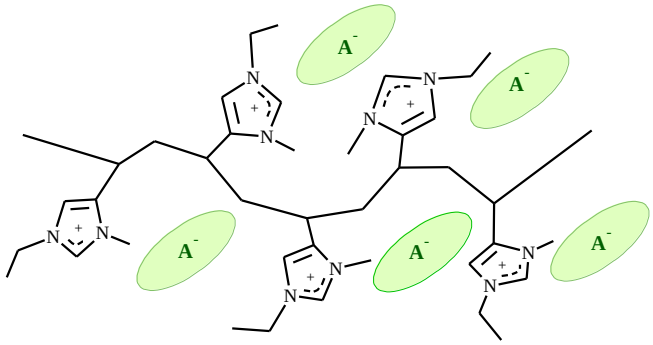

Figure 18 Pentad segment of the 1-ethyl-3-methyl-4-vinylimidazolium polymer

The cylindrical volume displaced by a rotating imidazolium group tethered to the polymer backbone at the 4 and 1 positions of the imidazolium ring and the bonds around which rotation is possible are depicted in Figure 19.

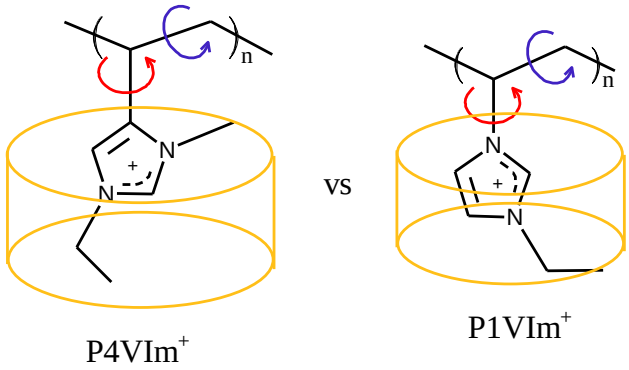

Figure 19 Asymmetry and rotational degrees of freedom in P4VIm+ and P1VIm+

In 1-vinyl- and 4-vinylimidazoliuim polymers, the hydrogen at the 2-position of the imidazole ring is somewhat acidic (pKa 21-23) [83], [84]. This acidic character can be the source of chemical and electrochemical instability. [85] In 2-methyl imidazolium moieties, this

problem is mitigated. [86] The present research is specifically concerned with the synthesis and polymerization, of 1-ethyl-3-methyl-4-vinylimidazolium and 1-butyl-2,3-dimethyl-4-vinylimidazolium triflates and the thermal and dielectric properties of polymers derived therefrom. (See **Figure 20**.)

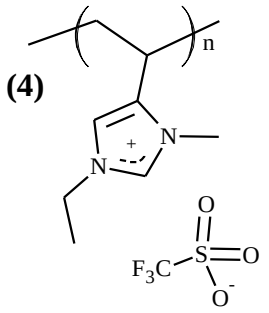

Poly(1-ethyl-3-methyl-4-vinylimidazolium triflate

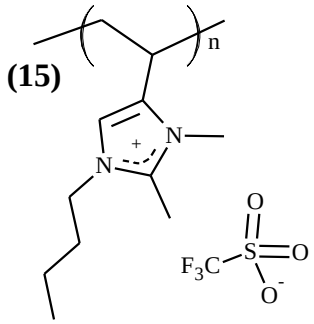

Poly(1-butyl-2,3-dimethyl-4-vinylimidazolium triflate

Figure 20 Structures of poly(1-ethyl-3-methyl-4-vinylimidazolium triflate) and poly(1-butyl-2,3-dimethyl-4-vinylimidazolium triflate)

5.2.1 Differential Scanning Calorimetry (DSC)

DSC thermograms were obtained under nitrogen using a TA Instruments DSC Q100 equipped with a liquid-nitrogen cooling system. All samples were prepared in an Ar-filled, Vacuum Atmospheres glove box. Polymer samples were placed in an open, hermetically-sealable, aluminum pan and heated to 100^{o}C for 15 minutes on the surface of a digital hot plate in the glove box. The aluminum pan was then capped and sealed. In the DSC, samples were ramped to 200^{o}C then cooled to -50^{o}C at a rate of 20^{o}C/min. Each sample was held at -50^{o}C and 200^{o}C, respectively, for 1 minute in between each heating and cooling cycle. T_g values are reported as midpoint glass transition temperatures, T_g-mid. The analysis was a 7-step process: (1) heating from 22^{o}C to 200^{o}C at 20^{o}C/min; (2) holding for 1 minute at 200 °C; (3) cooling from 200 to-50^{o}C at 20^{o}C/min; (4) holding for 1 minute at -50^{o}C; (5) heating from

-50ºC to 200ºC at 20ºC/min; (6) holding for 1 minute at 200 °C, and; (7) cooling from 200ºC to -50ºC at 20ºC/min. Steps 5-7 represent the first heating/cooling cycle. Each sample was subjected to at least three heating/cooling cycles with the requirement that the second and third heating cycles overlay each other. Correspondence in heating cycle and cooling cycle heat capacity changes were generally required to validate a heat capacity change as a glass transition. Additional validation was garnered by way of a final heating cycle from -50 to 200 °C, heating at 40 °C per minute. (*At increased heating rates, heating cycle heat capacity changes associated with the glass transition will be amplified and shifted to a somewhat higher temperature.)* It cannot be emphasized too strongly that obtaining accurate, repeatable, measures of the glass transition in poly(ionic liquid) 1-vinyl- and 4-vinylimidazolium salts requires substantial diligence and care.

5.2.2 Comparative Thermal Characteristics of Poly(1-ethyl-3-vinylimidazolium) and Poly(1-ethyl-3-methyl-4-vinylimidazolium) salts

The glass transition in 4-vinyl- and 1-vinylimidazolium polymers was evaluated, as described above. The results of the comparative DSC analysis of the glass transition temperatures of a set of ion-exchanged 4-vinylimidazolium polymers and 1-vinylimidazolium polymers are presented in Table I where heating-cycle and cooling-cycle glass transition values are tabulated. Cooling cycle T_g-mid values are somewhat lower than the heating cycle T_g-mid values. This may be a result of a longer time constant for the reformation of the glass, which results in a heat capacity change over broader temperature range in the cooling cycle [87]. **Figure 21** displays the second heating cycle and subsequent cooling cycle in the DSC thermogram for P4VIm$^+$TFSI$^-$. The thermogram is typical of those observed across the series

of poly(4-vinylimidazolium salts). DSC thermograms for all P4VIm$^+$ salts are displayed in the Appendix.

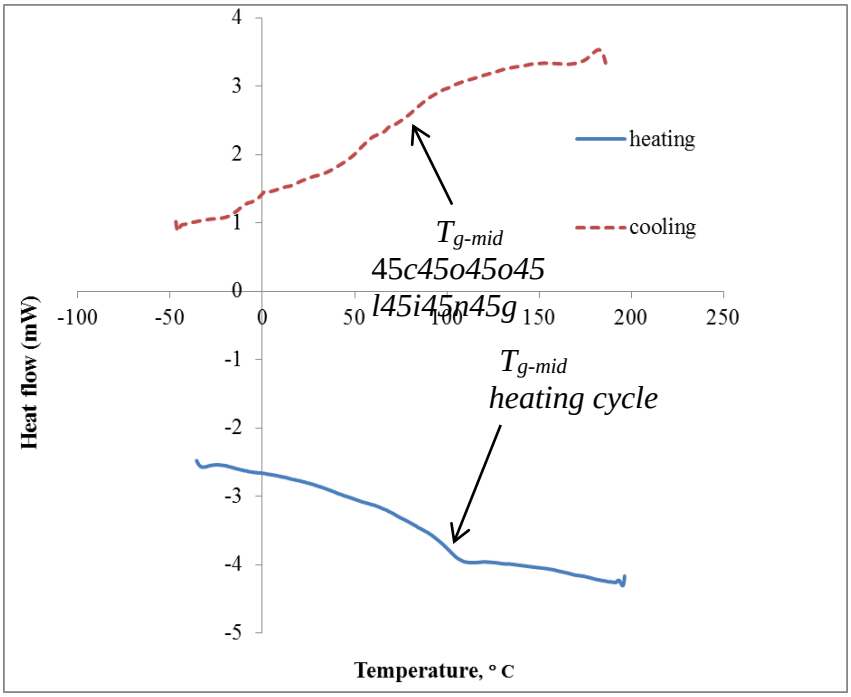

Figure 21 DSC scans of P4VIm+TFSI− during heating and subsequent cooling.

The correspondence of heating-cycle and cooling-cycle data provides significant support for the validity of the reported T_g values. Tetrafluoroborate, BF_4^-, hexafluorophosphate, PF_6^-, and hexafluoroarsenate, AsF_6^-, comprise a set of complex fluoride anions of increasing size. In the 1-ethyl-3-methyl-4-vinylimidazolum polymer set, the heating cycle T_g-mid increased from 186°C to 200°C and 213°C when the polymer was ion-exchanged to BF_4^-, PF_6^- and AsF_6^-, respectively. This result cannot be rationalized on the basis of the change in the ratio of the counter-ion charge, *q*, to the distance between the centers of cations and anions, *a*. Enhanced intersegmental and intramolecular interactions (bridging, by the anion, between imidazolium

moieties position 1,3 or 1,5 along the polymer chain) is likely to be the dominant factor governing the T_g increase in this series.

The 4-vinylimidazolium polymers with $TFSI^-$ and $C_2N_3^-$ anions exhibit the lowest glass transition temperatures. The lower glass transition temperatures of these two polymers may be a result of plasticization by large solvating anions, which, because of their soft nucleophilic character, allows for association between anion and cation over a larger distance.

Table 1 - Glass transition temperatures of poly(imidazolium salts)

	P4VIm$^+$ Salts		P1VIm$^+$ Salts	
Anion	Heating cycle T_g – mid (℃)	Cooling cycle T_g – mid (℃)	Heating cycle T_g – mid (℃)	Cooling cycle T_g – mid (℃)
BF_4^-	186	178	106	97
PF_6^-	200	180	141	113
AsF_6^-	213	208	122	-----
$CF_3SO_3^-$	153	140	140	124
$(CF_3SO_2)_2N^-$	88	63	97	74
$C_2N_3^-$	89	103	105	95

As a complement to our studies of poly(1-ethyl-3-methyl-4-vinylimidazolium salts), the glass transition characteristics of corresponding poly(1-vinylimidazolium salts), IUPAC or CAS identity being poly(1-ethyl-3-vinylimidazolium), were also evaluated. Table 1 displays the results. Heat capacity changes in the cooling cycle, consistent with the heating cycle glass transition temperatures, were observed in the BF_4^-, PF_6^-, $CF_3SO_3^-$, $TFSI^-$

and $C_2N_3^-$. In the AsF_6^- salt of the 1-ethyl-3-vinylimidazolium polymer, a heat capacity change that can be attributed to the glass transition was not observed in the cooling cycle.

The first difference of note between the glass transition characteristics of the 1-vinyl- and 4-vinylimidazolium polymers is that, in spite of the greater free volume required for the 1-ethyl-3-methyl-4-vinylimidazolium moiety, the glass transition temperatures of the 4-vinylimidazolium BF_4^-, PF_6^-, AsF_6^- and $CF_3SO_3^-$ salts are higher than those of the corresponding 1-vinylimidazolium salts. Another difference of note is that, in the 1-vinylimidazolium polymer set, the glass transition of the BF_4^-, PF_6^-, AsF_6^- series does not increase monotonically with increase of anion size. Instead, while the glass transition in this series of non-nucleophilic complex fluoride anions increases significantly in going from the BF_4^- salt to the PF_6^- salt, the T_g of the AsF_6^- salt is dramatically lower than that of the PF_6^- salt. This difference, no doubt, results from the fact that lateral overlap of imidazolium moieties is greater in the 4-vinylimidazolium polymer family and lesser in the 1-vinylimidazolium polymer family. Comparing the PF_6^- and AsF_6^- salts of the 1-vinylimidazolium polymer one sees the expected decrease in T_g with increasing anion size.

The glass transition temperatures of the $TFSI^-$ and dicyanamide, $C_2N_3^-$, derivatives of the 1-vinylimidazolium polymer are slightly higher than those for the corresponding 4-vinylimidazolium salts. As with the $TFSI^-$ and $C_2N_3^-$ salts of the 4-vinylimidazolium polymers, the 1-vinylimidazolium salts with soft, polarizable $TFSI^-$ and $C_2N_3^-$ anions exhibit the lowest glass transition temperatures.

Thermal gravimetric analysis of 4-vinyl- and 1-vinylimidazolium polymers

The comparative thermal gravimetric analysis (TGA) of the triflate polymers, presented in Figure 22, show that the 4-vinyl imidazolium polymer has greater thermal stability than the

1-vinylimidazolium polymer. The TGA results that were obtained in the present research for poly(1-ethyl-3-vinylimidazolium triflate), P1VIm$^{+}CF_3SO_3^{-}$, correspond well with those published by Marcilla *et al.* [88] Under nitrogen, P1VIm$^{+}CF_3SO_3^{-}$ suffers extensive mass loss at 400^{o}C to 448^{o}C. Significant mass loss in poly(1-ethyl-3-methyl-4-vinylimidazolium triflate), P4VIm$^{+}CF_3SO_3^{-}$, occurs in the 467^{o}C to 527^{o}C temperature range. The increased thermal stability is apparently due to the difference in the tethering point of the imidazolium ring to the polymer back-bone. The energy required to break the carbon-carbon bond is some 40 kJ/mol [89] greater than that required to break a carbon-nitrogen single bond. The modest reduction in mass below 400°C is due to loss of absorbed moisture.

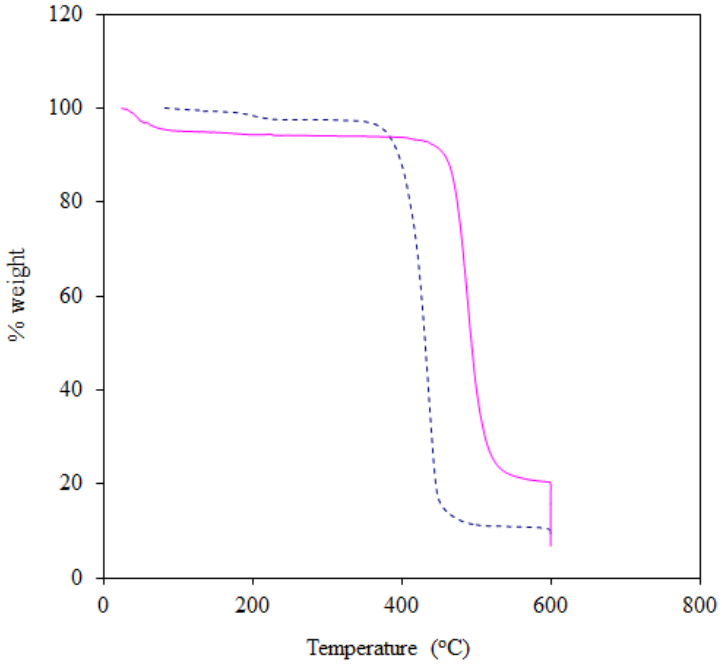

Figure 22 TGA of P1VIm+CF3SO3− [dashed blue line], and P4VIm+CF3SO3− [solid violet line].

5.2.3 Thermal Characteristics of Poly(1-butyl-2,3dimethyl-4-vinylimidazolium salts)

Glass transition characteristics of poly(1-butyl-2,3dimethyl-4-vinylimidazolium^{+}) Tf^{-}, PF_6^{-}, and $TFSI^{-}$ salts were also evaluated by differential scanning calorimetry. Second cycle DSC thermograms for the triflate polymer are shown in Figure 23 where plots of change in heat capacity in 20°C/min heating and cooling cycles are shown. An auxiliary 40°C/min rapid heating cycle, that served to validate the change in heat capacity as the glass transition [87], is included in the figure. Comparative TGA plots of poly(1-butyl-2,3-dimethyl-4-vinylimidazolium triflate) and poly(1-butyl-2,3-dimethyl-4-vinylimidazolium TFSI) and DSC thermograms for all poly(1-butyl-2,3-dimethyl-4-vinylimidazolium salts) are provided in the appendix.

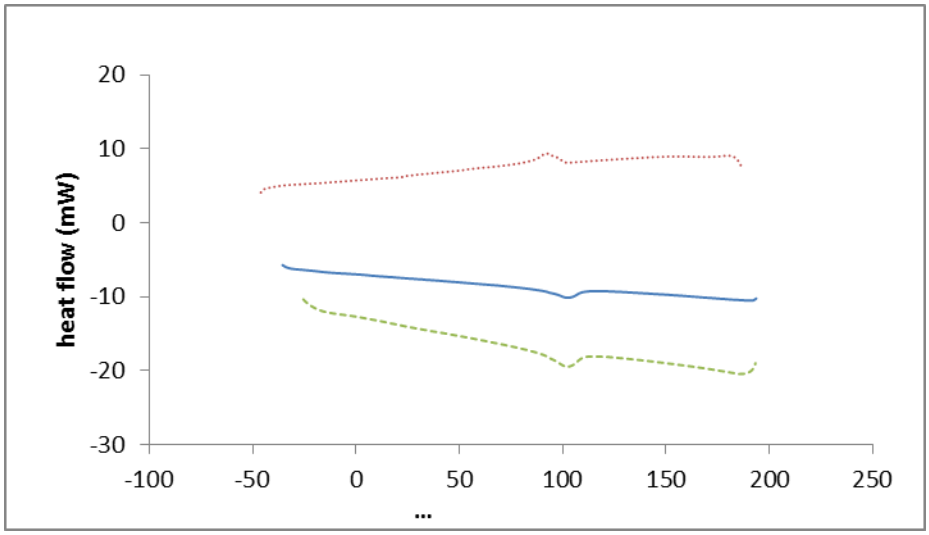

Figure 23 DSC scans for P23DMVIm+Tf −: solid blue line (20°C/min – heating cycle), dotted red line (20°C/min – cooling cycle), dashed green line (40°C/min – rapid heating cycle).

The appearance of the thermograms for P23DMVIm^{+}Tf $^{-}$, PF_6^{-}, and $TFSI^{-}$ are similar to each other with the heat capacity change around glass transition temperature for all salts in this group of 2-methyl imidazolium polymers exhibiting an unexpected “excess enthalpy” peak

often seen in aged polymer glasses [90]. The excess enthalpy peak in aged glasses is a result of densification of the glass. Extremely rapid aging of the 2-substituted imidazolium polymers is unexpected and one might speculate that it is related to the ionic liquid character of these polymers and the greater separation between the anion and cation in the 2-substituted polymer set. In the heating cycle, the mid and peak glass transition temperatures of the triflate salt are 98ºC, and 102ºC, respectively. At 99°C and 102°C, the mid and peak glass transition temperatures of the trifluoromethylsulfonylimide salt are virtually identical to those of the triflate salt. The heating cycle mid and peak glass transition temperatures for the hexafluorophosphate salt are only 84ºC and 90ºC, respectively. The glass transition temperatures of all three polymers are thus very close to each other. In light of the substantial differences in the glass transition temperatures of the corresponding $P4VIm^+$ salts, the proximity in the glass transition temperatures of the poly(1-butyl-2,3-dimethyl-4-vinylimidazolium) salts is particularly surprising. For comparison, the mid-point glass transition temperatures of 1-ethyl-3-methyl-4-vinylimidazolium polymers and 1-butyl-2,3-dimethyl-4-vinylimidazolium polymers are displayed in Table 2.

Table 2 - Comparative Tg of poly(1-butyl-2,3-dimethyl-4-vinylimidazolium) and poly(1-ethyl-3-methyl-4-vinylimidazolium) salts

Polymer composition	Triflate		$TFSI^-$		PF_6^-	
	$P23D4VIm^+$	$P4VIm^+$	$P23D4VIm^+$	$P4VIm^+$	$P23D4VIm^+$	$P4VIm^+$
Heating cycle mid-point Tg	98°C	153°C	99°C	88°C	84°C	200°C

As shown in Table 2, the glass transition temperatures for the $P4VIm^+$ salts vary from 88ºC for the $TFSI^-$ salt to 200ºC for the PF_6^- salt. Those for $P23D4VIm^+$ salts are between 84°C

and 98°C. In the case of PF_6^- and triflate, the glass transition temperatures for the 2-methylimidazolium polymer salts are substantially lower than those for the corresponding 4-vinylimidazolium polymers. In the case of the $TFSI^-$ salts, the T_g for the two polymers are similar. The $TFSI^-$ anion is the largest in the set and it is likely that the glass transition in both imidazolium $TFSI^-$ polymers is not elevated by attractive forces between the anion and cation.

Given no other molecular factors, it might be expected that, in accordance with historic analyses by Eisenberg [79] and Tsutsui and Tanaka [80], the glass transition temperature of an ionic polymer would be determined, as delineated in Equation 5.2, by the separation between the ionic moieties on the polymer and its counterion. The imidazolium polymers with a methyl group at the 2 position of the imidazolium ring, may force steric separation of the cation and anion to a degree that dramatically diminishes the contribution of counterion size to the equilibrium distance between the center of the anion and cation. Indeed the separation may be large enough that the onset of motion of the polymer backbone is decoupled from counterion motion. Figure 24 shows space-filling molecular renderings, created with ChemSketch-3D, of 1-butyl-2,3-dimethyl-4-vinylimidazolium triflate (B) and 1-ethyl-3-methyl-4-vinylimidazolium triflate polymer triads (A), wherein the position of the triflate anion relative to the 2-position of the imidazolium ring is depicted.

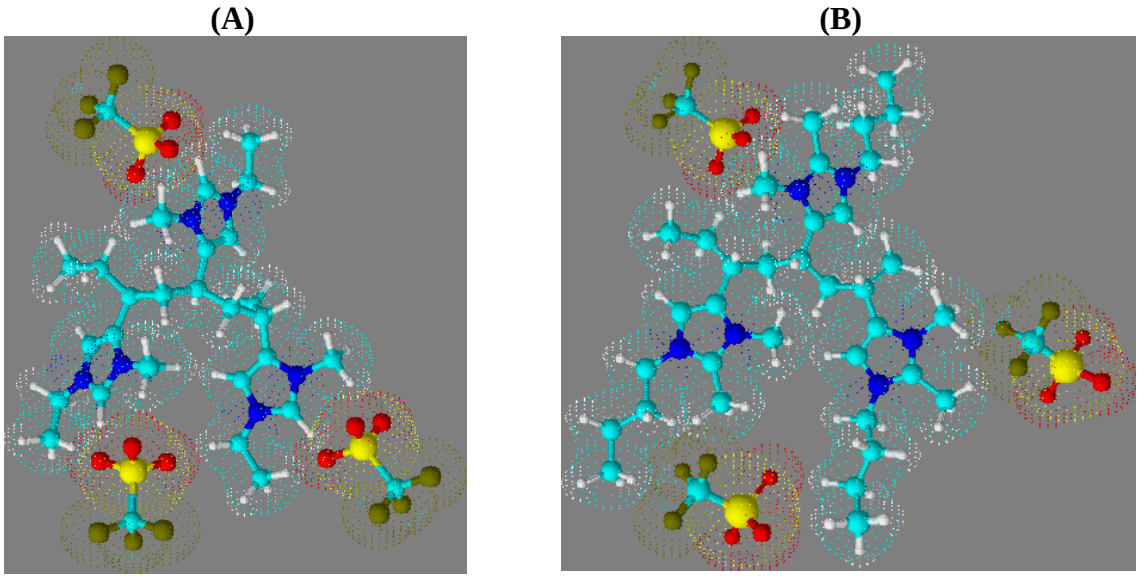

Figure 24 Space-filling molecular renderings of (A) 1-ethyl-3-methyl-4-vinylimidazolium triflate and (B) 1-butyl-2,3-dimethyl-4-vinylimidazolium triflate and polymer triads

While the proximity of the triflate anion to the imidazolium group is hindered in both triads, it is apparent that the 2-methyl substituent in P23D4VIm$^+$ forces the triflate anion to be further removed from imidazolium moiety. It may thus be reasonable to attribute the invariance in the glass transition of P23D4VIm$^+$ with different anions to steric separation enforced by having substituents on the 1, 2, 3, and 4 positions of the imidazolium moiety.

Chapter 6 Dielectric Properties of Imidazole Polymers Derived from Ionic Liquid 4-vinylimidazolium Monomers

Dielectric spectroscopy provides simultaneous measurements of dc conductivity and molecular relaxation modes. In broadband dielectric spectroscopy, the dipole moments of different materials can be observed at different frequencies. Molecular relaxations of larger molecules can usually be observed at lower frequencies. In **Figure 25,** it can be seen that the materials involved in this project, polymers or macromolecules, fall into the frequency regime between 1Hz and 1MHz. In this frequency regime different types of relaxation modes can be observed and these relaxation modes give us information on different properties of the materials tested.

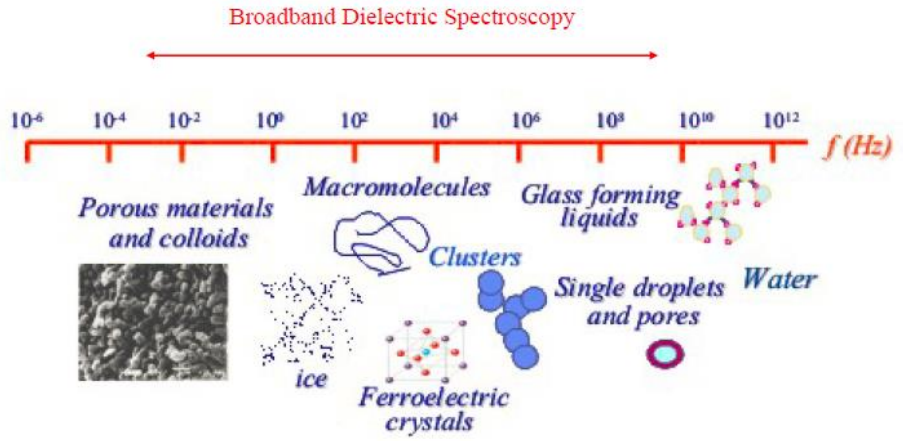

Figure 25 Frequency distribution for different types of molecules in Broadband Dielectric Spectroscopy

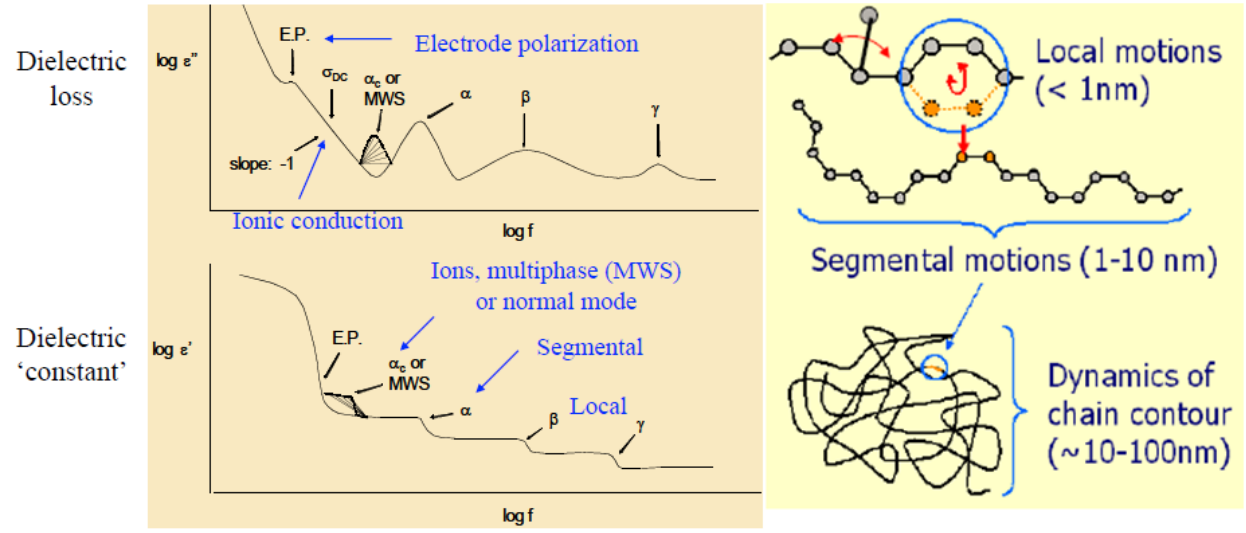

Figure 26 Different types of dipole relaxations in dielectric spectroscopy of polymers

In **Figure 26**, the relaxation modes that appear at high frequency are local dipole motions, sometimes called β or γ relaxations. This type of dipole motion is related to the mechanical properties of the material. At lower frequency one may observe segmental relaxation or α relaxation. This type of relaxation is usually related to the dynamic glass transition process which reflects the movements of the polymer backbone or large side-groups. At even lower frequency one may also observe electrode polarization and ionic conductivity.

Nakamura *et al*. have studied the relaxation characteristics of poly(1-ethyl-3-vinyl imidazolium trifluoromethylsulfonimide) ($PNVIm^{+}TFSI^{-}$) in the frequency range of 10 mHz to 2 MHz, and the temperature range of -90 to 90°C by dielectric spectroscopy [91] and dynamic mechanical spectroscopy. [92] Three relaxation modes were observed and identified as β, α, and EP (electrode polarization). The β relaxation mode, which is observed at low temperature (-90 to 0°C), was attributed to rotation around the C-N bond that tethers the imidazolium moiety

to the polymer main chain. The α-relaxation was attributed to ion-pair motion (see **Figure 27**).

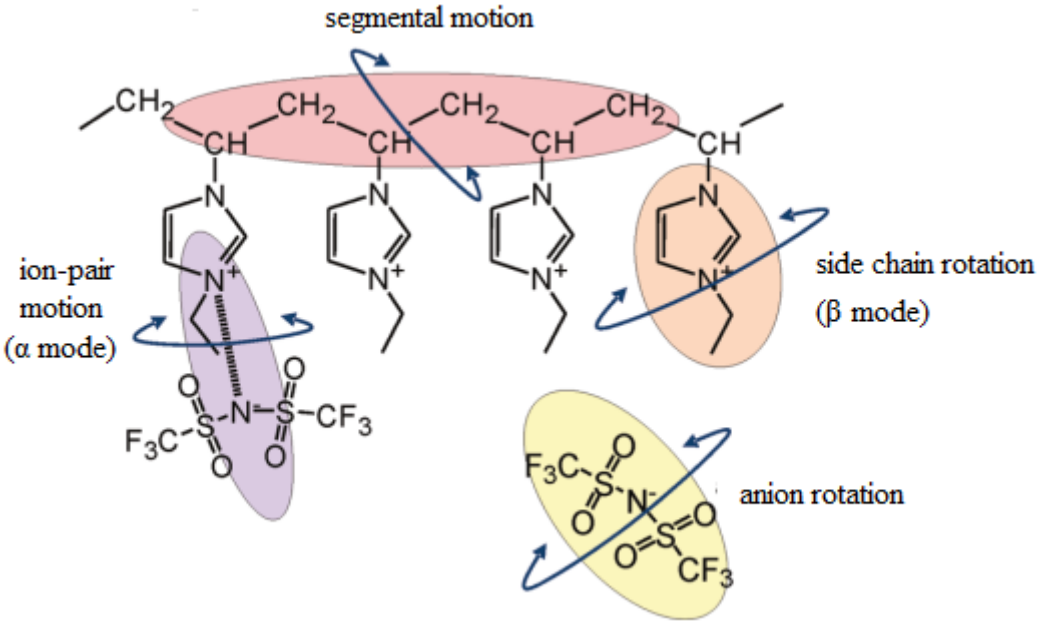

Figure 27 Relaxation modes for poly(1-ethyl-3-vinylimidazolium trifluoromethylsulfonimide) including ion-pair motion (α mode) , side-chain rotation (β mode) and segmental motion (not observed). Anion rotation was observed at very low temperature.

In a subsequent study of viscoelastic and dielectric relaxation behavior of poly(ionic liquids). [92] These workers reported on the influence of counterions on the dynamics of poly(1-butyl-3-vinylimidazolium) salts wherein the counterion was tetrafluoroborate (BF_4^-), hexafluorophosphate (PF_6^-), triflate (Tf^-), or bis(trifluoromethylsulfonylimide ($TFSI^-$). All poly(1-butyl-3-vinylimidazolium) salts also exhibited two dielectric relaxation modes. The faster mode derived from side chain rotation, and was independent of the nature of the anion and the glass transition, if X^- was not bulky. The slower mode reflected the lifetime of the ion pair formed between anion and the cation. Dielectric relaxation modes related to ion-pair

relaxation and rotational motions of the $TFSI^-$ anion were not observed. No relaxation modes were specifically associated with segmental motion of the imidazolium polymer chain.

In the present research, the dielectric relaxation behavior of a series of ionic liquid polymers derived from 1-ethyl-3-methyl-4-vinylimidazolium triflate [$P4VIm^+$ $CF_3SO_3^-$, $TFSI^-$, $C_2N_3^-$, BF_4^-, PF_6^-, and AsF_6^-]; 1-ethyl-3-vinylimidazolium triflate [$PNVIm^+$ $TFSI^-$, $C_2N_3^-$, and PF_6^-], and 1-butyl-2,3-dimethyl-4-vinylimidazolium triflate [$P2,3DM4VIm^+CF_3SO_3^-$, $TFSI^-$, and PF_6^-] have been evaluated in the frequency range of 20 Hz to $1x10^6$ Hz and the temperature range of 30-210°C. In three instances, [poly(1-ethyl-3-methyl-4-vinylimidazolium PF_6^-), poly(1-ethyl-3-vinylimidazolium PF_6^- and poly(1-ethyl-3-methyl-4-vinylimidazolium BF_4^-)] dipolar relaxations were analyzed by fitting the dielectric loss, ε'', using the Havriliak-Negami model, embodied in Equation 6.1, with $\Delta\varepsilon$, τ, β, γ, σ_0 and s as fitting parameters. **Figure 28** shows experimental ε" *vs* frequency data, the deconvoluted relaxation peaks, and the fit to Havriliak-Negami equation for poly(1-ethyl-3-methyl-4-vinylimidazolium PF_6^-) ($P4VIm^+PF_6^-$) at 90°C.

In order to find crucial information such as the position, shape and dielectric strength of a loss peak [93], [94], several model functions have been developed to characterize the dielectric spectroscopy of polymers. Using these methods, the measured information can be extracted and the physical properties of the tested polymer samples can be analyzed and compared with predictions. Moreover, separation and extraction of overlapping relaxation processes or conductivity contributions is possible. [95] Widely accepted model functions include Cole-Cole, [96] Cole-Davidson, [97], [98] and the Fuoss-Kirkwood-functions. [99] The most popular empirical model function is the Havriliak and Negami function, or HN-function [93], [100] which is defined in Equation 6.1:

$$\varepsilon^*_{HN}(\omega) - \varepsilon_\infty = \frac{\Delta\varepsilon}{(1 + (i\omega\tau_{HN})^{\beta_{HN}})^{\gamma_{HN}}} \qquad \text{Equation 6.1}$$

In Equation 6.1, β_{HN} and γ_{HN} are the fractional shape parameters, with $\beta_{HN} > 0$, and $\beta_{HN}\gamma_{HN} \leq 1$, due to the symmetric and asymmetric broadening of the loss peak. These two shape parameters are related to the slopes of $log(\varepsilon'')$ *versus* $log(\omega)$. τ_{HN} is defined as relaxation time, related to the peak frequency f_p and the shape parameters. [101]

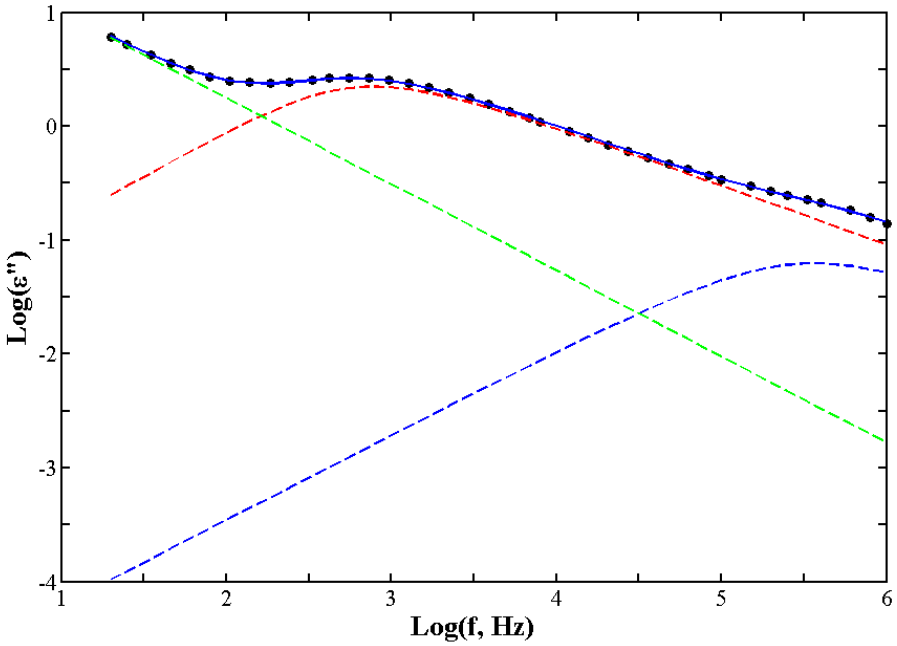

Figure 28 ε'' vs frequency for poly(1-ethyl-3-methyl-4-vinylimidazolium PF6-) at 90 °C. Points refer to measured data. Solid blue curve is the summation of individual fitted curves for the α' and α relaxations and dc conductivity reflecting the best fit to the data. Dashed red curve - deconvoluted α'-relaxation peak (Δε = 6.4, τ = 1.9×10-3 s, β= 0.83, γ = 0.6); dashed blue curve - deconvoluted α relaxation peak (Δε = 0.18, τ = 3.0×10-6 s, β = 0.74, γ= 0.86); dashed green line - dc conductivity (σ = 2.1×10-9 S/cm; s = 0.76).

The frequency of maximum loss, f_{max}, was most often evaluated directly from plots of tan δ (= ε''/ε') *vs* frequency. There was excellent correspondence between f_{max} values obtain from plots of tan δ *vs* frequency and f_{max} values obtained by fitting the dielectric loss, ε'', using the Havriliak-Negami model.

6.1 Comparison of dielectric characteristics of poly(ionic liquids) derived from 4-vinyl and N-vinylimidazolium polymers with no substitutent at the 2-position of the imidazolium ring

Figures 29 (a-f) display dielectric spectra (ε', ε" and tan δ versus frequency at 30 - 210°C) for P4VIm^{+}PF$_6^{-}$ and PNVIm^{+}PF$_6^{-}$. **Figures 29a** and **29b** show plots of dielectric constant, ε', *versus* frequency. Below 150°C, the dielectric constant in these two polymers is of the order of 70 and is substantially invariant with frequency. Above 110°C, the dielectric constant increases dramatically at frequencies below 10^5 Hz and is indicative of one or more relaxation processes. These relaxation processes are apparent in both the ε" and tan δ spectra, however, relaxation peaks are most clearly resolved in the tan δ spectra. In the ε" and tan δ spectra of PNVIm^{+}PF$_6^{-}$ (**Figures 29c and 29e**) one relaxation mode distinct from that for electrode polarization is observed in the temperature range of 30-130°C. The single peak in the dielectric spectra of the PNVIm^{+} PF$_6^{-}$ set may correspond to the relaxation that Nakamura assigned as the α–relaxation [91] in PNVIm^{+}TFSI^{-} and attributed to ion-pair motion. [96]

In the P4VIm^{+}PF6^{-} spectra set, (**Figure 29d and 29f**) two relaxation modes, distinct from that for electrode polarization, are apparent, the α-relaxation (observed in the 30-150°C temperature range) and a new relaxation peak (observed at lower frequency in the 130-210°C temperature range) that is labeled as α'.

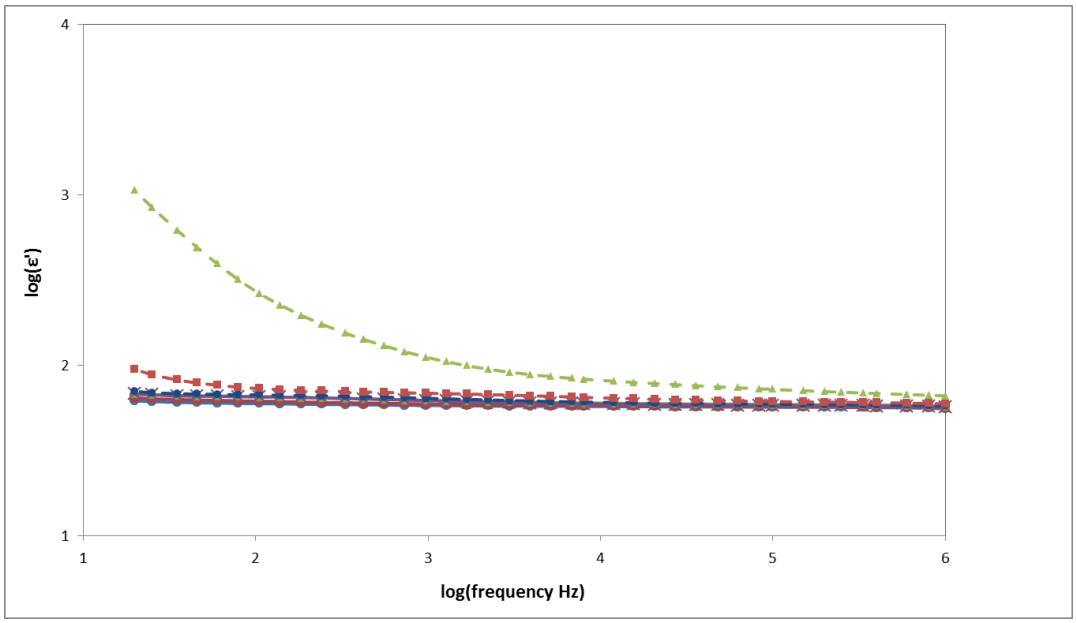

Figure 29(a) Frequency dependence of dielectric constant, ε', of PNVIm^{+}PF$_6^{-}$. [●–blue solid, 30°C; ■–red solid, 50°C; ▲–green solid, 70°C; ◆–black solid, 90°C; ●---blue dashed, 110°C; ■---red dashed, 130°C; ▲---green dashed, 150°C.

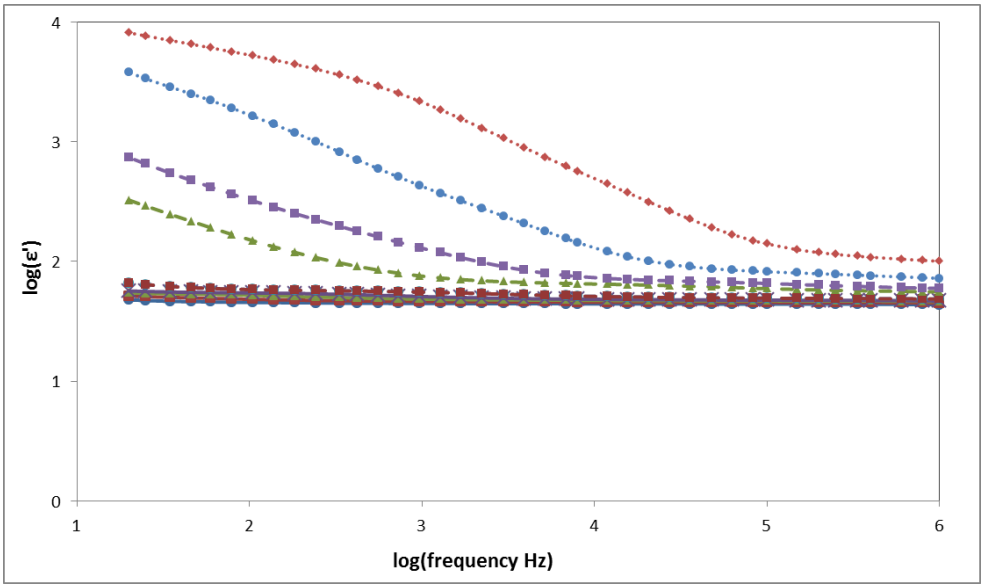

Figure 29(b) Frequency dependence of the dielectric constant, ε', of P4VIm^{+}PF$_6^{-}$. [●–blue solid, 30°C; ■–red solid, 50°C; ▲–green solid, 70°C; ◆–black solid, 90°C; ●---blue dashed, 110 °C; ■---red dashed, 130°C; ▲---green dashed, 150°C; ■---purple dashed, 170°C; ●···blue dotted, 190°C; ◆···orange dotted, 210°C.

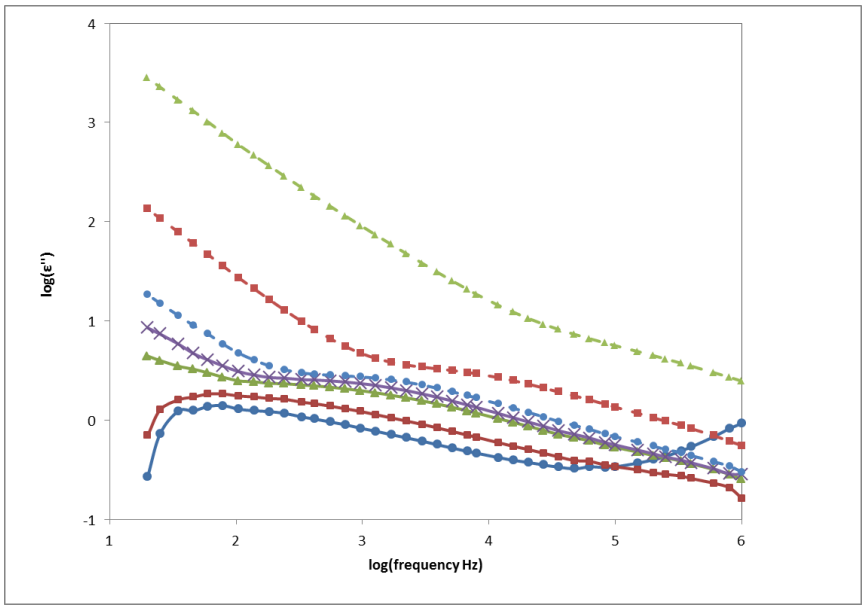

Figure 29(c) Frequency dependence of the dielectric loss, ε'', of $PNVIm^+PF_6^-$. [●–blue solid, 30°C; ■–red solid, 50°C; ▲–green solid, 70°C; ◆–black solid, 90°C; ●---blue dashed, 110°C; ■---red dashed, 130°C; ▲---green dashed, 150°C.

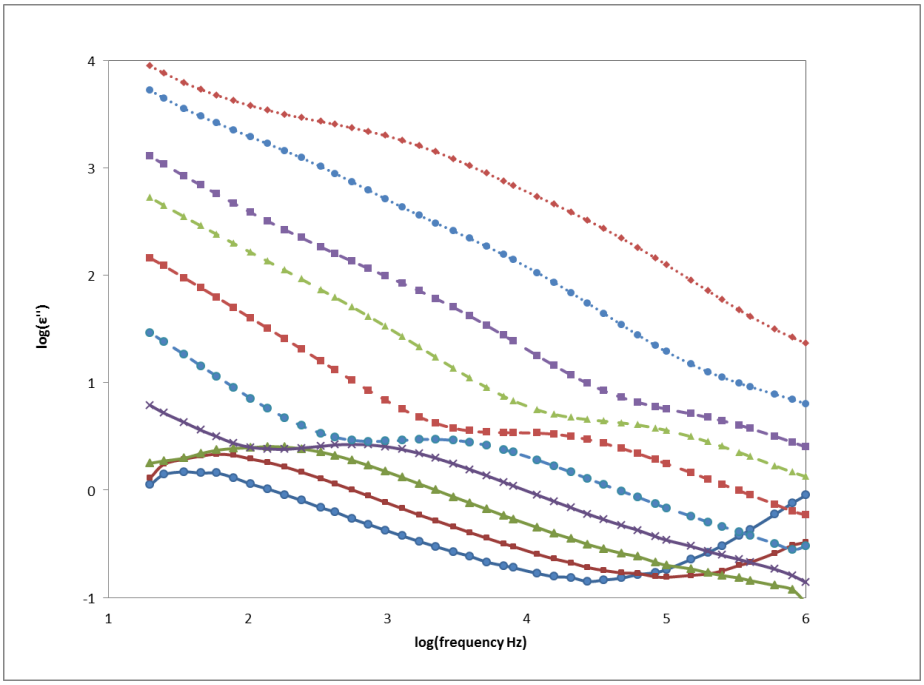

Figure 29(d) Frequency dependence of dielectric loss, ε'', of $P4VIm^+PF_6^-$. [●–blue solid, 30°C; ■–red solid, 50°C; ▲–green solid, 70°C; ◆–black solid, 90°C; ●---blue dashed, 110°C; ■---red dashed, 130 °C; ▲---green dashed, 150°C; ■---purple dashed, 170°C; ●···blue dotted, 190°C; ◆···orange dotted, 210°C.

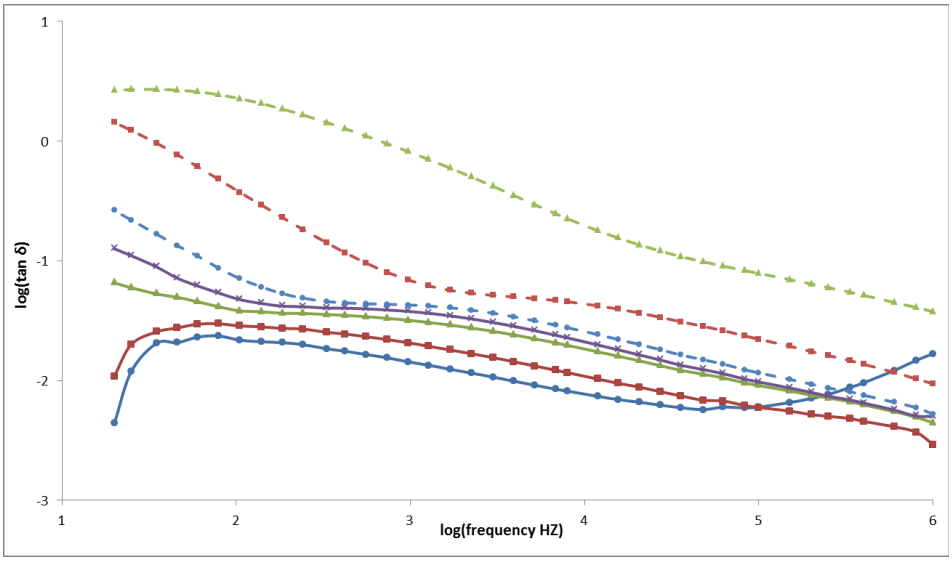

Figure 29(e) Frequency dependence of tan δ, of PNVIm^{+}PF$_6^{-}$. [●–blue solid, 30°C; ■–red solid, 50°C; ▲–green solid, 70°C; ◆–black solid, 90°C; ●---blue dashed, 110°C; ■---red dashed, 130°C; ▲---green dashed.

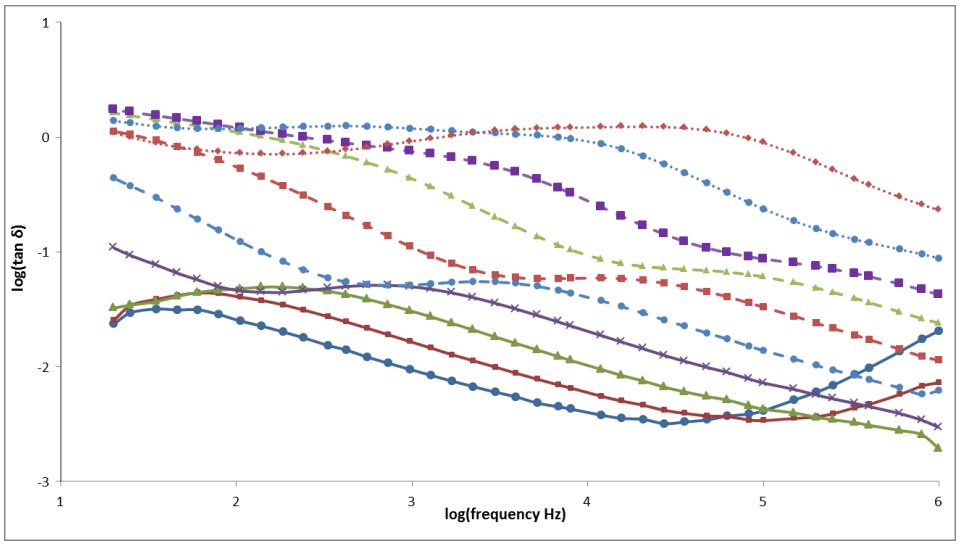

Figure 29(f) Frequency dependence of tan δ, of P4VIm^{+}PF$_6^{-}$. [●–blue solid, 30°C; ■–red solid, 50°C; ▲–green solid, 70°C; ◆–black solid, 90°C; ●---blue dashed, 110°C; ■---red dashed, 130°C; ▲---green dashed, 150°C; ■---purple dashed, 170 °C; ●···blue dotted, 190 °C; ◆···orange dotted, 210 °C.

Nakamura [91], [92] has clearly shown that there are additional β-relaxation modes in the lower temperature regime. In our work, the temperature range examined was 30-230°C, and the lower temperature β-relaxation modes were not accessible.

Because of its greater asymmetry and higher glass transition temperature, the α' relaxation is revealed in P4VIm$^+$PF$_6^-$ (but not in PNVIm$^+$PF$_6^-$). At the highest temperatures, 190°C and 210°C, the dielectric spectra of poly(4VIm$^+$PF$_6^-$) show a third peak at lower frequency (10^3-10^4 Hz) that, at this time, has neither been labeled, nor attributed to any specific relaxation phenomenon. P4VIm$^+$ polymers, whose glass transition temperatures are lower than that of P4VIm$^+$PF$_6^-$, do not show this third lower frequency peak.

Plots of tan δ *versus* frequency for P4VIm$^+$C$_2$N$_3^-$, P4VIm$^+$BF$_4^-$, P4VIm$^+$CF$_3$SO$_3^-$ and P4VIm$^+$TFSI$^-$ are displayed in **Figures 30, 31, 32 and 33**, respectively. Tan δ *versus* frequency plots for these poly(imidazolium) salts, are similar to that for the PF$_6^-$ salt in that α and α' relaxation peaks were generally observed.

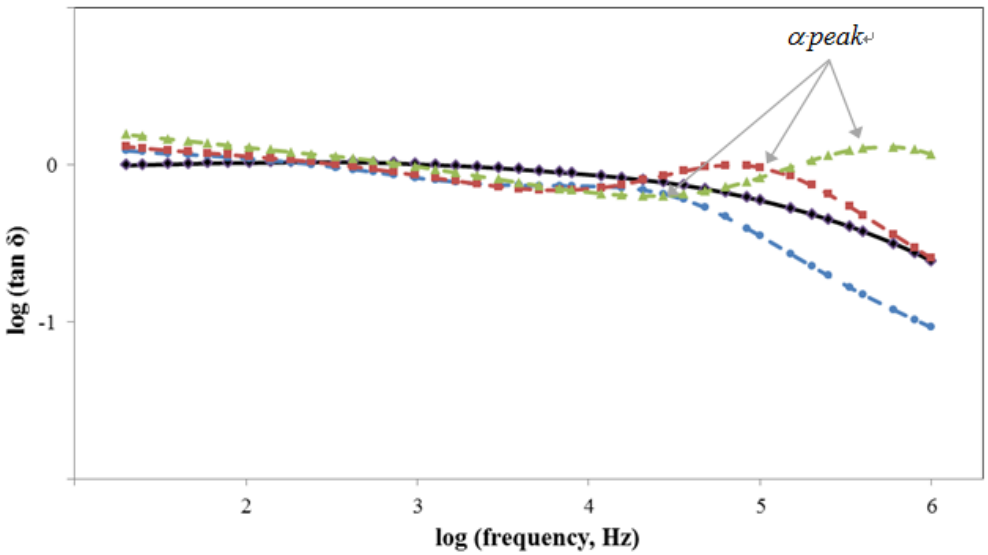

Figure 30 tan δ versus Frequency: P4VIm$^+$C$_2$N$_3^-$. [◆−black solid, 90 °C; ●---blue dashed, 110 °C; ■---red dashed, 130 °C; ▲---green dashed, 150 °C].

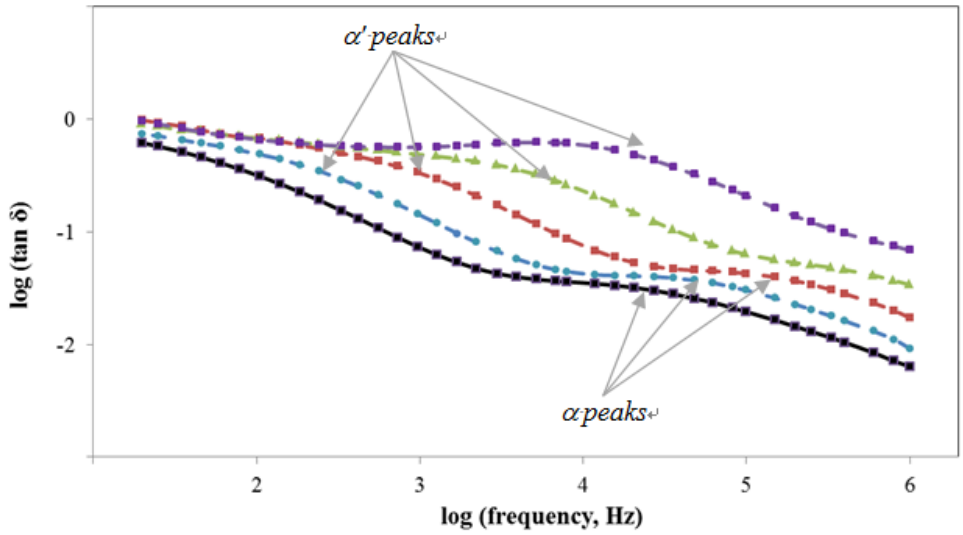

Figure 31 tan δ *versus* Frequency: P4VIm^{+}BF$_4^{-}$). [▪–black solid, 90 °C; ●–blue dashed, 110 °C; ▪---red dashed, 130 °C; ▲---green dashed, 150 °C; ▪---purple dashed, 170 °C].

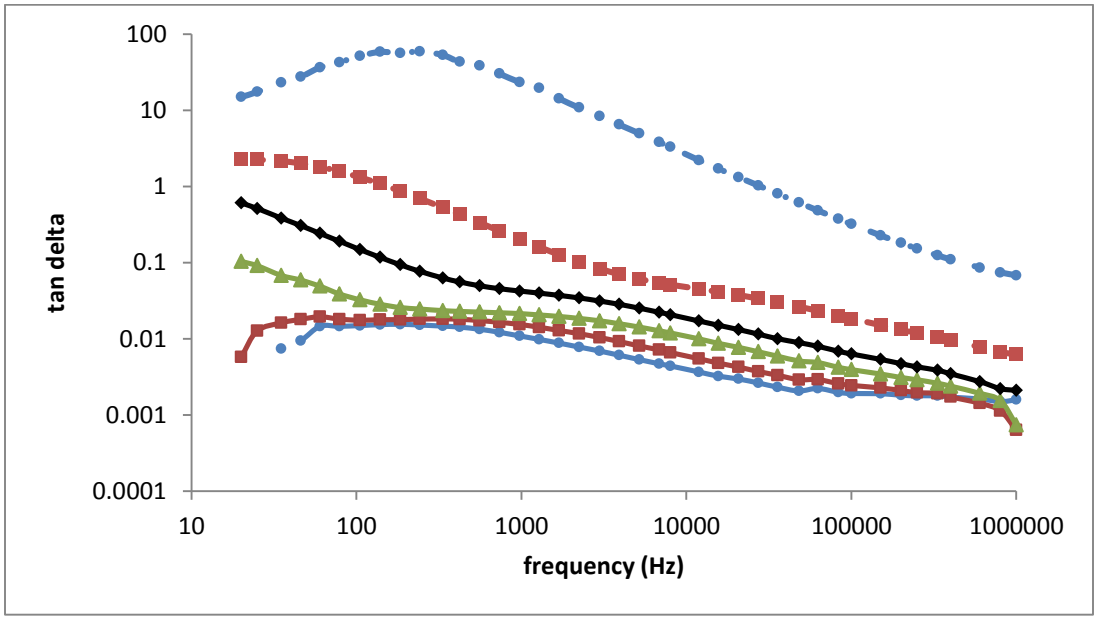

Figure 32 tan δ *versus* Frequency: P4VIm^{+} CF$_3$SO$_3^{-}$). [●–blue solid, 30 °C; ▪–red solid, 50 °C; ▲–green solid, 70 °C; ◆–black solid, 90 °C; ●---blue dashed, 110 °C; ▪---red dashed, 130 °C]

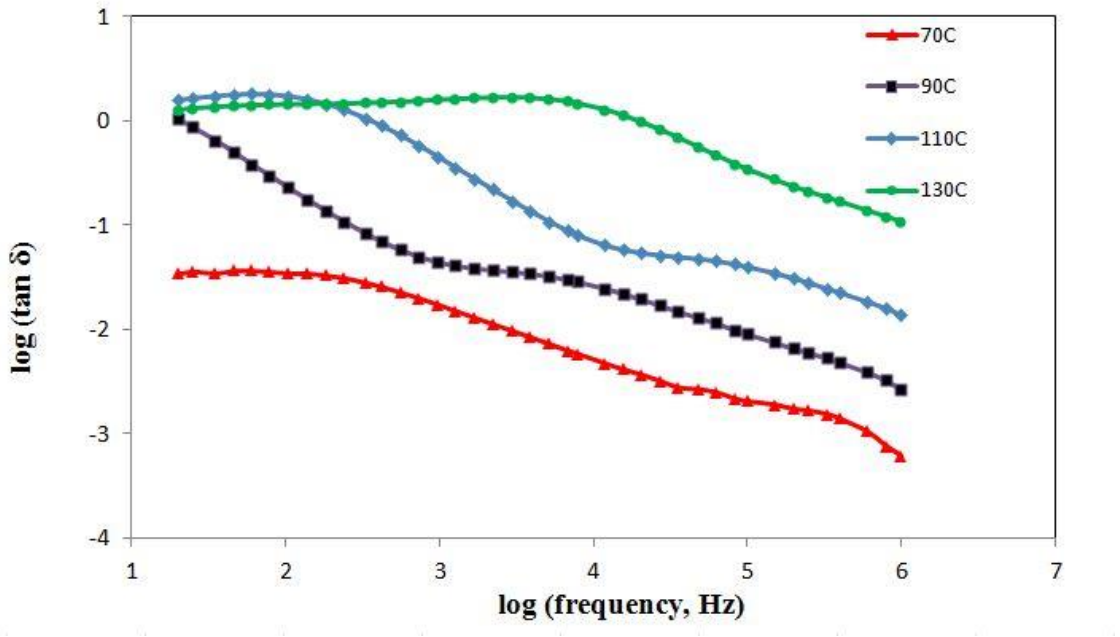

Figure 33 tan δ *versus* frequency, Poly(1-ethyl-3-methyl-4-vinyl-imidazolium TFSI). ▲– red line, 70°C ▪–Black line, 90°C; ◆–blue line 110°C; ●– green line, 130°C.

The anions that were employed differ in geometry and polarizability. The triflate salt is a classic semi-spherical "hard anion". TFSI and dicyanamide are soft, polarizable anions. Tetrafluoroborate, hexafluorophosphate and hexafluoroarsenate are a family non-nucleophilic complex anions derived from Lewis acids with increasing molecular volume.

In order to garner some insight into the nature of the relaxation peaks, an Arrhenius analysis was used as an approximation to allow an estimate of the activation energy to be made. The log of the maxima in each relaxation peak in the PF_6^- spectra were thus plotted against the reciprocal of the temperature, T, in kelvin. Arrhenius plots for the α-relaxation [observed in **Figure 29(b)** and **(e)**] and the α and α' relaxations [observed in **Figure 29(d)** and **(f)**] are presented in Figure **34(a) and (b)**. The plots displayed in **Figure 34(a)** and **(b)** include a least squares fit line that, over the modest temperature range (303-483 K) at which measurements were taken, is a surprisingly good fit to the data.

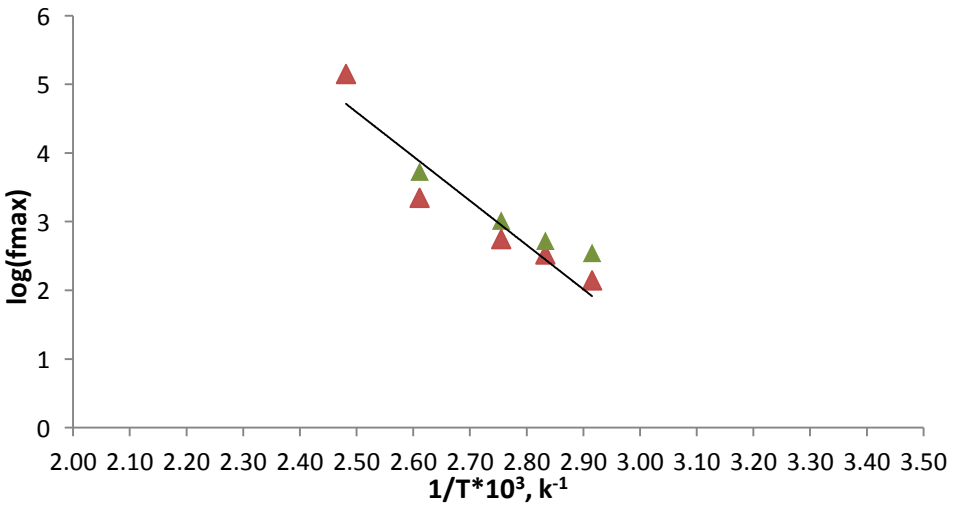

Figure 34 (a) Frequency-max *versus* 1/T (K): $PNVIm^{+}$ PF_6^{-} (▲, α-relaxation, data from tan δ plots; ▲, α-relaxation, data from deconvoluted ε'' vs frequency plots). Points refer to measured data. Lines are least squares fit to f_{max} data from deconvoluted ε'' plots.

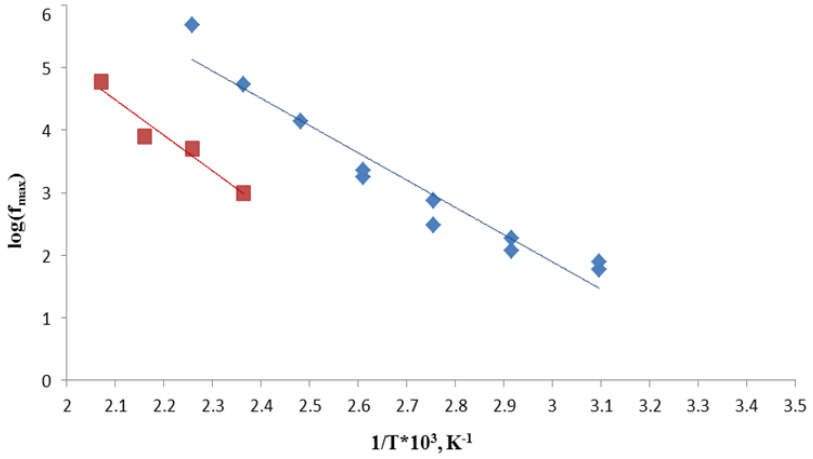

Figure 35 (b) Frequency-max *versus* 1/T (K): $P4VIm^{+}PF_6^{-}$ (◆, α-relaxation, from tan δ; ◆, α-relaxation, from deconvoluted ε''); $P4VIm^{+}PF_6^{-}$ (■, α'-relaxation, from tan δ). Points refer to measured data. Lines are least squares fit to f_{max} data from deconvoluted ε'' plots.

In a plot of tan δ *versus* temperature at a fixed frequency, the nature of a relaxation peak can sometimes be recognized by the temperature position of peaks. In **Figure 36**, two peaks can be

seen in the tan δ plot of poly(1-ethyl-3-methyl-4-vinylimidazolium PF_6^-) and poly(1-ethyl-3-methyl-4-vinylimidazolium $TFSI^-$) at 20Hz. At this frequency, the relaxation peaks can be associated with large-scale, segmental motions of polymer chains. The positions of these two relaxation peaks on the temperature axis match the DSC results shown in Table 2.

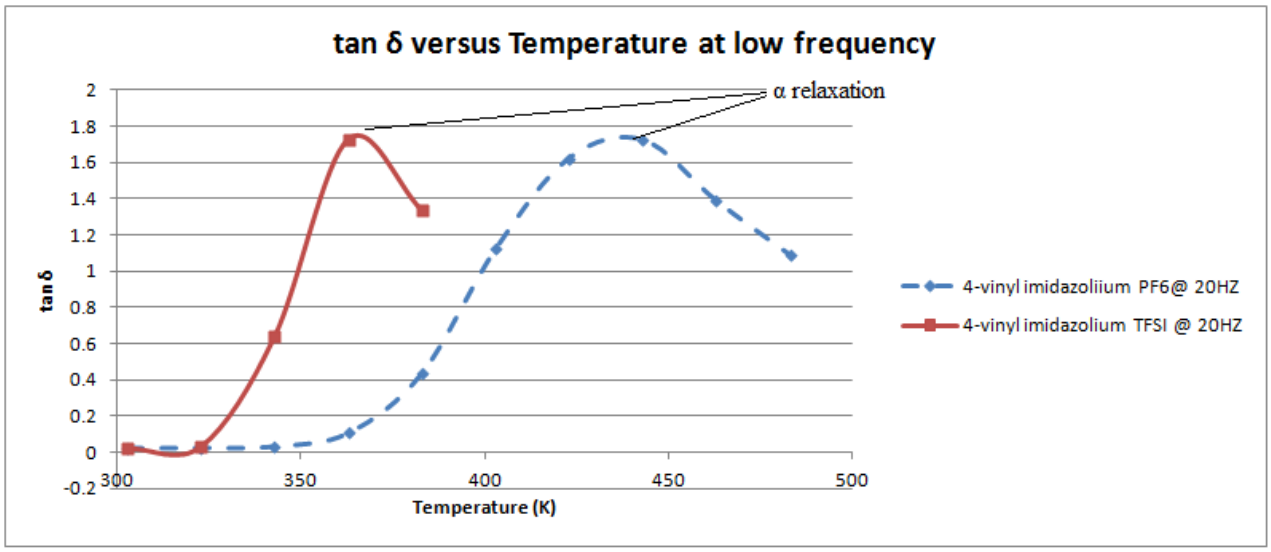

Figure 36 Tan δ versus temperature for poly(1-ethyl-3-methyl-4-vinylimidazolium PF_6^-) and Poly(1-ethyl-3-methyl-4-vinylimidazolium $TFSI^-$) at 20Hz.

Table 3 presents fitting parameters, $\Delta\varepsilon$ (dielectric strength) and σ_0 (dc conductivity), for the α and α' relaxations in $P4VIm^+PF_6^-$ and $P4VIm^+BF_4^-$. The high temperature, low frequency data may have large errors in the fit parameters because of the strong conduction effect and weak relaxation peak seen there. The α' relaxation is "stronger" than the α relaxation in both $P4VIm^+PF_6^-$ and $P4VIm^+BF_4^-$. The $\Delta\varepsilon$ values for α' increase with increasing temperature in both materials; however, the α process has a much weaker temperature dependence than α', especially in $P4VIm^+PF_6^-$. The conductivity increases with temperature by several orders of magnitude in $P4VIm^+PF_6^-$, but only slightly in $P4VIm^+ BF_4^-$. In both the α and α' relaxations, the relaxation

strength increases with temperature. The increase in relaxation strength with temperature for the α and α' relaxations, is not expected for a segmental mode relaxation. The conductivity increases with temperature by several orders of magnitude in P4VIm^{+}PF$_6^{-}$, but increases only slightly in P4VIm^{+} BF$_4^{-}$.

Table 3 - Temperature dependence of conductivity, σ_0, and relaxation strength, Δε, for the α and α' processes in P4VIm^{+}PF$_6^{-}$ and P4VIm^{+}BF$_4^{-}$.

Polymer	T (K)	Δε(α)	Δε(α')	σ_0 (S/cm)
4-vinyl PF_6	343	5.1	--	2.8 E-11
	363	5.7	--	9.9 E-10
	383	8.0	--	2.3 E-08
	403	7.3	--	6.1 E-08
	423	8.1	30	2.0 E-07
	443	7.1	74	4.0 E-07
	463	96	890	1.4 E-06
4-vinyl BF_4	363	2.4	--	8.1 E-09
	383	3.2	28	2.9 E-08
	403	2.8	46	4.7 E-08
	423	3.2	51	5.2 E-08
	443	4.8	92	7.1 E-08

Fragiadakis, et al. [102] studied a system of more conventional copolymer ionomers and report that large values of the dielectric increment may be associated with ion motion. Indeed, for the α' relaxation, $\Delta\varepsilon$ values range from 30-890 for P4VIm^{+}PF$_6^{-}$ and from 28-92 for P4VIm^{+}BF$_4^{-}$. Accordingly, the α and α' relaxations are attributed to ion-pair motion, with the onset of segmental motion perhaps being correlated with ion-pair motion. Plots of Δε *versus* temperature are shown in **Figure 37 (a)** and **(b)**. For both polymers, it can be seen from **Figure 37** that the relaxation strength Δε is higher for α' relaxations than that for α relaxations, indicating more intensive molecular motions. Additionally, in α' relaxations, the relaxation strength Δε appears to be flat until the temperature reaches 440K, then it increases abruptly.

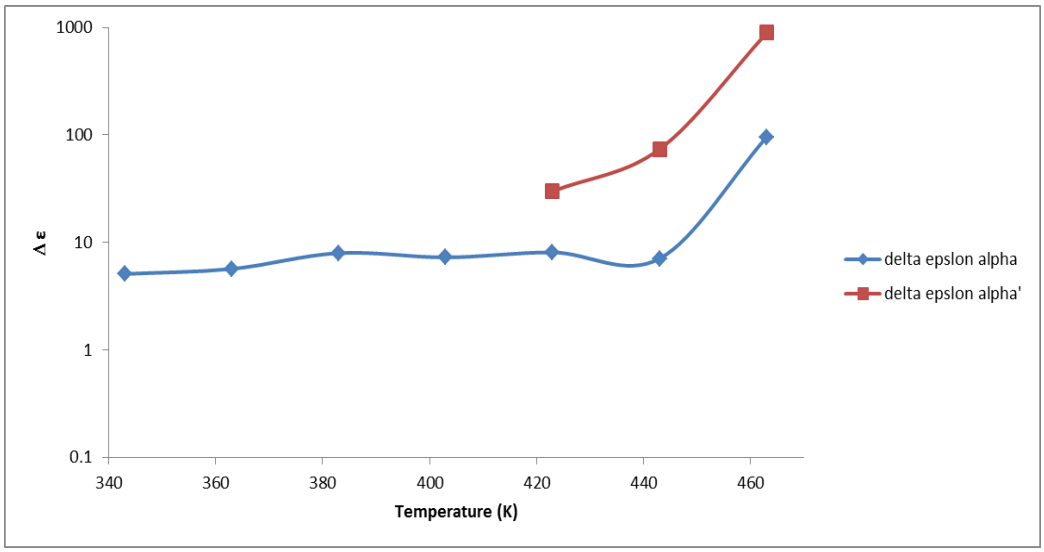

(a)

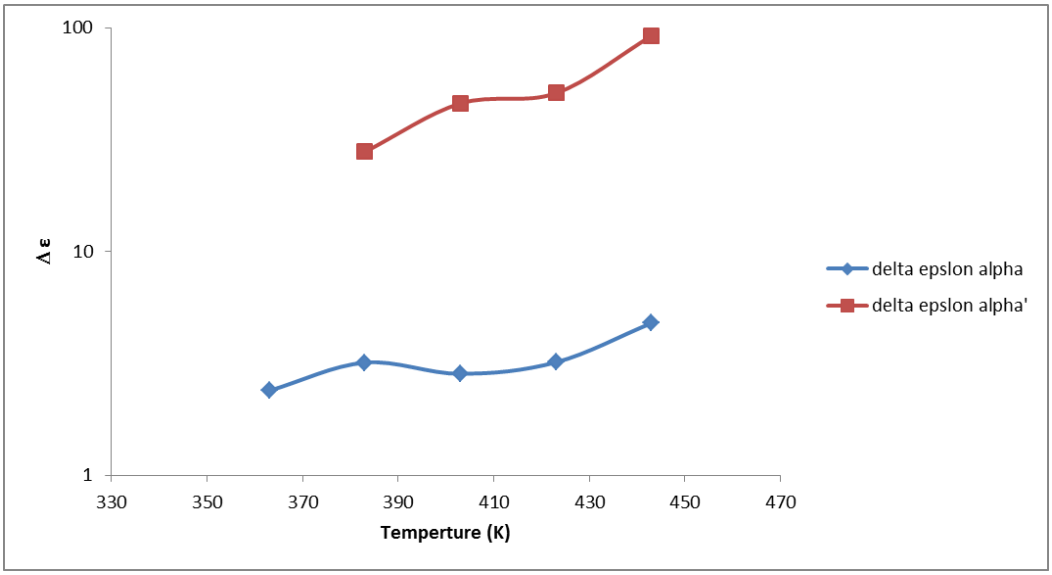

(b)

Figure 37 (a) Temperature dependence of relaxation strength, Δε, for the α (blue) and α' (red) processes in P4VIm^{+}PF$_6^{-}$. (b) Temperature dependence of relaxation strength, Δε, for the α (blue) and α' (red) processes in P4VIm^{+}BF$_4^{-}$.

In any discussion of the origin of relaxation peaks in the dielectric spectra of ionic polymers one is obligated to consider the possibility of ion aggregation. Ion aggregates would be most expected in the triflate system in which the anion is "hard" – not highly polarizable. Soft anions

like TFSI and dicyanamide would be least likely to suffer from ion aggregation. The similarity of dielectric spectral characteristics across the series of ion-exchanged $P4VIm^+$ salts leads us to discount the impact of ion aggregation and any consequent interfacial polarization peaks. While critical X-ray diffraction or viscoelastic studies which could rule out ion aggregation have not been carried in our $P4VIm^+$ system, the recent viscoelastic study by Nakamura *et al.* [91], indicating the absence of ion aggregates in poly(1-butyl-3-vinylimidazolium salts), supports the probability that ion aggregation is not a factor in any features of the dielectric spectra of $P4VIm^+$ salts.

Activation energies were calculated from the slope of the plots of frequency *versus* 1/T (K) for five 4-vinylimidazolium polymer salts ($CF_3SO_3^-$, BF_4^-, PF_6^-, $C_2N_3^-$, and $TFSI^-$). These data are presented in Table 4. The activation energy of the α-relaxation appears to scale with the glass transition temperature, with E_a-α being lowest for the $TFSI^-$ and $C_2N_3^-$ salts. The activation energy of the α'-relaxation process was variable; however, it was highest in the $TFSI^-$ and $C_2N_3^-$ salts and lowest with the $CF_3SO_3^-$ and BF_4^- salts. The differences between the activation energies of the α and α' processes were least pronounced in $P4VIm^+$ PF_6^- and $P4VIm^+CF_3SO_3^-$. The activation energies of the α relaxation process in $P4VIm^+$ PF_6^- and $P4VIm^+$ $C_2N_3^-$ are similar to those in $PNVIm^+$ PF_6^- and $PNVIm^+C_2N_3^-$. These differences in the apparent activation energies of the α and α' relaxation processes may be related to how tightly the anion is coupled to the imidazolium cation.

Table 4 E_a of α and α' relaxations in $P4VIm^+$ salts

$P4VIm^+$	E_a (KJ/mol), α relaxation	E_a (KJ/mol), α' relaxation	Heating Cycle T_g -mid, °C
BF_4^-	72	28	186
PF_6^-	83*	109	200
$CF_3SO_3^-$	40	18	213
$C_2N_3^-$	31†	102	88
$TFSI^-$	28	141	81

* *E_a of $PNVIm^+$ PF_6^- = 107 KJ/mol.*
† *E_a of $PNVIm^+$ $C_2N_3^-$ = 12 KJ/mol.*

In light of the substantial difference in the activation energies of the α and α' relaxations of the $P4VIm^+C_2N_3^-$ and $P4VIm^+TFSI^-$ one might speculate these large soft (highly polarizable) anions are not tightly coupled and that the nature of the ion-pair motion associated with α and α' relaxations are inverted with the α-relaxation being more reflective of ion-pair motion preceding segmental motion.

Agapov and Sokolov [6] have proposed that, in some glass-forming systems, ion diffusion can be decoupled from structural relaxation, with the extent of decoupling being characterized by the deviation of the temperature dependence of the characteristic structural relaxation time, τ, from a simple Arrhenius behavior. This deviation can be uniquely captured in the fragility index, m, (a measure of the steepness of the temperature dependence of τ at the glass transition temperature, T_g) [103]. At this juncture, more extensive dielectric relaxation studies over a broader temperature range are needed to unequivocally elucidate the molecular origins of the relaxation processes and the degree of correlation between anion mobility and the glass transition in 4-vinylimidazolium polymer salts. While such measurements are planned, the present work

represents a significant body of new data on the glass transition and dielectric relaxation characteristics of families of poly(1-ethyl-3-methyl-4-vinylimidazolium) and poly(1-ethyl-3-vinylimidazolium) salts.

6.2 Dielectric Properties of Imidazole polymers derived from ionic liquid 1-butyl-2,3-dimethyl-4-vinylimidazolium monomers

The dielectric relaxation characteristics of poly(1-butyl-2,3-dimethyl-4-vinylimidazolium triflate (Tf^-), and trifluoromethylsulfonylimide ($TFSI^-$) were evaluated and compared to triflate and $TFSI^-$ salts of 1-ethyl-3-methyl-4-vinylimidazolium polymers.

Figure 38 displays the dielectric storage parameter, ε', *versus* frequency in log-scale for TFSI and triflate salts of 1-butyl-2,3-dimethyl-4-vinylimidazolium and 1-ethyl-3-methyl-4-vinylimidazolium polymers. The temperature dependence of the ε' for P23D4VIm$^+$TFSI$^-$, P23D4VIm$^+$Tf$^-$, and P4VIm$^+$TFSI$^-$ is much greater than that for P4VIm$^+$Tf$^-$, [**38 (a), (b), (c)** and as compared to **38 (d)**]. This is probably because of the lower glass transition temperatures (see Table 2) of these three polymers. The dielectric constant tends to saturate at high frequency for all the four polymers.

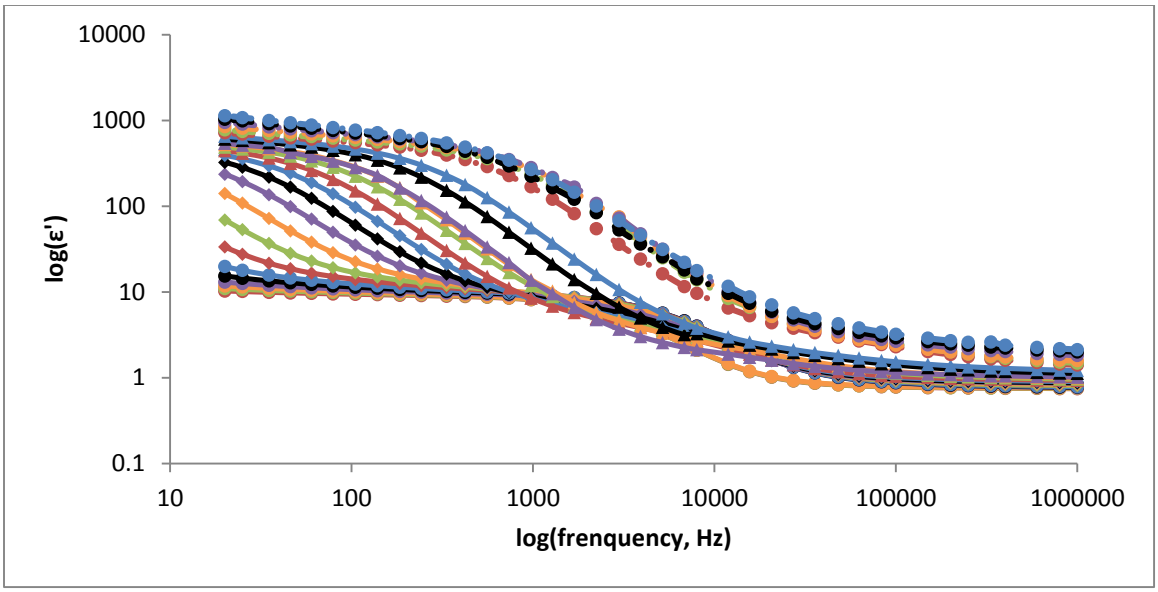
10000
1000
100
10
1
0.1
log(ε')
10
100
1000
10000
100000
1000000
log(frenquency, Hz)

(a)

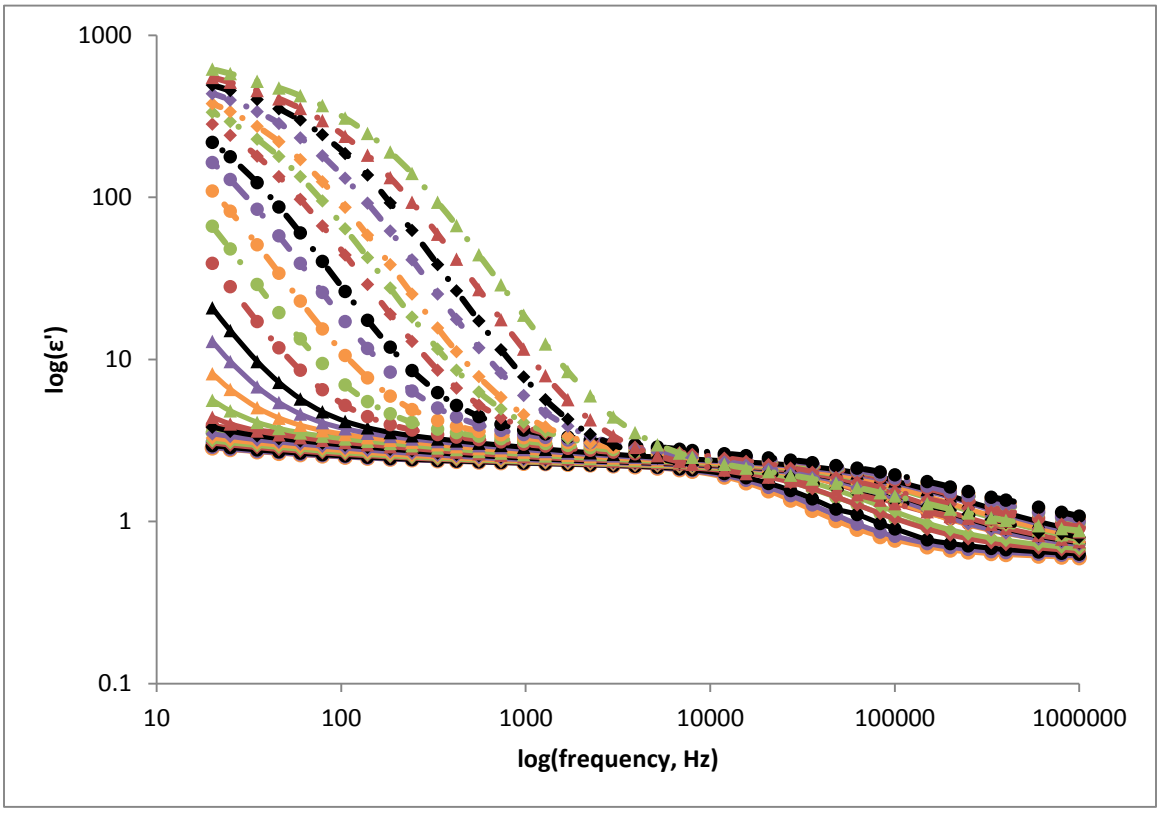
1000
100
10
1
0.1
log(ε')
10
100
1000
10000
100000
1000000
log(frequency, Hz)

(b)

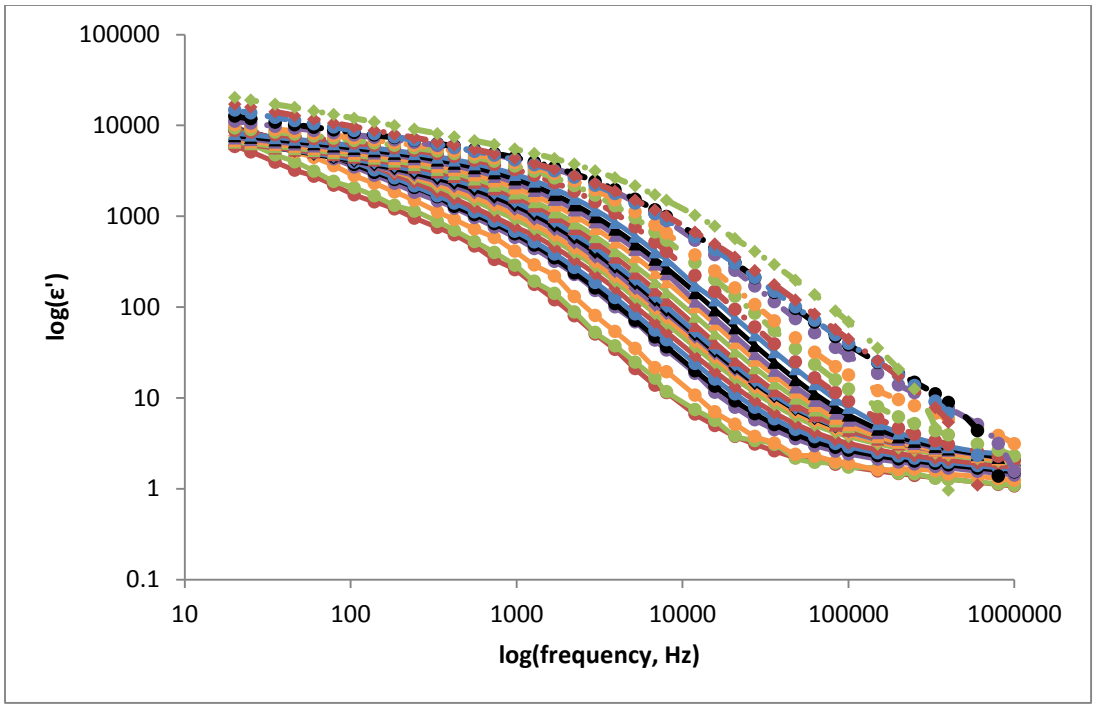

(c)

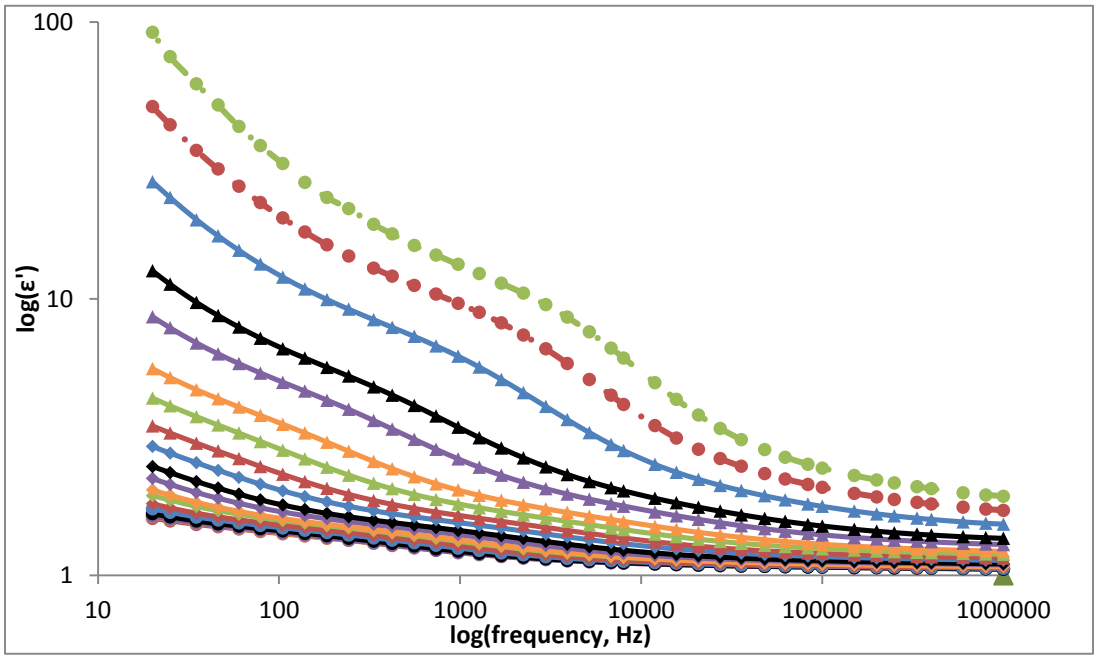

(d)

Figure 38 Log-scale ε' versus frequency for (a) poly(1-butyl-2,3-dimethyl-4vinylimidazolium TFSI⁻) (b) poly(1-butyl-2,3-dimethyl-4vinylimidazolium triflate) (c) poly(1-ethyl-3-methyl-4-vinylimidazolium TFSI⁻) (d) poly(1-ethyl-3-methyl-4-vinylimidazolium triflate)

Figure 39 (a-d) show plots of the dielectric loss parameter, ε", *versus* frequency in log-scale for TFSI and triflate salts of 1-butyl-2,3-dimethyl-4-vinylimidazolium and 1-ethyl-3-methyl-4-vinylimidazolium polymers. Two sets of relaxation peaks are apparent in the dielectric spectra of all four ionic liquid polymer salts. The intensity of the relaxation peaks in the P4VIm^{+}TFSI^{-} and P4VIm^{+}Tf^{-} spectra is lower than that in the spectra of P23D4VIm^{+}TFSI and P23D4VIm^{+}Tf^{-}. This can likely be attributed to the greater relative asymmetry of the tetra-substituted 1-butyl-2,3-dimethyl-4-vinylimidazolium moiety.

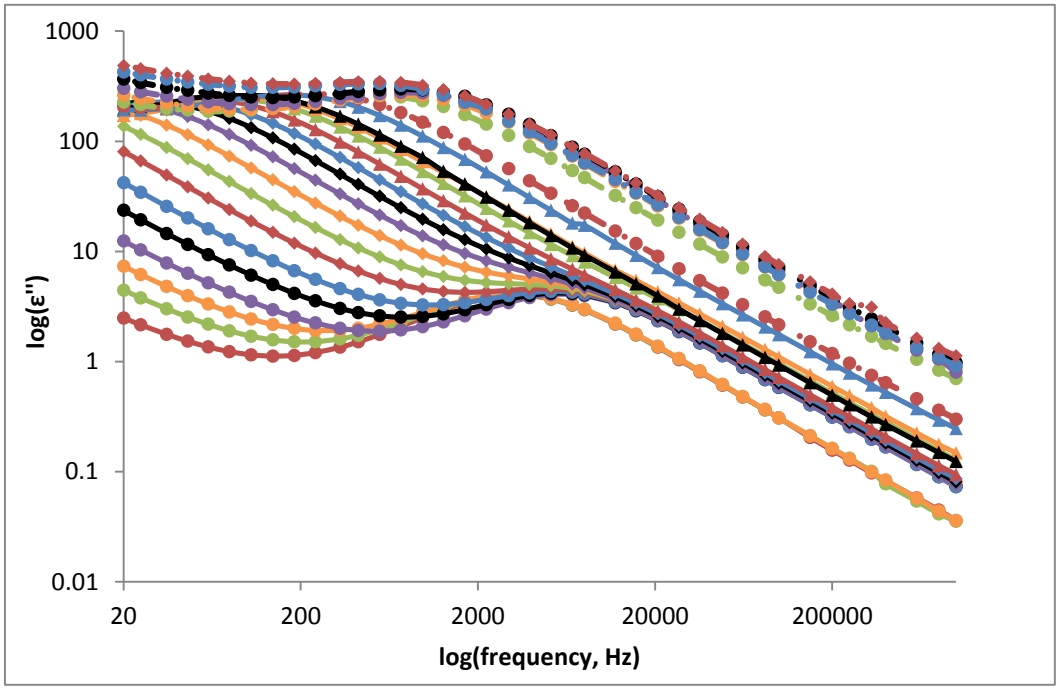

(a)

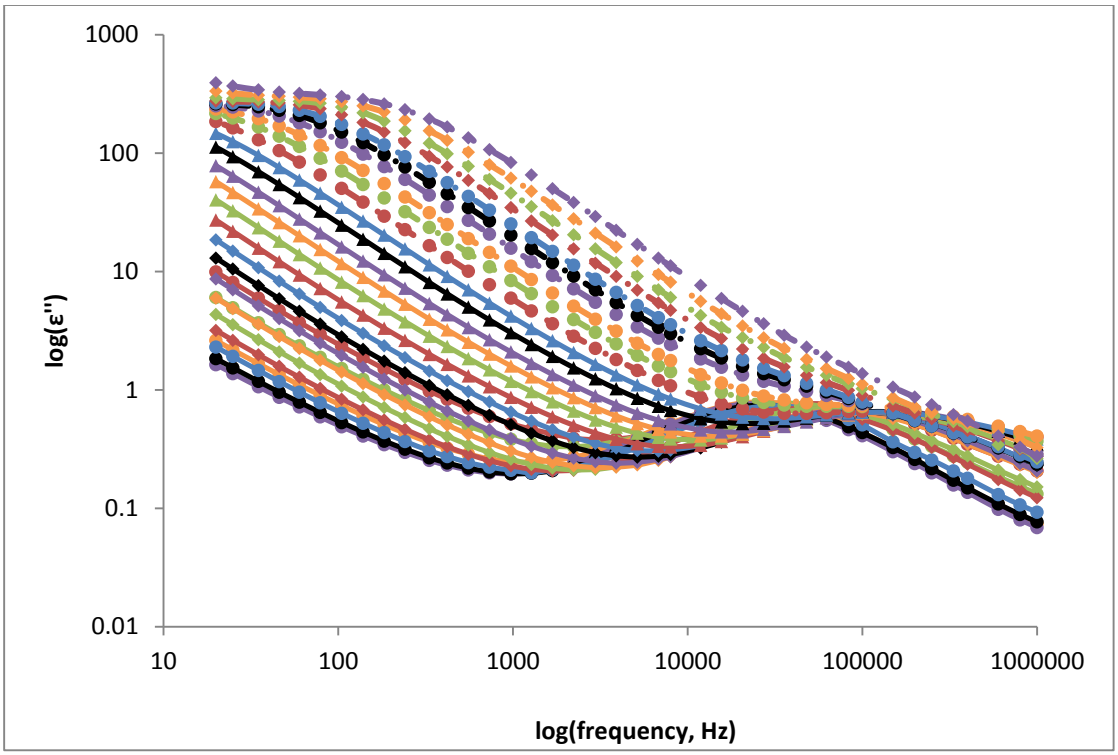
1000
100
10
1
0.1
0.01
log(ε'')
10
100
1000
10000
100000
1000000
log(frequency, Hz)

(b)

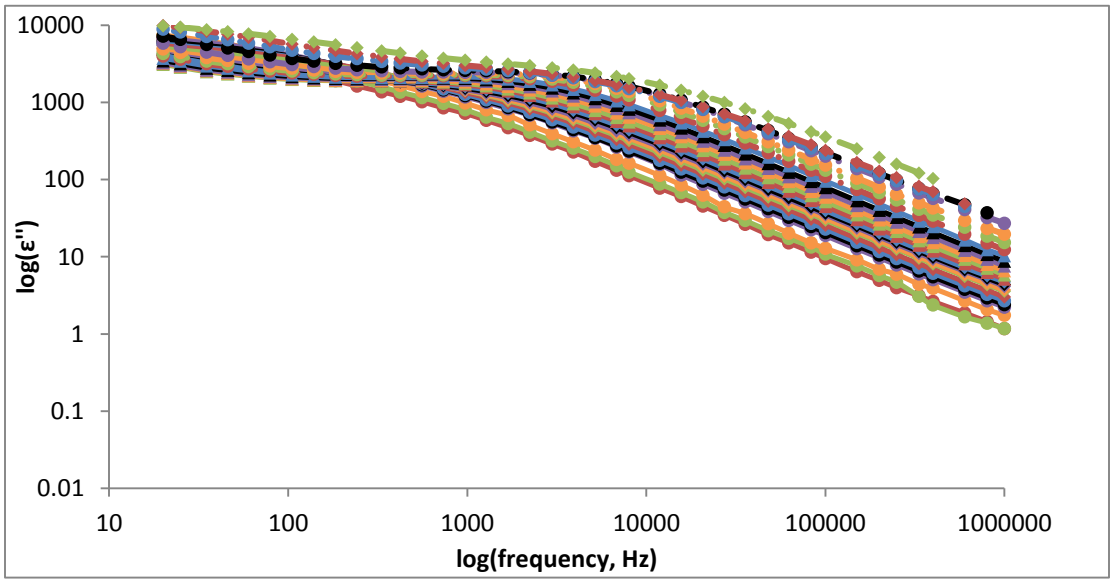
10000
1000
100
10
1
0.1
0.01
log(ε'')
10
100
1000
10000
100000
1000000
log(frequency, Hz)

(c)

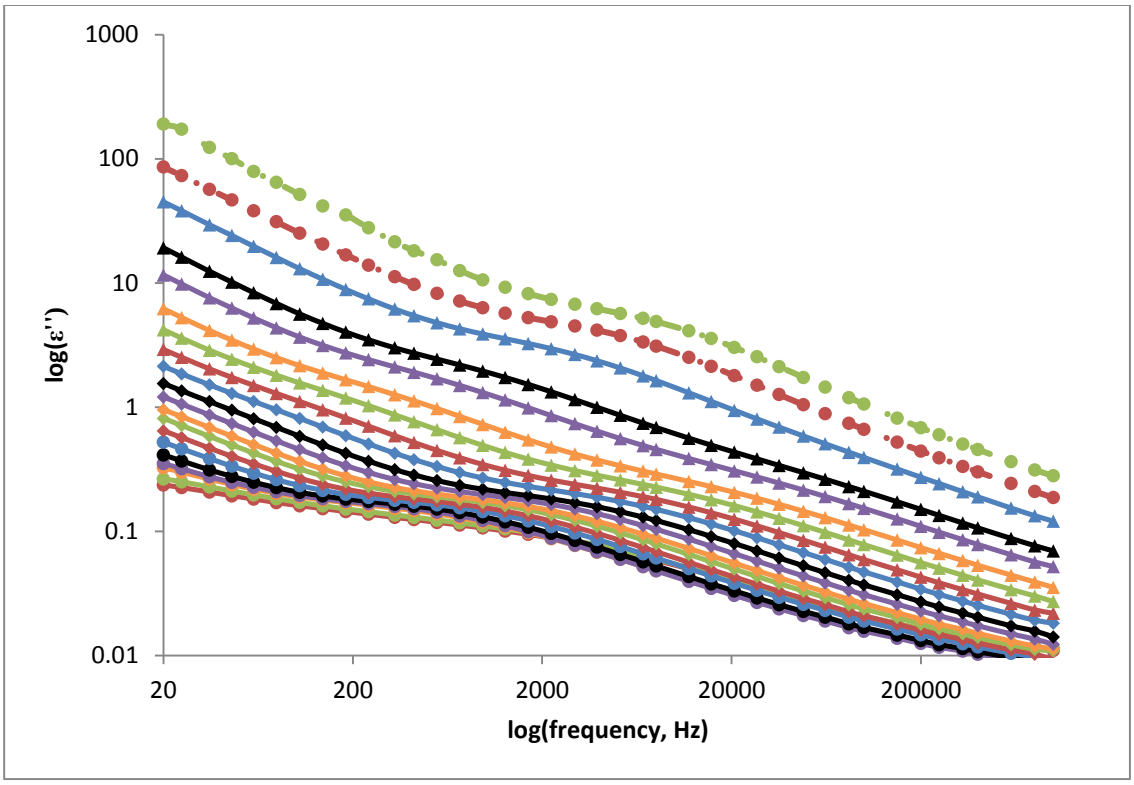

(d)

Figure 39 Log-scale ε'' versus frequency for (a) poly(1-butyl-2,3-dimethyl-4vinylimidazolium TFSI) (b) poly(1-butyl-2,3-dimethyl-4vinylimidazolium triflate) (c) poly(1-ethyl-3-methyl-4-vinylimidazolium TFSI) (d) poly(1-ethyl-3-methyl-4-vinylimidazolium triflate)

The maximum frequency of dipolar relaxations in poly(1-ethyl-3-methyl-4-vinylimidazolium) Tf^- and $TFSI^-$ was analyzed by fitting the dielectric loss ε'' using the Havriliak-Negami model, in Equation (6.1). That for poly(1-butyl-2,3-dimethyl-4-vinylimidazolium) Tf^- and $TFSI^-$ was taken directly from plots of frequency *versus* tan δ.

Figure 40 (**a** and **b**) and **Figure 41** (**a** and **b**) show comparative plots of tan δ (dissipation factor) *versus* frequency, at temperatures ranging from 30°C to 150°C, for $TSFI^-$ and triflate salts of $P23D4VIm^+$ and $P4VIm^+$. Included within the figures are 3-dimensional surface plots [log (tanδ) *vs* temperature *vs* log(frequency)] that may be advantageous in visualization of the relative intensity of the relaxation processes. In the 3-D surface plots, the highest intensity shows as red,

lowest is dark blue; green is intermediate intensity. In all four dielectric spectra, two relaxation modes, α and α', analogous to those described in Section 6.1 for $P4VIm^+$ salts, were observed. In the dielectric spectra of the $P23D4VIm^+$ salts, shown in **Figure 40**, the relaxation peaks are strong and clearly delineated.

(a) **$P23D4VIm^+TFSI^-$**

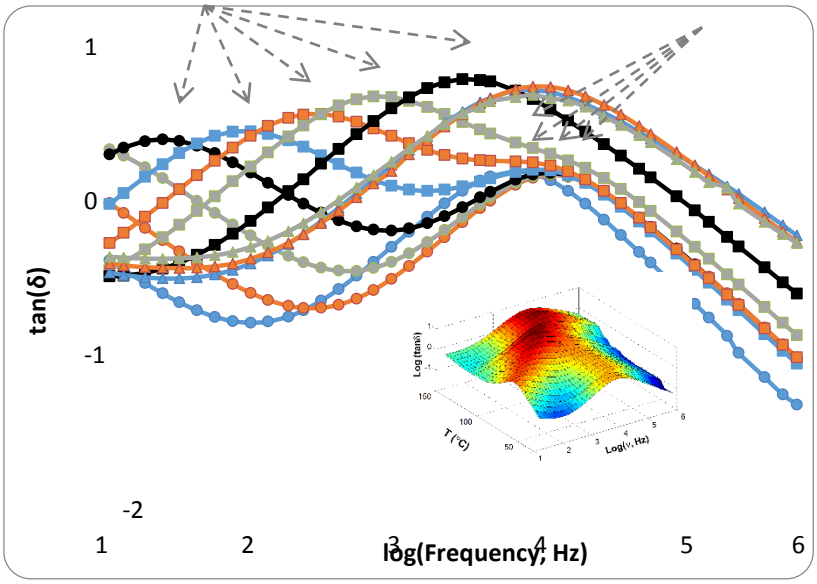

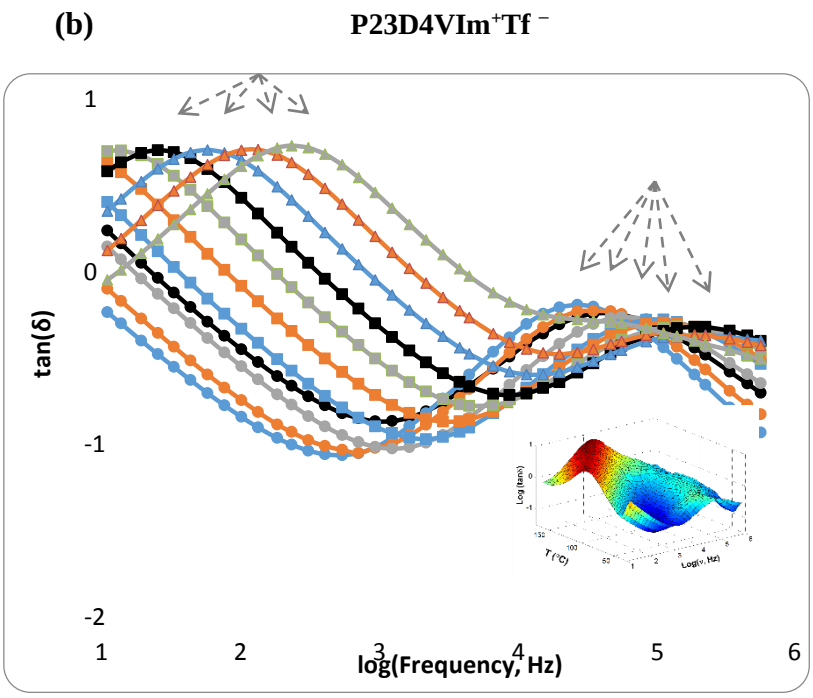

Figure 40 (a and b)Frequency dependence of tan δ for (a) P23D4VIm^{+}TFSI^{-}, (b) P23D4VIm^{+}TF −. Data points of different shape and color connected by solid or dashed lines of the same color are measured data at different temperatures: ● blue solid, 40 °C; ● red solid, 50 °C; ● green solid, 60 °C; ● black solid, 70 °C; ■ blue solid, 80 °C; ■ red solid, 90 °C; ■ green solid, 100 °C; ■ black solid, 120 °C; ▲blue solid, 130 °C; ▲red solid, 140 °C; ▲green solid, 150 °C. The 3-D inset plots show log(tanδ) vs. temperature vs. log(ν). The highest intensity shows as red, intermediate is green, lowest is dark blue.

Peaks for the α relaxation process in P23D4VIm^{+}TFSI^{-} nearly span the entirety of the frequency space. Peaks for the α'-relaxation process span a smaller range of frequencies and overlap the frequencies at which peaks for the α process are observed. Peaks for the α relaxation process in P23D4VIm^{+}Tf^{-} appear over a frequency range of 20 Hz – 10^{3} Hz. The positional frequency resolution of the relaxation processes in both P23D4VIm^{+}TFSI^{-} and P23D4VIm^{+}Tf $^{-}$ is substantive; however, the resolution of the peaks in P23D4VIm^{+}Tf $^{-}$ is most pronounced (see **Figures 40a and 40b**). It should also be noted that the intensity of the α–relaxation is greater than that of the α'-relaxation. The greater positional resolution of the α and α' relaxation processes in

P23D4VIm^{+}Tf^{-}, as compared to that in the corresponding TFSI^{-} salt, may be a result of the greater dipole moment of the triflate anion, 0.94 *e* Å (4.52 D), *versus* 0.13 *e* Å (0.62 D) for TFSI^{-}. [104]

Figure 41 (a and b) display plots of frequency *versus* tan δ for P4VIm^{+}TFSI^{-} and P4VIm^{+}Tf^{-}. The α' relaxation in P4VIm^{+}TFSI^{-} is more intense and more clearly resolved than the α-relaxation; with the α-relaxation peaks being largely subsumed under the envelope of the α'-relaxation process (see **Figure 41a**). The intensity of the α–relaxation in the dielectric spectra of the P4VIm^{+}Tf^{-} (shown in **Figure 41b**) is greater than that of the α' relaxation. The peaks for the α and α' relaxations in P4VIm^{+}Tf^{-} are not as intense or as clearly resolved as those in P23D4VIm^{+}Tf^{-}. The greater asymmetry of the P23D4VIm^{+} cation is the likely origin of the greater resolution and increased intensity of the relaxation peaks.

(a) **P4VIm^{+}TFSI^{-}**

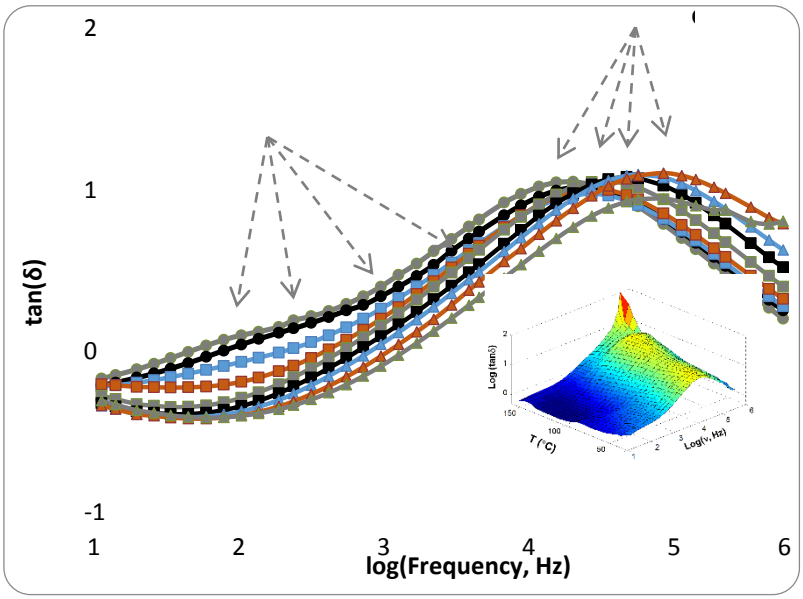

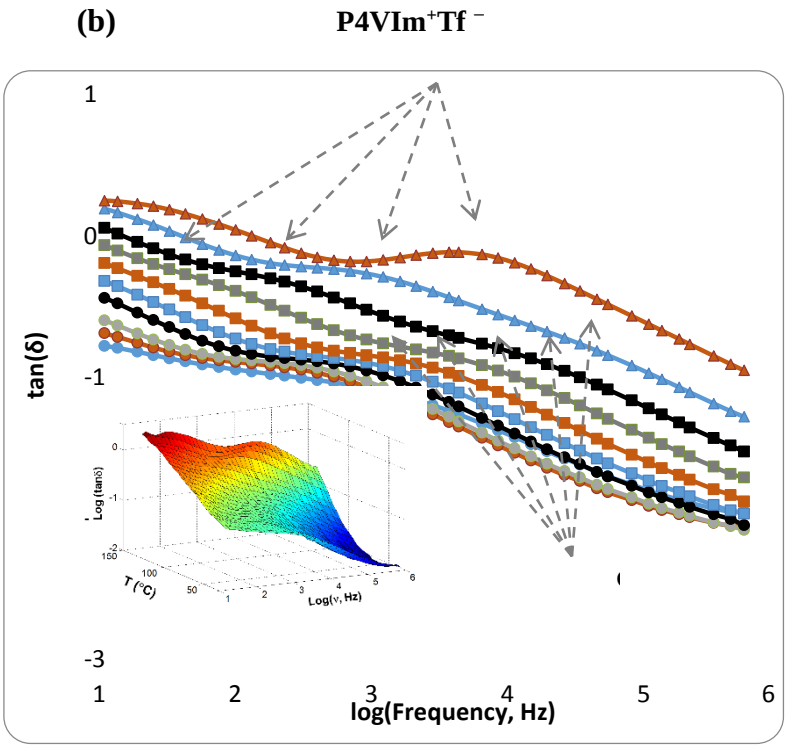

Figure 41 (a and b)Frequency dependence of tan δ for (a) P4VIm^{+}TFSI^{-}, and (b) P4VIm^{+}CF$_3$SO$_3^{-}$. Data points of different shape and color connected by solid or dashed lines of the same color are measured data at different temperatures: ● blue solid, 40 ºC; ● red solid, 50 ºC; ● green solid, 60 ºC; ● black solid, 70 ºC; ■ blue solid, 80 ºC; ■ red solid, 90 ºC; ■ green solid, 100 ºC; ■ black solid, 120 ºC; ▲blue solid, 130 ºC; ▲red solid, 140 ºC; ▲green solid, 150 ºC. The 3-D inset plots show log(tanδ) vs. temperature vs. log(ν). The highest intensity shows as red, intermediate is green, lowest is dark blue.

The α and α' relaxations in P4VIm^{+}Tf^{-} are more discreet that those in P4VIm^{+}TFSI^{-}. As in the case of P23D4VIm^{+}Tf^{-}, the increased resolution in P4VIm+Tf^{-} (**see Figure 41b**) may be related to the greater dipole moment of the triflate anion. Because of the substantial overlap in the α and α' peaks, dipolar relaxation of P4VIm^{+} salts was analyzed, by fitting the dielectric loss ε'' using the Havriliak-Negami model, in Equation. (6.1). Experimental ε" vs frequency data, the deconvoluted α-relaxation peak, and the fit to the Havriliak-Negami equation for P4VIm^{+}Tf^{-} at 120 °C are provided in the Appendix. Excel spreadsheets provide data in five degree increments from 30 - 150 ºC.

The activation energy of the relaxation processes in the triflate and $TFSI^-$ salts of $P23D4VIm^+$ and $P4VIm^+$ was estimated from the slope of least squares fit lines in plots of the log of the frequency of each relaxation peak *versus* the reciprocal of the temperature, T, over the temperature range (303-423 K) at which measurements were taken. Arrhenius plots of the α and α' relaxation processes are presented in **Figures 42 (a and b)**, respectively. In **Figure 42 (a)**, it is apparent that the slopes of the plots for $P4VIm^+TFSI^-$ (black solid circles, ●), $P23D4VIm^+TFSI^-$ (red solid circles, ●) and $P23D4VIm^+Tf^-$ (green solid circles, ●) are similar and substantially different from that for $P4VIm^+Tf^-$ (blue solid circles, ●). The glass transition temperatures of $P4VIm^+TFSI^-$, $P23D4VIm^+TFSI^-$ and $P23D4VIm^+Tf^-$ are also similar. In **Figure 42 (b)**, the slopes of the lines for TFSI salts of $P4VIm^+$ and $P23D4VIm^+$ are similar and differ from those for the triflate salts which themselves differ from each other.

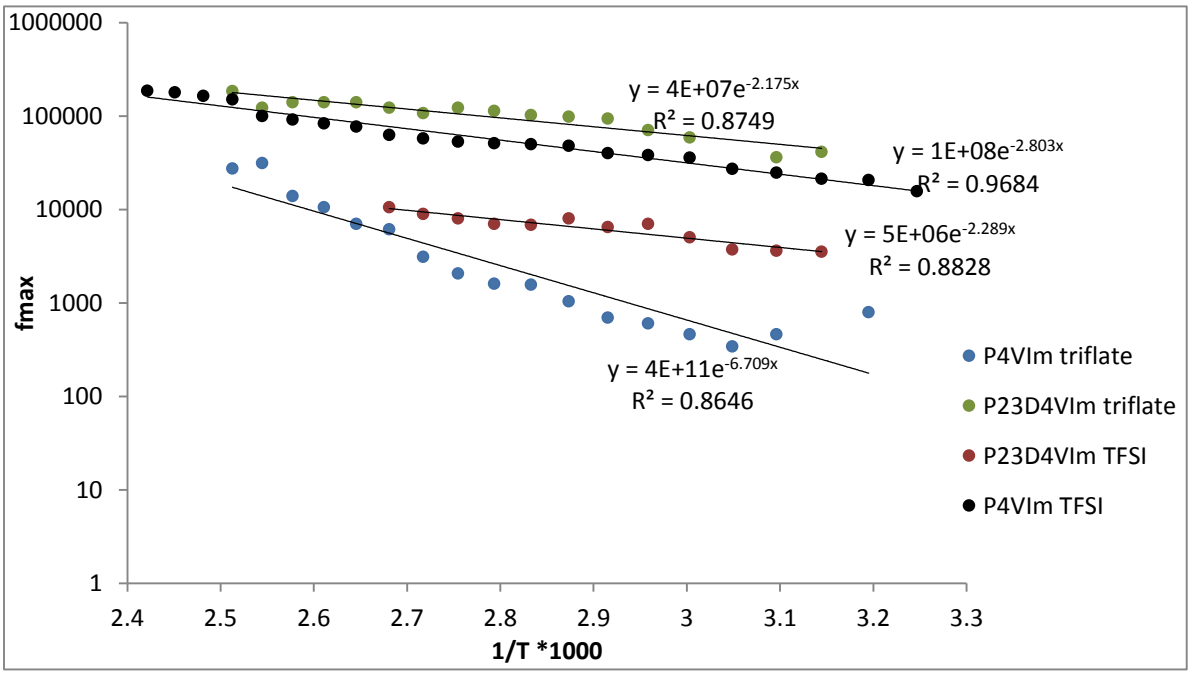

(a)

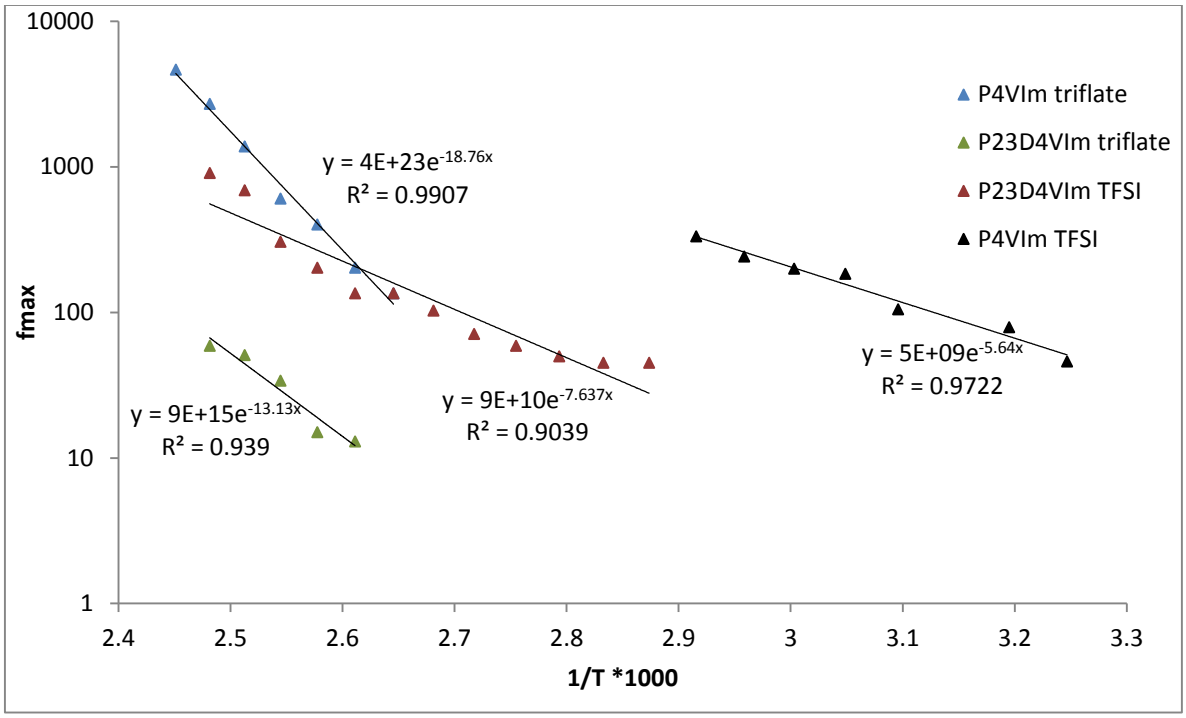

(b)

Figure 42 Arrhenius plots for P4VIm+ and P23D4VIm+ with two anions for (a) α'- and (b) α- relaxation; the fitting parameters are labeled

The activation energy for the α relaxation processes, presented in Table.5, ranges from 18-56 KJ/mol and scales with the glass transition temperatures of the respective salts. The correlation coefficients for the fit of the least square lines to the data were 0.86, 0.97, 0.87, and, 0.88 for $P4VIm^{+}Tf^{-}$, $P4VIm^{+}TFSI^{-}$, $P23D4VIm^{+}Tf^{-}$ and $P23D4VIm^{+}TFSI^{-}$, respectively.

Table 5 – E_a of α and α' relaxations in $P23DMVIm^{+}$ and $P4VIm^{+}$ salts

Polymer	Anion	E_a (KJ/mol), α relaxation	E_a (KJ/mol), α' relaxation
$P4VIm^{+}$	$TFSI^{-}$	23	47
	Tf^{-}	56	156
$P23DMVIm^{+}$	$TFSI^{-}$	19	63
	Tf^{-}	18	109

The activation energy for the α' relaxation processes of the triflate salts (156 KJ/mol and 109 KJ/mol) are much larger than those of the TFSI salts (47 KJ/mol and 63 KJ/mol). The correlation coefficients for the least square fit to the α' relaxation processes are 0.99, 0.97, 0.94, and, 0.92 for $P4VIm^{+}\ Tf^{-}$, $P4VIm^{+}TFSI^{-}$, $P23D4VIm^{+}Tf^{-}$ and $P23D4VIm^{+}TFSI^{-}$, respectively. On the basis of the activation energies of the α and α' relaxation processes, one might speculate that ion motion associated with the α relaxation is closely coupled to segmental motion of the polymer backbone and that ion motion associated with the α' relaxation is related to translational motion of the counterion and is substantially decoupled from the glass transition.

The relaxation time, calculated as $\tau = 1/(2\pi f_{max})$, *versus* temperature K is also shown in **Figure 43**.

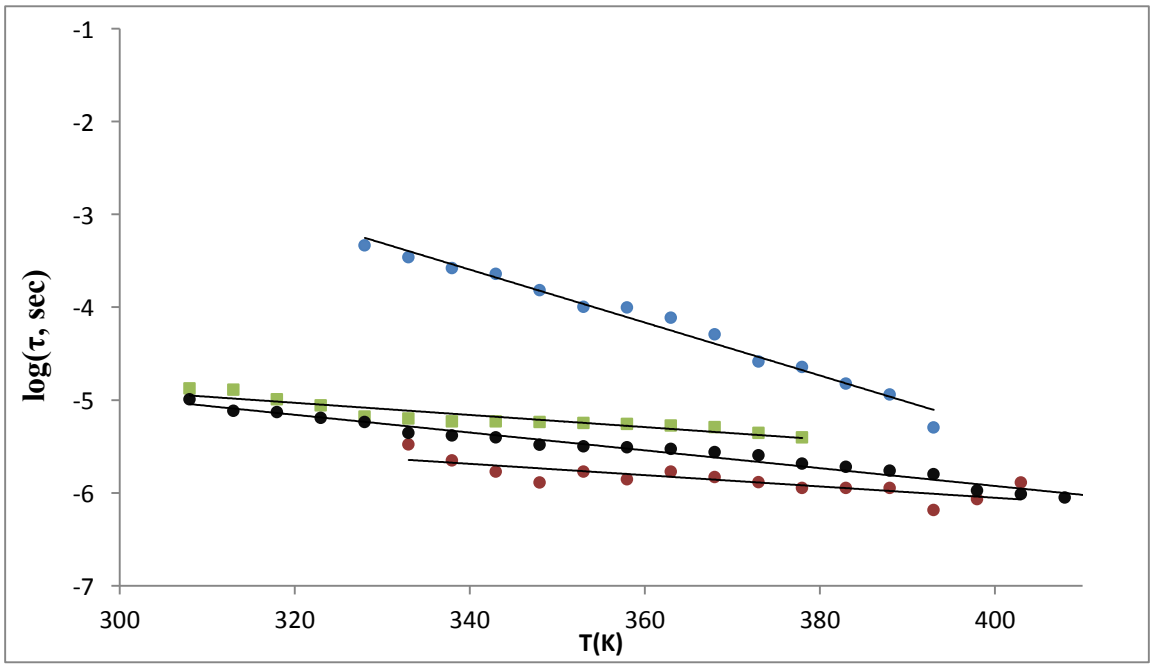

(a)

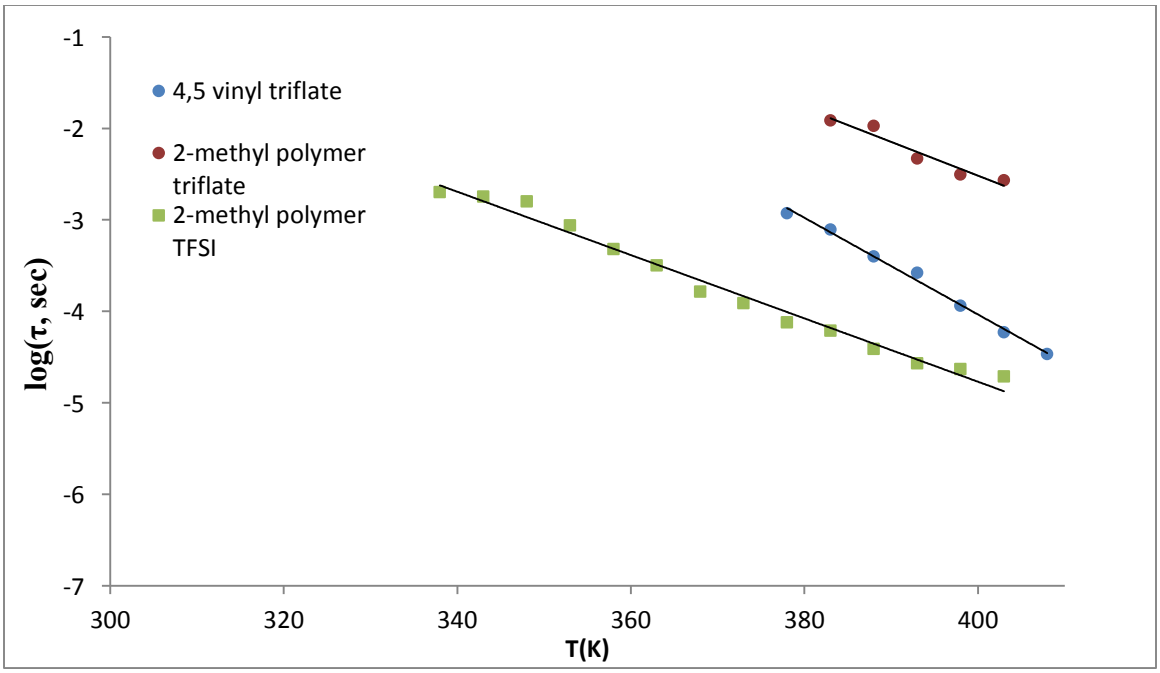

(b)

Figure 43 Relaxation time versus temperature for P4VIm+ and P23D4VIm+ with two anions for (a) α'- and (b) α- relaxation

The conductivity of the four polymers was analyzed and extracted from the dielectric data using the method shown in **Figure 29**. The extracted conductivity data are plotted *versus* temperature for three polymers, shown in **Figure 44**. For all three polymers, the ionic conductivity increases with increasing temperature as expected. The ionic conductivity of P23D4VIM TFSI and triflate reaches 10^{-3} mS/cm, which is comparable for the number reported in other literatures[1], [73]. For P23D4VIM with two anions, the ionic conductivity increases linearly up to about 350K, around their glass transition temperatures, then it saturates.

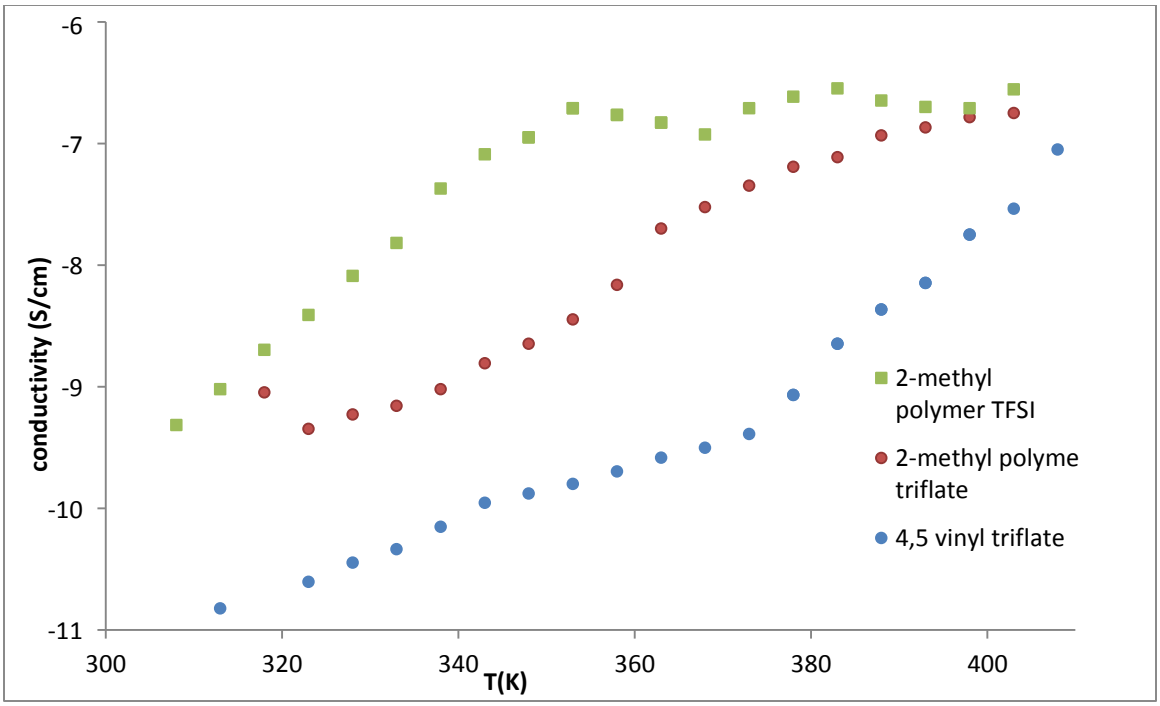

Figure 44 Conductivity versus temperature T

Figure 45 shows plots of tan δ *versus* temperature at fixed frequency for P23D4VIM and P4VIm triflate. For P23D4VIM^{+}triflate one sees a peak at about 100ºC in the low frequency (20Hz) plot. This is roughly the glass transition temperature of P23D4VIM^{+}triflate, and indicates that this relaxation is coupled to the glass transition process. At 1000 Hz, this relaxation moves to about 160°C. Because the glass transition temperature of P4VIm triflate is 153°C, maxima are pushed to temperatures in excess of 440 K and peaks are no observed.

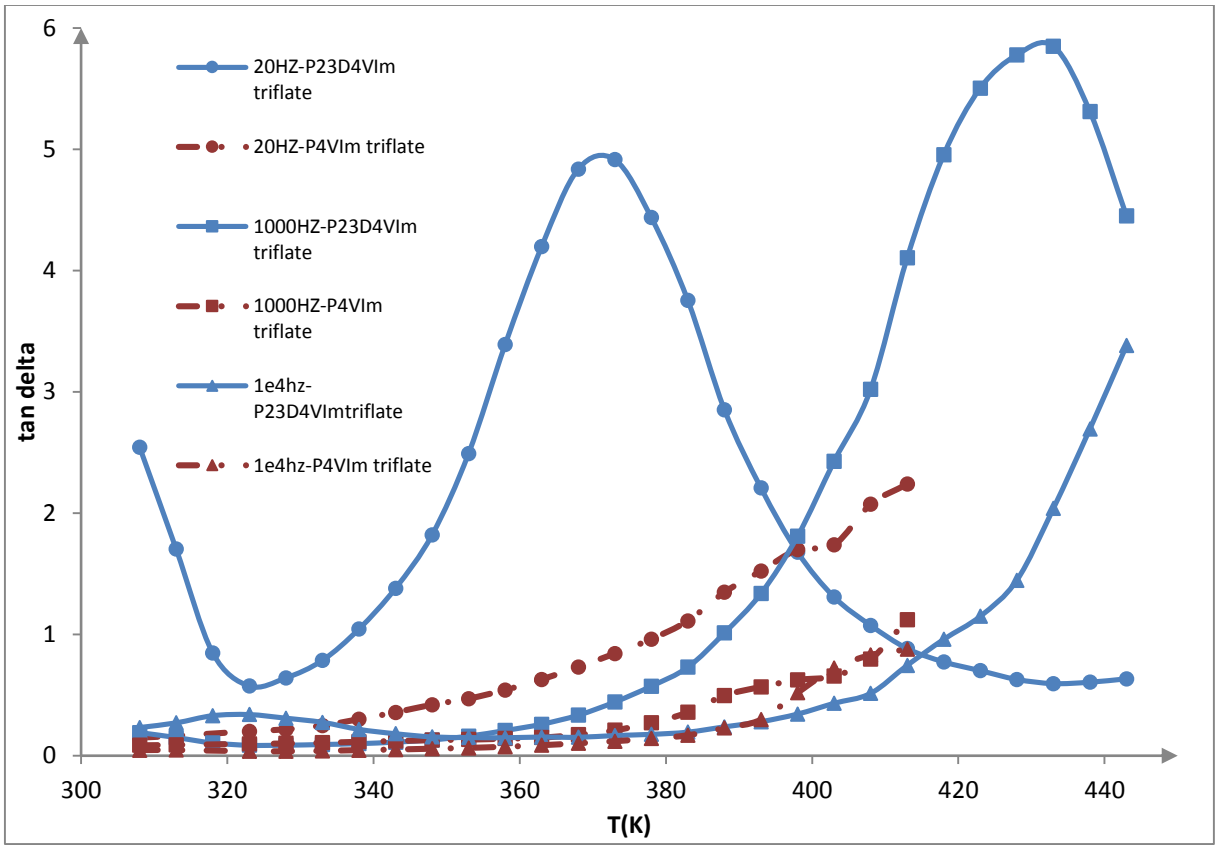

Figure 45 Tan δ versus temperature at fixed frequency for P23D4VIM and P4VIm triflate

Summary and Conclusions

A robust process for the synthesis of 1-ethyl-3-methyl-4-vinylimidazolium triflate (EM-4-VIm^+ $CF_3SO_3^-$), was developed. This new monomer was synthesized in a pure, dry (water-free) state by direct alkylation of 1-methyl-5-vinylimidazole in CH_2Cl_2 or ethyl acetate solution with ethyl triflate at 0 °C. While the monomer tends to polymerize spontaneously at ambient temperature or when exposed to water, it can be stored and handled without polymerization as long as it is kept dry in its crystalline state and held at temperatures below 0 °C. EM-4-VIm^+ $CF_3SO_3^-$ is readily polymerized with a free-radical initiator; and, the resulting polymer has been ion-exchanged to create a family of 4-vinylimidazolium polymers in which the counter-ion ranged from BF_4^-, PF_6^-, and AsF_6^- to dicyanamide ($C_2N_3^-$), *bis*-trifluoromethylsulfonamide ($TFSI^-$), and, triflate ($CF_3SO_3^-$).

This same process was employed in the synthesis of 1-ethyl-3-vinylimidazolium triflate (N-VIm^+ $CF_3SO_3^-$) and its subsequent polymerization and ion exchange.

The trends in the glass transition characteristics of the various 4-vinylimidazolium and N-vinylimidazolium polymers were similar; however, the glass transition temperatures of P4VIm^+ BF_4^-, PF_6^-, AsF_6^-, and, $CF_3SO_3^-$ salts were significantly higher than those of the corresponding poly(N-vinylimidazolium) salts. This difference and the increase in T_g in going from BF_4^- to AsF_6^- in the 4-vinylimidazolium series was attributed to enhanced intramolecular bridging between imidazolium moieties position 1,3 or 1,5 along the polymer chain.

In the 30-210 °C temperature range, the dielectric relaxation spectra of the 4-vinylimidazolium polymer salts exhibited two relaxation modes. The N-vinylimidazolium polymer salt exhibited only one relaxation mode in that temperature range. The single mode

appears to correspond to the α-relaxation peak, assigned to ion-pair motion in $PNVIm^+$ $TFSI^-$, by Nakamura *et al*. [92] The second relaxation peak, that is apparent at lower frequency in the dielectric spectra of the 4-vinylimidazolium polymer salts, was identified in this work as the α'-relaxation and is also associated with ion-pair motion. Assuming the relaxation processes to be Arrhenius in nature, the activation energy of the α-relaxation in $P4VIm^+$ BF_4^-, PF_6^-, $CF_3SO_3^-$, $TFSI^-$ and $C_2N_3^-$ salts ranged from 83 to 28 KJ/mol. The activation energy of the α-relaxation in poly(4-vinylimidazolium $TFSI^-$ and $C_2N_3^-$) was lowest, ranging from 31 to 28 KJ/mol. The activation energy of the α-relaxation in $P4VIm^+$ salts appears to scale with the glass transition temperature of the various salts. The activation energy of the α'-relaxation in $P4VIm^+$ $TFSI^-$ and $C_2N_3^-$, (141 and 102 KJ/mol), respectively, was dramatically higher than that for the α-relaxation (28 and 31 KJ/mol, respectively).

1-butyl-2,3-dmethyl-4-vinylimidazolium triflate was synthesized in a pure, dry (water-free) state by direct alkylation of 1-butyl-2-methyl-4-vinylimidazole in CH_2Cl_2 with methyl triflate at 0 °C. $2,3D4VIm^+Tf^-$ was polymerized with a free-radical initiator, and the resulting polymer was ion-exchanged to create hexafluorophosphate (PF_6^-), and *bis*-trifluoromethylsulfonimide ($TFSI^-$) salts. The glass transition characteristics of the PF_6^- and triflate salts of $23D4VIm^+$ polymers are anomalous as compared to those of PF_6^- and triflate salts of 4-vinyl and N-vinylimidazolium polymers. The invariance in the glass transition of $P23D4VIm^+$ with different anions was attributed to steric separation enforced by having substituents on the 1, 2, 3, and 4 positions of the imidazolium moiety that dramatically diminishes the contribution of counterion size to the equilibrium distance between the center of the anion and cation. Indeed the separation may be

large enough that the onset of motion of the polymer backbone is decoupled from counterion motion.

The α and α' relaxations of the triflate salts of P23D4VIm$^+$ and P4VIm$^+$ are more clearly resolved than in the corresponding TFSI salts. The α and α' relaxations in P23D4VIm$^+$ $CF_3SO_3^-$ are more clearly resolved than the α and α' relaxations in P4VIm$^+$ $CF_3SO_3^-$. On the basis of these observations, it is proposed that translational motion of the anions is substantially decoupled from the polymer and has little influence on the glass transition in PV23D4Im$^+$triflate and TFSI$^-$, and P4VIm$^+$TFSI$^-$. It is also suggested that translational motion of the anion is reflected in the α' relaxation and that, because of its greater dipole moment, this motion is most clearly reflected in the dielectric spectra of triflate salts.

References

[1] Michel, A.; Frank, E.; Douglas, M.; Hiroyuki, O. "Ionic-liquid Materials for the Electrochemical Challenges of the Future" *Nature Materials* **2009**, *8*, pp. 621 – 629.

[2] Kishimoto, K.; Yoshio, M.; Mukai, T.; Yoshizawa, M.; Ohno, H.; Takashi, K. "Nanostructured anisotropic ion-conductive films" *J. Amer. Chem.Soc.*, **2003,** *125(11),* 3196–3197.

[3] Yoshio, M.; Kagata, T.; Hoshino, K.; Ohno, H. "One-dimensional ion-conductive polymer films: Alignment and fixation of ionic channels formed by self-organization of polymerizable columnar liquid crystals*," J. Amer. Chem. Soc.*, **2006**, *128(16),* 5570–5577.

[4] D. Linden, T. B. Reddy, "Handbook of Batteries" *Fuel and Energy Abstracts*, **2002.**

[5] Scott, M. P.; Rahman M.; Brazel, C. S. "Application of ionic liquids as low-volatility plasticizers for PMMA," *European Polymer Journal* **2003**, *39(10),* 1947-1953.

[6] Agapov A. L.; Sokolov, A. P.; "Decoupling Ionic Conductivity from Structural Relaxation: A Way to Solid Polymer Electrolytes?" *Macromolecules*, **2011**, *44*, 4410–4414.

[7] Winter, M.; Brodd, R. J. "What Are Batteries, Fuel Cells, and Supercapacitors?" *Chem. Rev.*, **2004**, 104, pp.4245-4269.

[8] Skoog, D. A. & West, D. M.(1980). Principles of Instrumental Analysis (2nd ed.) Saunders College, Philadelphia.

[9] Harris, D. C. "Quantitative Chemical Analysis", 6th edition, W. H. Freeman and Company, New York, **2003**.

[10] Kishimoto, K.; Yoshio, M.; Mukai, T.; Yoshizawa, M.; Ohno, H.; Takashi, K. "Nanostructured anisotropic ion-conductive films," *J. Amer. Chem. Soc.* **2003**, *125*, 3196.

[11] Tarascon, J.M.; Armand, M. "Issues and challenges facing rechargeable lithium batteries" *Nature*, **2001**, *414*, 359-367.

[12] Stenger-Smith, J. D.; Webber, C. K.; Anderson, N.; Chafin, A.P.; Zong, K.; Reynolds, J. "Poly(3,4-alkylenedioxythiophene)-based supercapacitors using ionic liquids as supporting electrolytes," *J. Electrochem. Soc.*, **2002**, *148(8),* A973-A977.

[13] Mifler, J. R.; Simon, P. "Fundamentals of Electrochemical Capacitor Design and Operation" *The Electrochemical Society Interface Spring*, **2008.**

[14] C. Liu, Z. Yu, D. Neff, A. Zhamu, B. Z. Jang, " Graphene-Based Supercapacitor with an Ultrahigh Energy Density" *Nano Lett.*, **2010**, 10*(12)*, 4863–4868.

[15] Yoon, S.; Lee, J.; Hyeon, T.; Oh, S. M. "Electric Double-Layer Capacitor Performance of a New Mesoporous Carbon" *J. Electrochem. Soc.*, **2000**, *147 (7)*, 2507-2512.

[16] Kotz, R.; Carle, M. "Principles and Applications of Electrochemical Capacitors" *Electrochimica Acta*, **2000**, *45*, 2483–2498.

[17] Simon, P.; Gogotsi, Y. "Materials for Electrochemical Capacitors" *Nature Materials* **2008**, *7*, 845 – 854.

[18] D. Pech, M. Brunet, P. L. Taberna, P. Simon, "Elaboration of a Microstructured Inkjet-printed Carbon Electrochemical Capacitor" *J. Power Sources* **2010,** *195,*1266–1269.

[19] E. Frackowiak, "Supercapacitors Based on Carbon Materials and Ionic Liquids" *J. Braz. Chem. Soc.*, **2006**, *17(6)*

[20] Lewandowski, A.; Widerska, A. S. "Electrochemical Capacitors with Polymer Electrolytes Based on Ionic Liquids" *Solid State Ionics*, **2003,** *161*, pp. 243–249.

[21] Sato, T.; Masuda, G.; Takagi, K. "Electrochemical Properties of Novel Ionic Liquids for Electric Double Layer Capacitor Applications" *Electrochimica Acta*, **2004**, *49(21)*, 3603–3611.

[22] Balducci, A.; Soavi, F.; Mastragostino, M. "The Use of Ionic Liquids as Solvent-free Green Electrolytes for Hybrid Supercapacitors" *Appl. Phys. A*, **2006**, *82(4)*, 627–632.

[23] Wei, D.; Ng, T. W. "Application of novel room temperature ionic liquids in flexible Supercapacitors" *Electrochemistry Communications*, **2009**, *11(10)*, 1996–1999.

[24] Liu, X.; Osaka, T. "Properties of Electric Double-Layer Capacitors with Various Polymer Gel Electrolytes" *J. Electrochem. Soc.*, **1997**, *144(9)*, 3066-3071.

[25] Ishikawa, M.; Ihara, M.; Morita, M.; Matsuda, Y. X. "Electric Double Layer Capacitors with New Gel Electrolytes" *Electrochimica Acta*, **1995**, *40(13)*, 2217-2222.

[26] Tarascon, J.M.; Armand, M. "Issues and Challenges Facing Rechargeable Lithium Batteries" *Nature*, **2001**, *414(15)*, 359-367.

[27] Zhang, S. S.; Foster, D.; Read, J. "Discharge Characteristic of a Non-aqueous Electrolyte Li/O_2 Battery" *J. Power Sources*, **2010**, *195 (4)*,1235–1240.

[28] Goodenough, J. B.; Kim, Y. "Challenges for Rechargeable Li Batteries" *Chem. Mater.*, **2010**, *22*, 587–603.

[29] Fang, S.; Yang, L.; Wang, J.; Zhang, H.I.; Tachibana, K.; Kamijima, K. "Guanidinium-based Ionic Liquids as New Electrolytes for Lithium Battery" *J. Power. Sour*ces, **2009**, *191(2)*, 619–622.

[30] Stracke, M.P.; Migliorini, M.V.; Lissner, E.; Schrekker, H.S.; Dupont, J.; Gonlves, R.S. "Imidazolium Ionic Liquids as Electrolytes for Manganese Dioxide Free Leclanche Batteries" *Applied Energy*, **2009,** *86 (9)*, 1512–1516.

[31] Yang, Y.; McDowell, M. T.; Jackson, A.; Cha, J. J.; Hong, S. S.; Cui, Y. "New Nanostructured Li_2S/Silicon Rechargeable Battery with High Specific Energy" *Nano Lett.*, **2010**, *10(4)*, 1486–1491.

[32] Dudney, N. J.; "Thin Film Micro-Batteries" *Electrochem. Soc. Interface*, **2008**

[33] Zhang, D.; Li, R.; Huang, T.; Yu, A. "Novel Composite Polymer Electrolyte for Lithium Air Batteries" *J. Power Sour*ces, **2010**, *195 (4)*, 1202–1206.

[34] Chew, S. Y.; Sun, J.; Wang, J.; Liu, H.; Forsyth, M.; MacFarlane, D.R. "Lithium-polymer Battery Based on An Ionic Liquid–Polymer Electrolyte Composite for Room Temperature Applications" *Electrochimica Acta*, **2008**, *53(22)*, 6460–6463.

[35] Croce, F.; Appetecchi, G. B.; Persi, L.; Scrosati, B. "Nanocomposite Polymer Electrolytes for Lithium Batteries" *Nature*, **1998**, *394*, 456-458.

[36] Krebs, F. C. "Fabrication and processing of polymer solar cells: A review of printing and coating techniques," *Solar Energy Materials & Solar Cells*, **2009**, *93(4)*, 394–412.

[37] Gevorkian, P. - Sustainable energy systems engineering: the complete green building design resource. pg. 498, New York : McGraw-Hill, ©2007.

[38] http://en.wikipedia.org/wiki/Solar_cell

[39] Fenton, D. E.; Parker, J. M.; Wright, P. V. "Ionic Conductivity and Electrochemical Stability of Poly[oligo(ethylene glycol)oxalate]-Lithium Salt Complexes," *Polymer*, **1973,** *14(11)*, 589-589.

[40] Armand, M. "The history of polymer electrolytes" *Solid State Ionics*, **1994,** *69(3-4)*, 309-319.

[41] Berthier, C.; Gorecki, W.; Minier, M.; Armand, M. B.; Chabagno, J. M.; Rigaud, P. "Microscopic investigation of ionic conductivity in alkali metal salts-poly (ethylene oxide) adducts" *Solid State Ionics*, **1983**, *11*(1), 91-95.

[42] Angell, C. A., "On the Importance of the Metastable Liquid State and Glass Transition Phenomenon to Transport and Structure Studies in Ionic Liquids. I. Transport Properties" *The Journal of Physical Chemistry*, **1966,** *70(9)*, 2793-2803.

[43] Lampreia, M. I.; Barreira, F., "Transport properties of molten tetra-alkylammonium picrates - I. Viscosity," *Electrochim. Acta,* **1976,** *21(7),* 485-489**.**

[44] Barreira, M. L.; Barreira, F., "Transport properties of molten *tetra*-alkylammonium picrates—II conductivity," *Electrochim. Acta,* **1976,** *21(7),* 491-49.

[45] Ratner, M. A.; Shriver, D. F., "Ion transport in solvent-free polymers," *Chemical Reviews,* **1988,** *88(1),* 109-124.

[46] Duclot, M. J., in P. Vashishta, J. N. Mundy, & G. K. Shenoy, (Eds.), Fast ion transport in solids, North Holland, Amsterdam. **1979**

[47] Armand, M. B., "Polymer electrolytes," *Annual Review of Materials Science,* **1986,** *16*, 245-261.

[48] Bartholomew, R. F. "Transport processes in molten binary acetate systems," *J. Phys. Chem.* **1970,** *74(12),* 2507-2512.

[49] Williams, M. L.; Landel, R. F.; Ferry, J. D. "The temperature dependence of relaxation mechanisms in amorphous polymers and other glass-forming liquids," *J. Amer. Chem. Soc.,* **1955,** *77(14),* 3701-3707.

[50] Adam, G., Gibbs, J. H. "On the temperature dependence of cooperative relaxation properties in glass-forming liquids," *J. Chem. Phys.* **1965**, *43(1),* 139-146.

[51] Fernicola, A.; Scrosati, B.; Ohno, H. "Potentialities of ionic liquids as new electrolyte media in advanced electrochemical devices," *Ionics,* **2006**, *12*, 95-102.

[52] Fuller, J.; Breda, A. C.; Carlin, R. T. "Ionic liquid–polymer gel electrolytes from hydrophilic and hydrophobic ionic liquids," *Journal of Electroanalytical Chemistry,* **1998**, *459(2)*, 29–34.

[53] Fuller, J.; Breda, A. C.; Carlin, R.T. "Ionic Liquid-Polymer Gel Electrolytes," *J. Electrochem. Soc.*, **1997,** *144(4),* L67-L69.

[54] Sun, J.; Jordan, L.R.; Forsyth, M.; MacFarlane, D.R. "Acid–Organic base swollen polymer membranes," *Electrochimica Acta*, **2001**, *46*, 1703–1708.

[55] Johnson, K. E. "What's an ionic liquid?" *Interface-Electrochemical Society*, ***2007,*** *16*(1), 38-41.

[56] Galinski, M.; Lewandowski, A.; Stępniak, I. "Ionic Liquid as Electrolyte," *Electrochimica Acta,* **2006,** *51(26),* 5567–5580.

[57] Rogers, R. D. "Materials Science: Reflections on Ionic Liquids" *Nature*, **2007**, *447*, 917-918.

[58] Kamal, A.; Chouhan, G.; "A Task-specific Ionic Liquid [bmim]SCN for the Conversion of Alkyl Halides to Alkyl Thiocyanates at Room Temperature" *Tetrahedron Lett.* **2005**, *46(9)*, 1489-1491.

[59] Tiyapiboonchaiya, C.; MacFarlane, D. R.; Sun, J.; Forsyth, M. "Polymer-in-ionic-liquid Electrolytes" *Macromolecular Chem. Phys*. **2002**, *203(13)*, 1906-1911.

[60] Bansal, D.; Cassel, F.; Croce, F.; Hendrickson, M.; Plichta, E.; Salomon, M. "Conductivities and Transport Properties of Gelled Electrolytes with and without an Ionic Liquid for Li and Li-Ion Batteries" *J. Phys. Chem. B*, **2005**, *109(10)*, 4492–4496.

[61] Egashira, M.; Todo, H.; Yoshimoto, N.; Morita, M. "Lithium Ion Conduction in Ionic Liquid-based Gel Polymer Electrolyte" *J. Power Sources* **2008**, *178(2)*, 729-735.

[62] Tamada, M.; Ueda, S.; Hayashi, T.; Ohno, H. "Thermally Stable Polymer Gel Electrolytes Composed of Branched Polyimide and Ionic Liquid/Zwitterion Mixture Prepared by *in situ* Polycondensation," *Chem. Lett.* **2008**, *37(1)*, 86-87.

[63] Snedden, P.; Cooper, A. I.; Scott, K.; Winterton, N. "Cross-Linked Polymer−Ionic Liquid Composite Materials" *Macromolecules*, **2003**, *36(12)*, 4549–4556.

[64] Hirao, M.; Ito, K.; Ohno, H. "Preparation and Polymerization of New Organic Molten Salts: *N*-alkylimidazolium Salt Derivatives," *Electrochimica Acta*, **2000,** *45 (8-9)*, 1291–1294.

[65] Scott, M. P.; Rahman, M.; Brazel, C. S. "Application of Ionic Liquids as Low-volatility Plasticizers for PMMA," *European. Polymer Journal*, **2003**, *39(10)*, 1947-1953.

[66] Susan, M. A. B. H.; Kaneko, T.; Noda, A.; Watanabe, M. "Ion Gels Prepared by *in situ* Radical Polymerization of Vinyl Monomers in an Ionic Liquid and their Characterization as Polymer Electrolytes," *J. Am. Chem. Soc.*, **2005**, *127(13)*, 4976–4983.

[67] Lewandowski, A.; Swiderska, A. "New Composite Solid Electrolytes Based on a Polymer and Ionic Liquids" *Solid State Ionics* **2004**, *169 (1-4)*, 21-24.

[68] Chen, H.; Choi, J. H.; Cruz, D. S.; Winey, K. I.; Elabd, Y. A. "Polymerized Ionic Liquids: The Effect of Random Copolymer Composition on Ion Conduction" *Macromolecules*, **2009**, *42(13)*, 4809–4816.

[69] Ye, Y.; Elabd, Y. A.; "Anion Exchanged Polymerized Ionic Liquids: High Free Volume Single Ion Conductors" *Polymer*, **2011,** *52 (5)*, 1309-1317.

[70] Marcilla, R.; Blazquez, J. A.; Rodriguez, J.; Pomposo, J. A.; Mecerreyes, D. "Tuning the Solubility of Polymerized Ionic Liquids by Simple Anion-exchange Reactions" *J. Polymer Sci. (Part A): Polymer Chem.*, **2004**, *42 (1)*, 208-212.

[71] Ogihara, W.; Washiroa, S.; Nakajima, H.; Ohno, H. **"**Effect of Cation Structure on the Electrochemical and Thermal Properties of Ion Conductive Polymers Obtained from Polymerizable Ionic Liquids" *Electrochim. Acta*, **2006,** *51(13),* 2614-2619.

[72] Matsumi, N.; Sugai, K.; Miyake, M.; Ohno, H. "Polymerized Ionic Liquids *via* Hydroboration Polymerization as Single Ion Conductive Polymer Electrolytes," *Macromolecules*, **2006**, *39(20),* 6924–6927.

[73] Weber, R. L.; Yuesheng Y.; Andrew L. S.; Steven M. B.; Elabd, Y. A.; Mahesh K. M. "Effect of nanoscale morphology on the conductivity of polymerized ionic liquid block copolymers." *Macromolecules* **2011**, *44(14),* 5727-5735.

[74] Bottcher, C. J. F; Bordewijk P. Theory of Electric Polarization, Vol. II., Dielectrics in Time-dependent Fields, Elsevier - Amsterdam, Oxford, New York, **1978.**

[75] Schiavone, R. J.; Overberger, C. G. "Reactions and polymerization of 1-trityl-4-vinylimidazole," *Journal of Polymer Science, Part A - Polymer Chemistry* **1988,** *26*, 107-115.

[76] Overberger, C. G.; Kawakami, Y. "Esterolytic activity of imidazole-containing polymers: Synthesis and characterization of copoly[1-alkyl-4 or 5-vinylimidazole/4 (5)-vinylimidazole] and its catalytic activity in the hydrolysis of p-nitrophenyl acetate." *Journal of Polymer Science: Polymer Chemistry Edition*, **1978**, *16(6),* 1237-1248.

[77] Wang, J.; Smith, T. W. "Synthesis and polymerization of liquid ionic 1-methyl-3-alkyl-5-vinylimidazolium salts," *Polymer Preprints*, (American Chemical Society, Division of Polymer Chemistry) **2004**, *45(2)*, 290-291.

[78] Yang, F. "Synthesis and Characterization of Ionic Liquid Monomers and Polymers Derived from 2-substituted-1, 3-dialkyl-4 (5)-vinylimidazolium salts," **2013**, ROCHESTER INSTITUTE OF TECHNOLOGY.

[79] Eisenberg, A. "Glass transitions in ionic polymers," *Macromolecules* **1971**, *4*, 125-129.

[80] Tsutsui, T.; Tanaka, T. "Role of electrostatic forces in the glass transition temperatures of ionic polymers," *Polymer*, **1977**, *18*, 817.

[81] Angell, C. A. "Formation of Glasses from Liquids and Biopolymers," *Science* **1995,** *267 (5206),* 1924-1935**.**

[82] Agapov, A.; "Decoupling phenomena in dynamics of soft matter," Dissertation presented to the Graduate Faculty of the University of Akron, December **2011**.

[83] Alder, R.W.; Allen, P. R.; Williams, S. J. "Stable carbenes as strong bases," *J. Chem. Soc. Chem. Commun.* **1995**, 1267-1268.

[84] Amyes, T.L.; Diver, S.T.; Richard, J.P.; Rivas, F.M.; Toth, K. "Formation and stability of N-heterocyclic carbenes in water: The carbon acid pK_a of imidazolium cations in aqueous solution," *J. Am. Chem. Soc.* **2004**, *126*, 4366-4374.

[85] Handy, S. T.; Okello, M. "The 2-Position of Imidazolium Ionic Liquids: Substitution and Exchange," *J. Org. Chem.* **2005**, *70*, 1915-1918.

[86] Seki, S.; Kobayashi, Y.; Miyashiro, H.; Ohno, Y.; Usami, A.; Mita, Y.; Kihira, N.; Watanabe, M.; Terada N. "Lithium Secondary Batteries Using Modified-Imidazolium Room-Temperature Ionic Liquid," *J. Phys. Chem. B*, **2006**, *110*, 10228-10230.

[87] Gabbott, P. "A Practical Introduction to Differential Scanning Calorimetry," in Principles and Application of Thermal Analysis", Blackwell Publishing Ltd.: Oxford, **2008.**

[88] Marcilla, R.; Blazquez, A. J.; Rodriguez, J.; Pomposo, J. A.; Mecerreyes, D. "Tuning the solubility of polymerized ionic liquids by simple anion-exchange reactions," *Journal of Polymer Science: Part A: Polymer Chemistry* **2003**, *42*, 208-212.

[89] Gabbott, P. (Ed.), Principles and applications of thermal analysis, John Wiley & Sons, **2008.**

[90] Sakatsuji W.; Konishi T.; Miyamoto Y. "Enthalpy relaxation and annealing effect in polystyrene," *Phys Rev E Stat Nonlin Soft Matter Phys*. **2013**, *88(1)*, 012605.

[91] Nakamura, K.; Saiwaki, T.; Fukao, K. "Dielectric Relaxation Behavior of Polymerized Ionic Liquid," *Macromolecules* **2010**, *43*, 6092–6098.

[92] Nakamura, K.; Saiwaki, T.; Fukao, K. Inoue, T. "Viscoelastic Behavior of the Polymerized Ionic Liquid Poly[1-ethyl-3-vinylimidazolium *bis*(trifluoromethanesulfonylimide)]," *Macromolecules* **2011**, *44*, 7719–7726.

[93] Havriliak, S.; Negami, S. "A complex plane representation of dielectric and mechanical relaxation processes in some polymers," *J. Polymer Sci. Part C*, **1966**, *16*, 99.

[94] Kremer, F.; Schonhals, A., Broadband Dielectric Spectroscopy, Springer: Berlin, Germany, **2002**.

[95] Runt, J. P., & Fitzgerald, J. J. (1997). Dielectric spectroscopy of polymeric materials: Fundamentals and applications. Washington, DC: American Chemical Society.

[96] Cole, K.S.; Cole, R.H. "Transverse impedance of the squid giant axon during current flow," *The Journal of general physiology*, **1941**, *24(4)*, 535-549.

[97] Davidson, D.W.; Cole, R.H. "Dielectric relaxation in Glycerine," *J. Chem. Phys.* **1950**, *18(10)*,1417.

[98] Davidson, D.W.; Cole, R.H. "Dielectric Relaxation in Glycerol, Propylene Glycol, and n-Propanol," *J. Chem. Phys.*, **1951**, *19(12)*,1484.

[99] Fuoss, R. M.; Kirwood, J. G. "Electrical properties of solids. VIII. Dipole moments in polyvinyl chloride-diphenyl systems," *J. Amer. Chem. Soc.* **1941**, *63(2)*, 385-394

[100] Williams G., "Dielectric Relaxation Spectroscopy of Amorphous Polymer Systems: The Modern Approaches," in: E. Riande , Keynote Lectures in Selected Topics of Polymer Sciences, Madrid, pg.1, **1995.**

[101] Schlosser, E.; Kastner, S.; Friedland, K.J. "Evaluation method for the determination of the dielectric-relaxation spectrum of polymers obtained from periodical and quasi-static test results" *Plaste and Kautschuk*, **1981**, *28(2)*, 77-83

[102] Fragiadakis, D.; Dou, S.; Colby, R. H.; Runt, J., "Molecular mobility and Li^+ conduction in polyester copolymer ionomers based on poly(ethylene oxide)," *J. Chem. Phys.* **2009**, *130*, 064907

[103] Kunal, K.; Robertson, C. G.; Pawlus, S.; Hahn, S. F.; Sokolov, A. P. "Role of Chemical Structure in Fragility of Polymers: A Qualitative Picture" *Macromolecules* **2008**, *41*, 7232-7238.

[104] Kobrak, M. N.; Li, Hualin, "Electrostatic interactions in ionic liquids: the dangers of dipole and dielectric descriptions," *Phys. Chem. Chem. Phys.*, **2010**, *12*, 1922-1932.

Appendix

Comparative thermogravimetric analysis of Poly(1-butyl-2,3-dimethyl-4-vinylimidazolium salts)

Thermal gravimetric analysis (TGA) of poly(1-butyl-2,3-dimethyl-4-vinylimidazolium) triflate and TFSI salts of was carried out under a nitrogen atmosphere with a TA Instruments TGA 2050. The temperature was increased from 25-600^{o}C at 20 ^{o}C/min under a nitrogen atmosphere, and then held at 600^{o}C for 10 minutes under an air atmosphere. TGA mass loss profiles for triflate and $TFSI^{-}$ salts of poly(1-butyl-2,3-dimethylimidazolium) are shown in **Figure S1**. The thermal stability of the triflate and $TFSI^{-}$ salts is similar. Significant mass loss in the $TFSI^{-}$ salt occurs between 430 and 505 °C; that in the triflate salt occurs between 440 and 505 °C.

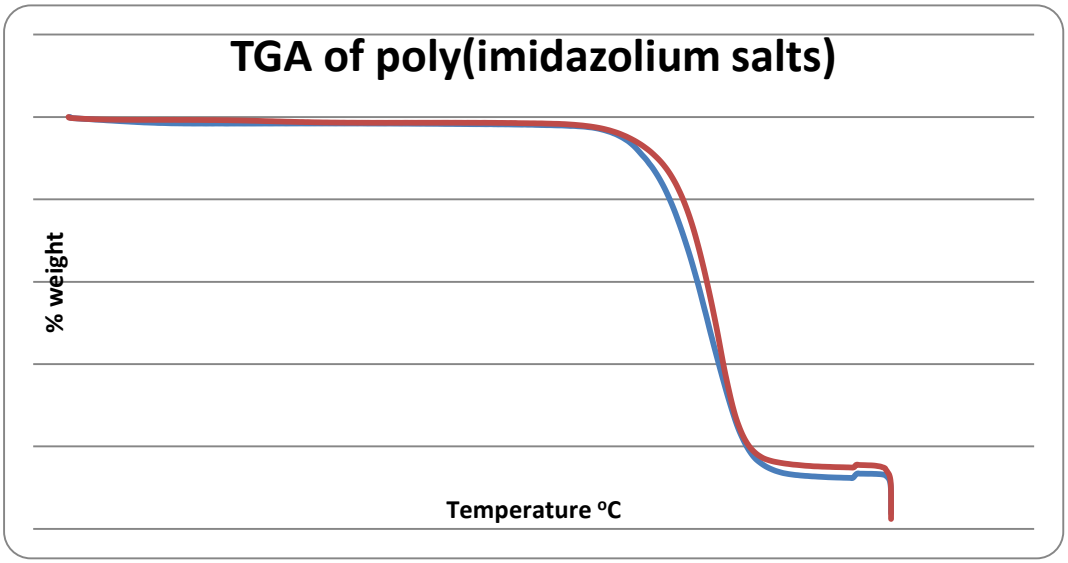

Figure S1 TGA of poly(1-butyl-2,3-dimethyl-4-vinylimidazolium triflate)(red) and poly(1-butyl-2,3-dimethyl-4-vinylimidazolium TFSI)(blue).

DSC thermograms for N-vinylimidazolium polymers

Poly(1-ethyl-3-vinylimidazolium) triflate exhibits a heat capacity change in the heating cycle that can reasonably be assigned as its onset glass transition temperature, T_g-onset, (128^{o}C). In the cooling cycle it exhibits a corresponding heat capacity change at 136^{o}C (see **Figure S2**).

The lowest temperatures for heat capacity changes in the family of poly(1-ethyl-3-vinylimidazolium) salts set were seen at around 90^{o}C for the heating cycle in trifluoromethylsulfonylimide (TFSI) (**Figure S3**) and dicyanamide (**Figure S4**) salts. In the cooling cycle, there is a 25^{o}C difference, in the temperature for onset of heat capacity change (95^{o}C and 120^{o}C) for the TFSI and dicyanamide salts, respectively.

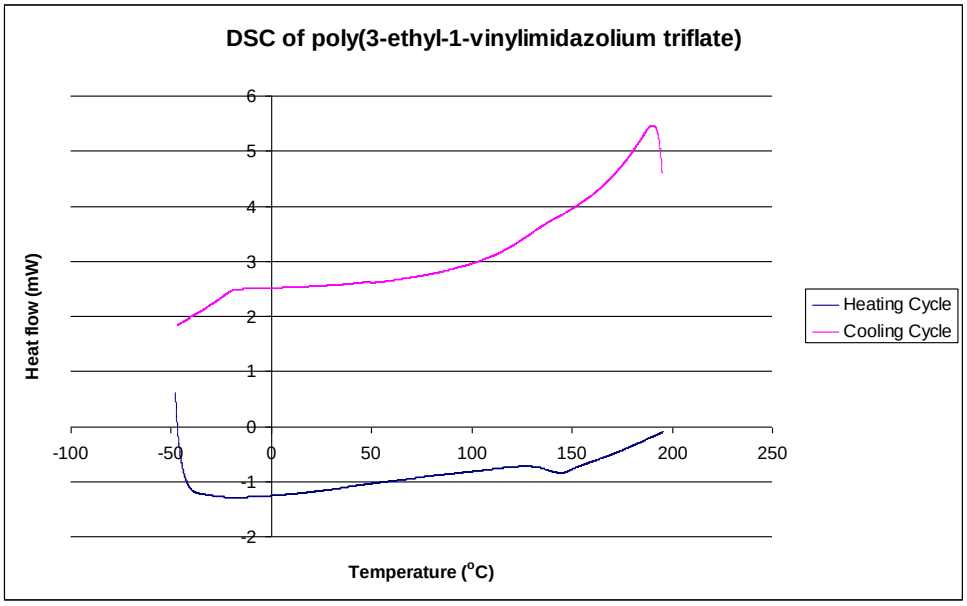

Figure S2 DSC scan of poly(1-ethyl-3-vinylimidazolium triflate) from -50oC to 200oC

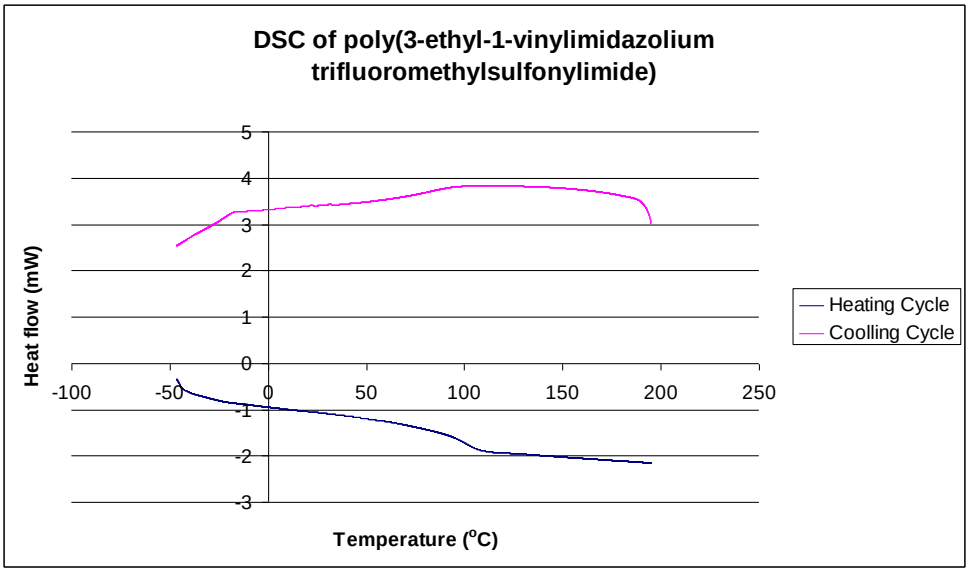

Figure S3 DSC scan of poly(1-ethyl-3-vinylimidazolium TFSI) from -50oC to 200oC

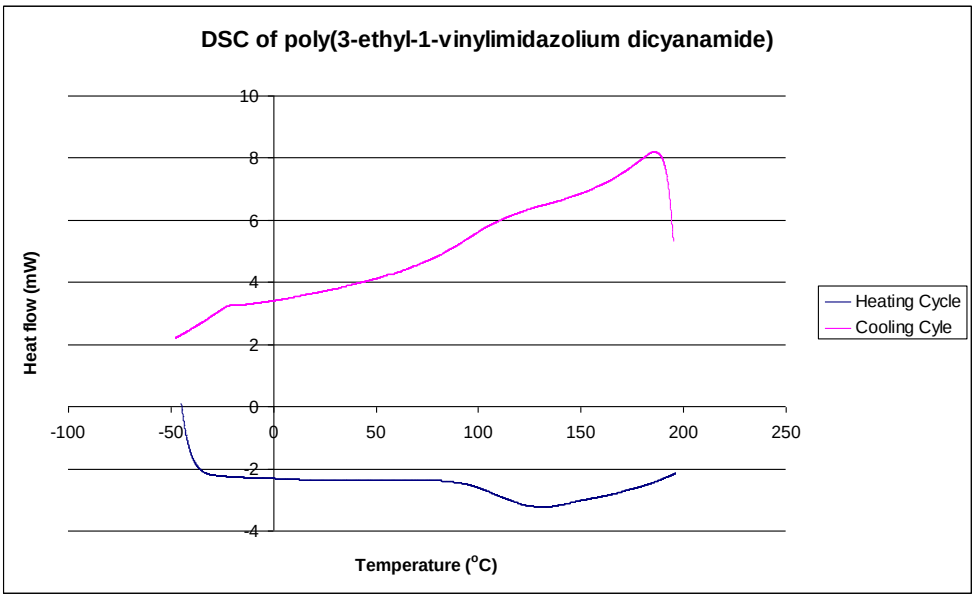

Figure S4 DSC scan of poly(1-ethyl-3-vinylimidazolium dicyanamide) from -50oC to 200oC

The DSC thermogram of poly(1-ethyl-3-vinylimidazolium hexafluorophosphate), **Figure S5,** exhibits onset heat capacity changes in the heating cycle at about 130°C and 167°C. In the cooling cycle the onset of the change in heat capacity is at about and 138°C.

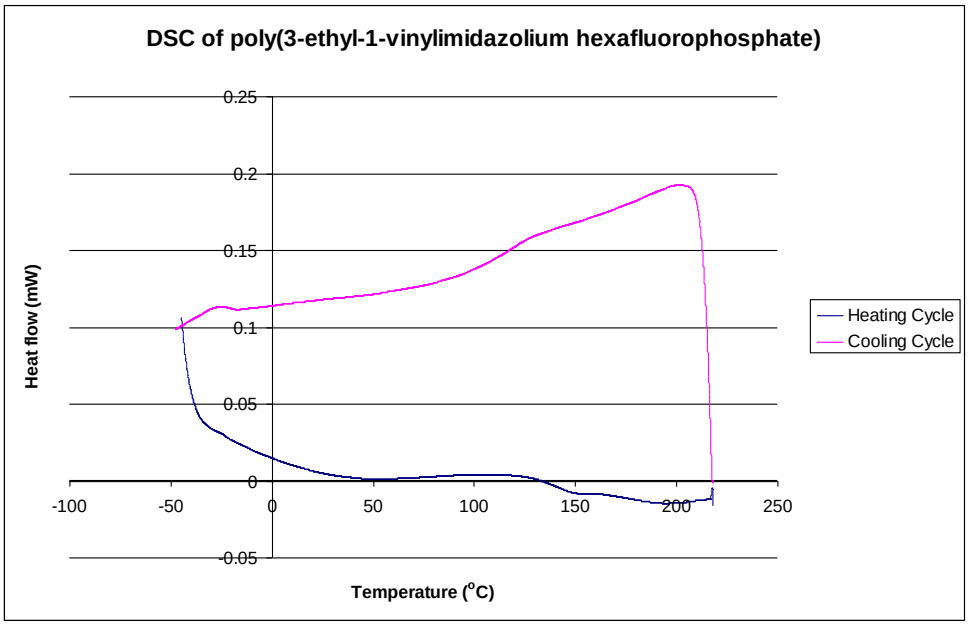

Figure S5 DSC scan of poly(3-ethyl-1-vinylimidazolium hexafluorophosphate) from -50oC to 220oC

The hexafluoroarsenate of the *N*-vinylimidazolium polymer, **Figure S6**, exhibits a heat capacity in the heating cycle, T_g-onset, at about 121°C.

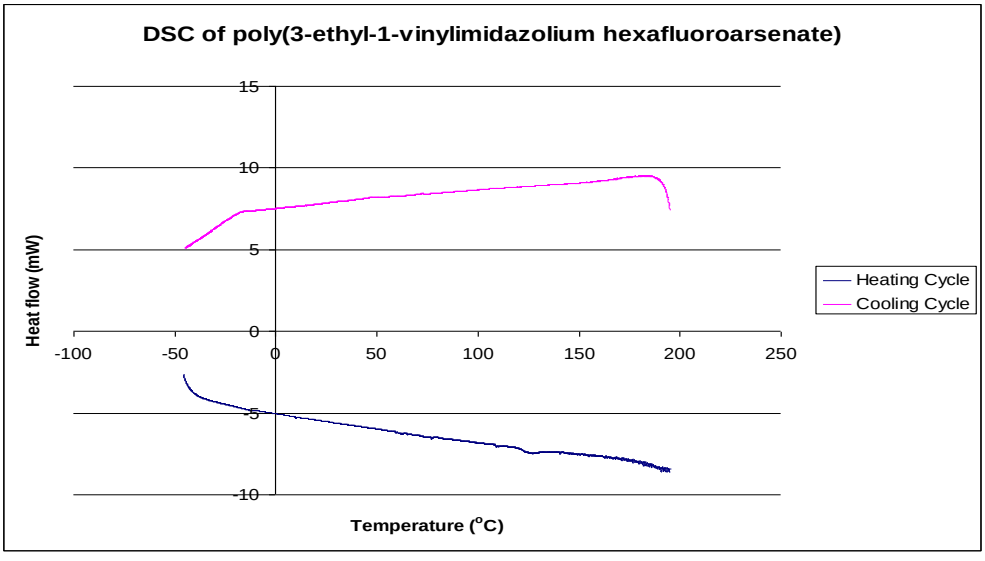

Figure S6 DSC scan of poly(1-ethyl-3-vinylimidazolium hexafluoroarsenate) from -50oC to 200oC

The onset heat capacity changes seen for the tetrafluoroborate salt of the N-vinylimidazolium polymer (**Figure S7**) occur at about 98ºC in the heating cycle and at about 118ºC in the cooling cycle.

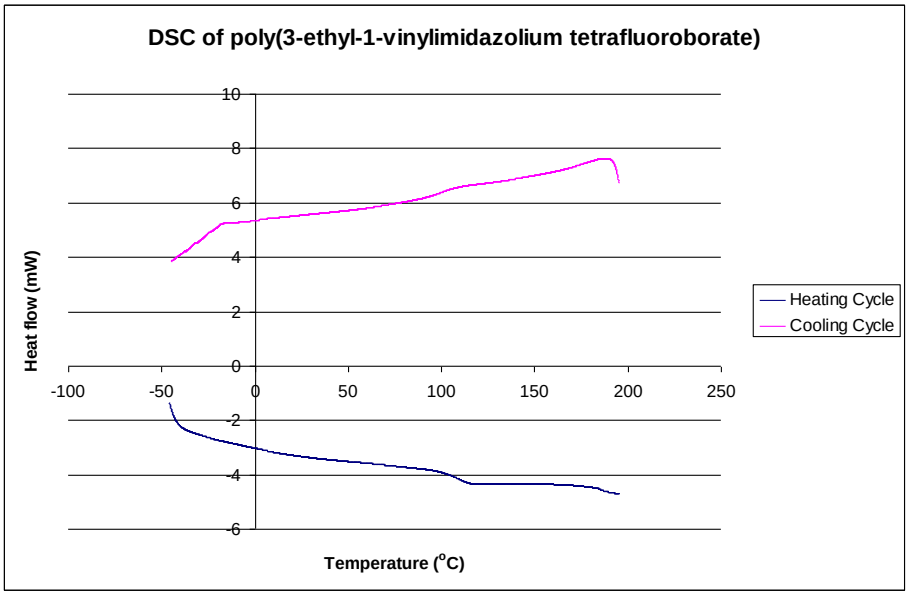

Figure S7 DSC scan of poly(3-ethyl-1-vinylimidazolium tetrafluoroborate) from -50oC to 200oC

DSC Thermograms of Poly(1-ethyl-3-methyl-4-vinyl imidazolium salts)

The heat capacity changes seen for the hexafluoroarsenate salt of the 4-vinylimidazolium polymer (**Figure S8**) are at about 206ºC in the heating cycle and 234ºC in the cooling cycle.

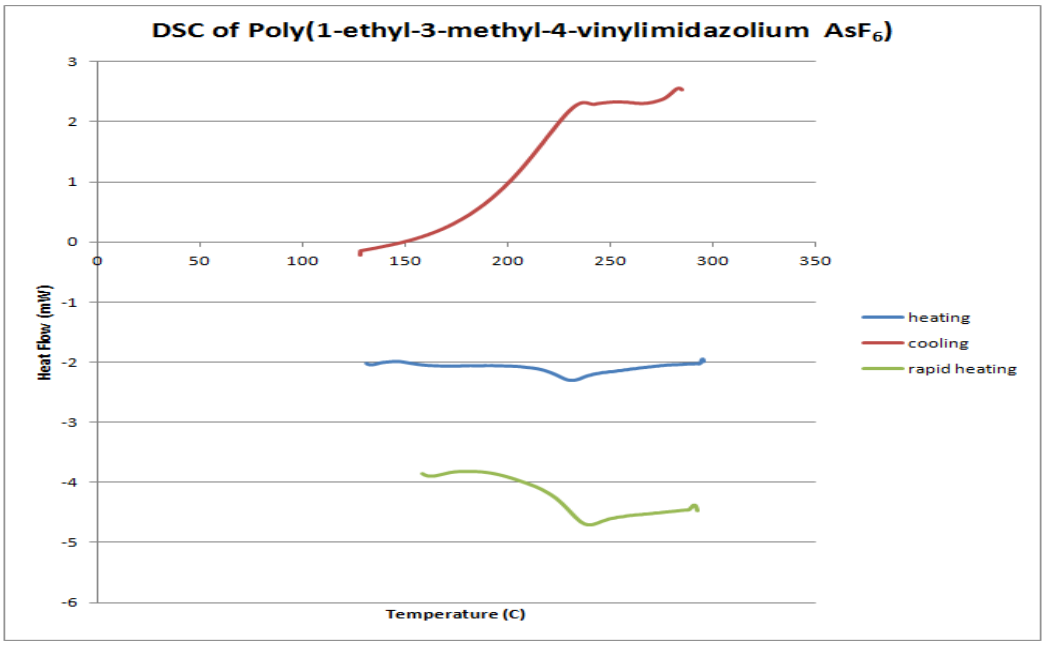

Figure S8 DSC scan of poly(1-ethyl-3-methyl-4-vinylimidazolium hexafluoroarsenate) from -50oC to 200oC

The heat capacity changes seen for the triflate salt of the 4-vinylimidazolium polymer (**Figure S9**) are at about 145^{o}C in the heating cycle and 150^{o}C in the cooling cycle.

The hexafluorophosphate of the 4-vinylimidazolium polymer, **Figure S10,** exhibits an onset heat capacity change in the heating cycle at 187^{o}C and 200^{o}C in the cooling cycle.

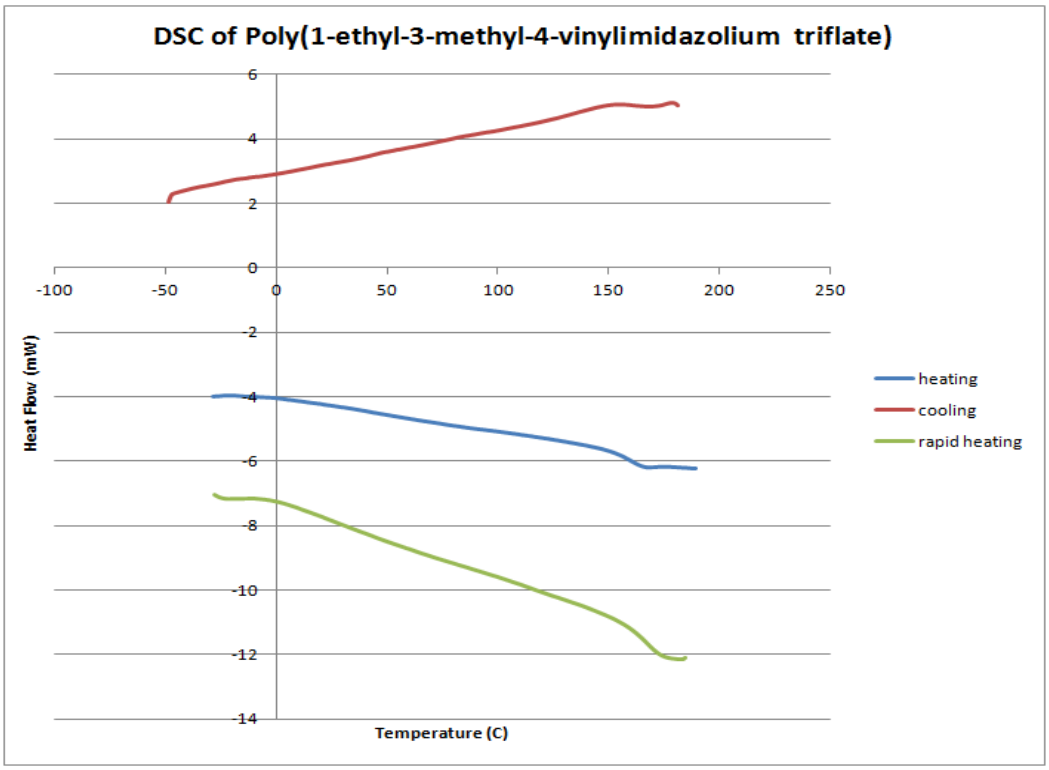

Figure S9 DSC scan of poly(1-ethyl-3-methyl-4-vinylimidazolium triflate) from -50oC to 200oC

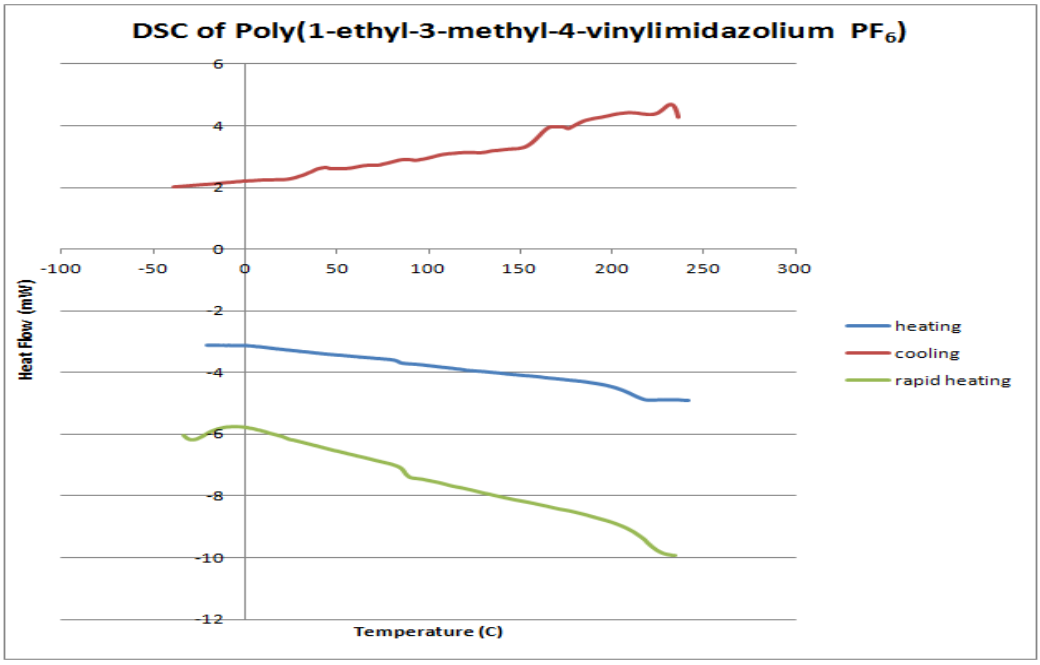

Figure S10 DSC scan of poly(1-ethyl-3-methyl-4-vinylimidazolium hexafluorophosphate) from -50oC to 200oC

The heat capacity changes seen for the trifluoromethylsulfonylimide(TFSI) of the 4-vinylimidazolium polymer (**Figure S11**) on the heating cycle is 72^{o}C and the cooling cycle has a heat capacity change at 92^{o}C.

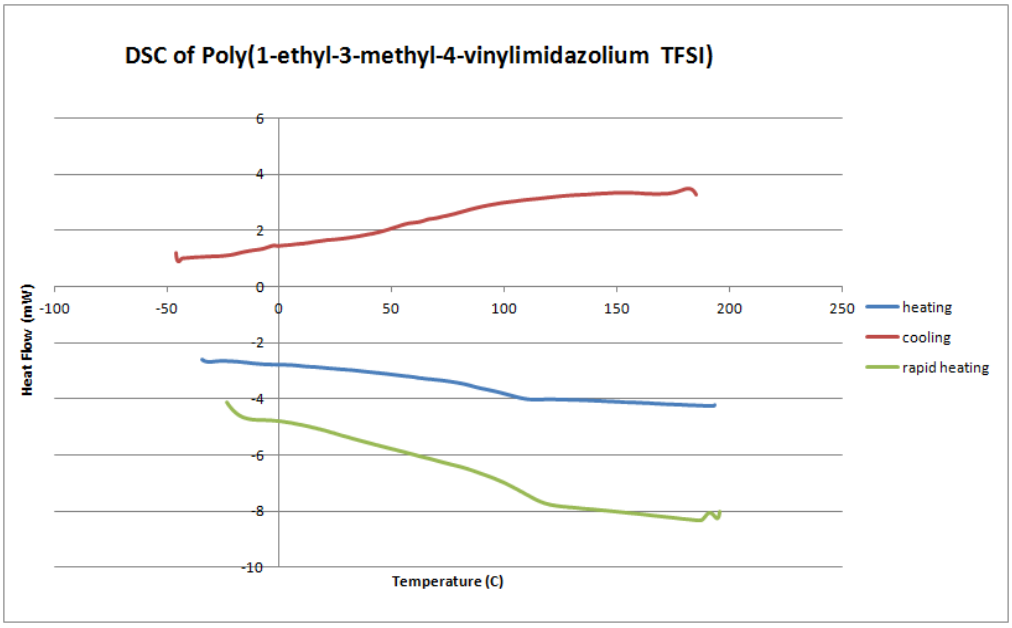

Figure S1 DSC scan of poly(1-ethyl-3-methyl-4-vinylimidazolium trifluoromethylsulfonylimide) from -50oC to 200oC

The onset heat capacity changes in the DSC scan for the tetrafluoroborate salt of the 4-vinylimidazolium polymer (**Figure S12**) occur at about 178^{o}C in the heating cycle and 198^{o}C in the cooling cycle.

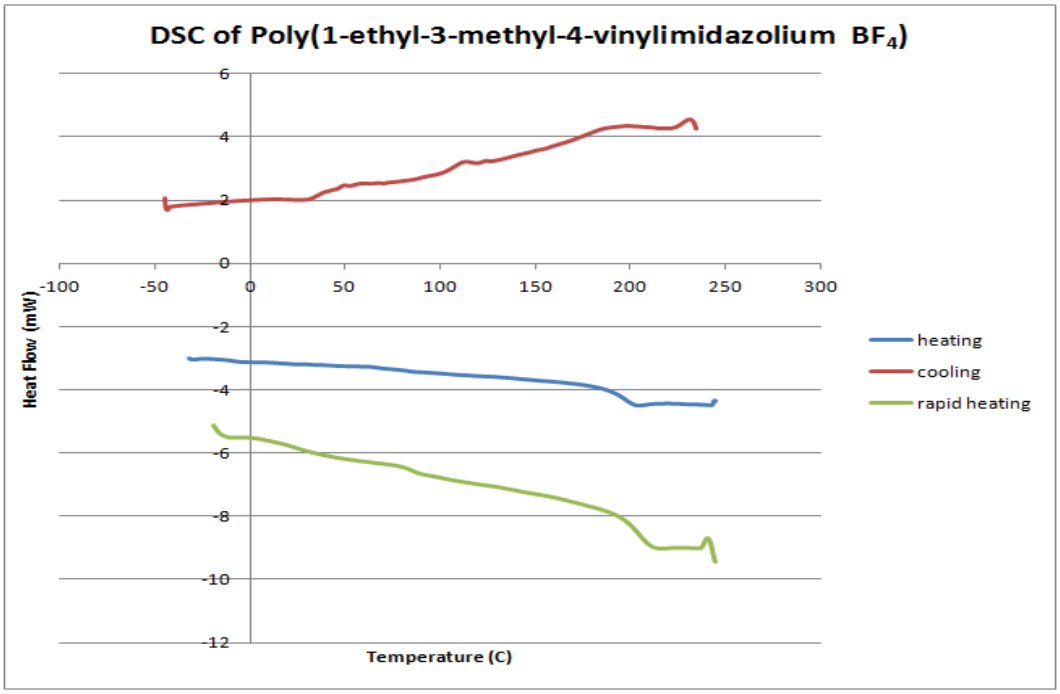

Figure S2 DSC scan of poly(1-ethyl-3-methyl-4-vinylimidazolium tetrafluoroborate) from -50oC to 200oC

In the heating cycle, the onset temperature for heat capacity changes in poly(1-ethyl-3-methyl-4-vinylimidazolium dicyanamide) occurs at about 73^{o}C. In the cooling cycle the onset temperature is about 114^{o}C.

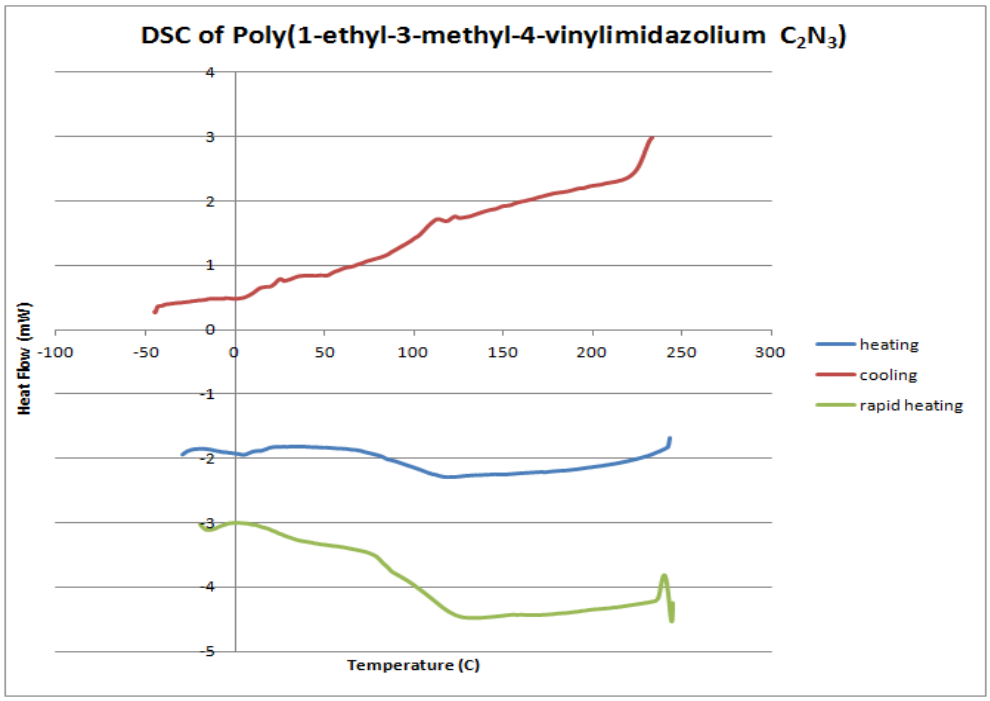

Figure S3 DSC scan of poly(1-ethyl-3-methyl-4-vinylimidazolium dicyanamide) from -50oC to 200oC

DSC Thermograms of poly(1-butyl-2,3-dimethyl-4-vinylimidazolium) salts

Glass transition characteristics of poly(1-butyl-2,3-dimethyl-4-vinylimidazoliium) triflate, hexaflurophosphate and trifluoromethylsulfonylimide salts were also evaluated by differential scanning calorimetry. DSC thermograms for the triflate, TFSI and PF_6^- salts of the polymer are shown in **Figure S14, S15** and **S16,** respectively, where heating and cooling cycles and an auxiliary 40°C/min rapid heating cycle displayed.

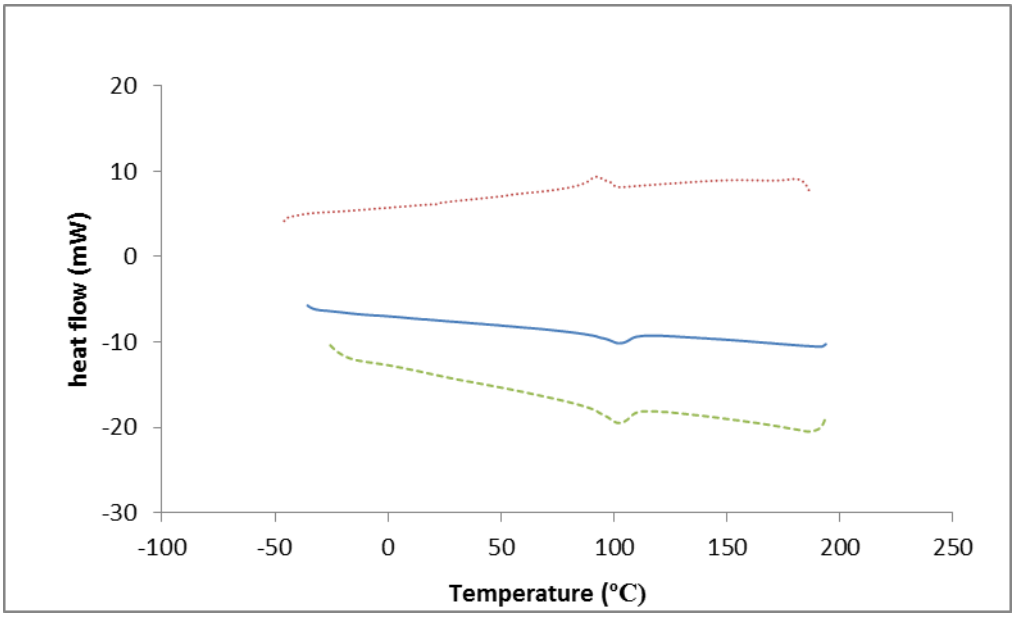

Figure S4 DSC scans for poly(1-butyl-2,3-dimethyl-4-vinylimidazolium triflate): solid blue line (20°C/min – heating cycle), dotted red line (20°C/min – cooling cycle), dashed green line (40°C/min – rapid heating cycle).

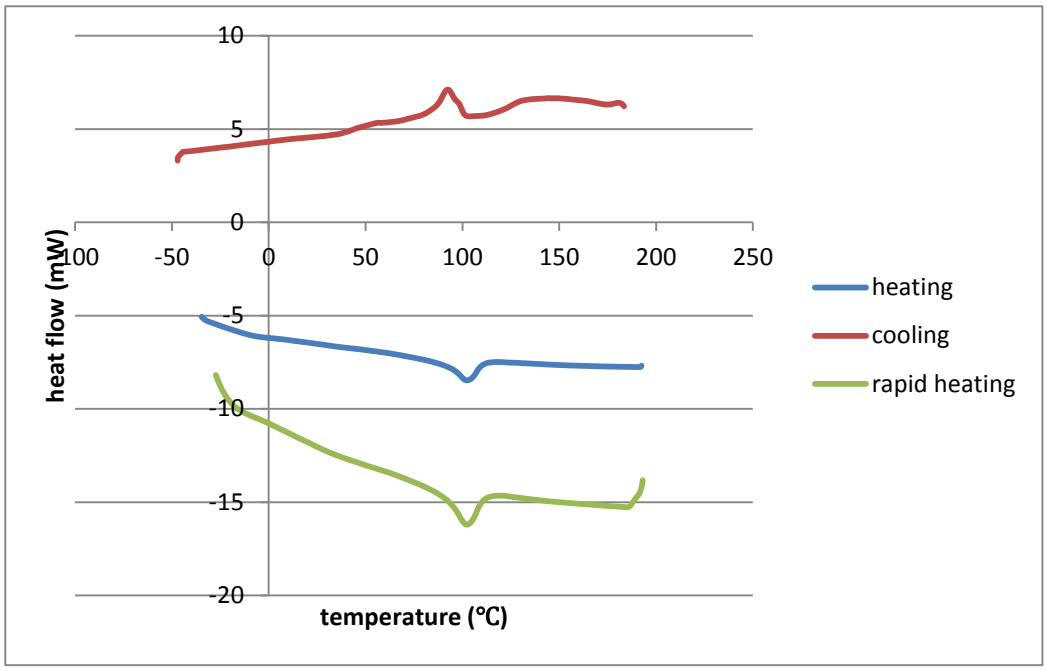

Figure S5 DSC scans for poly(1-butyl-2,3-dimethyl-4-vinylimidazolium TFSI): solid blue line (20°C/min – heating cycle), dotted red line (20°C/min – cooling cycle), dashed green line (40°C/min – rapid heating cycle).

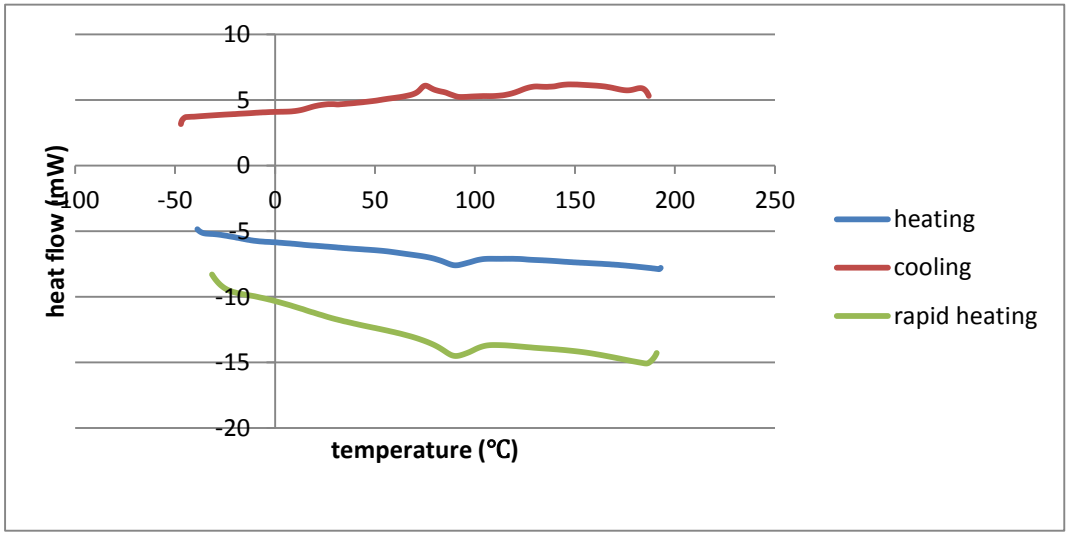

Figure S6 DSC scans for poly(1-butyl-2,3-dimethyl-4-vinylimidazolium PF6): solid blue line (20°C/min – heating cycle), dotted red line (20°C/min – cooling cycle), dashed green line (40°C/min – rapid heating cycle).

H-N Fit for poly(1-ethyl-3-methyl-4-vinylimidazolium triflate)

The fit to the Havriliak-Negami equation for P4VIm^{+}Tf^{-} at 120 °C is shown below.

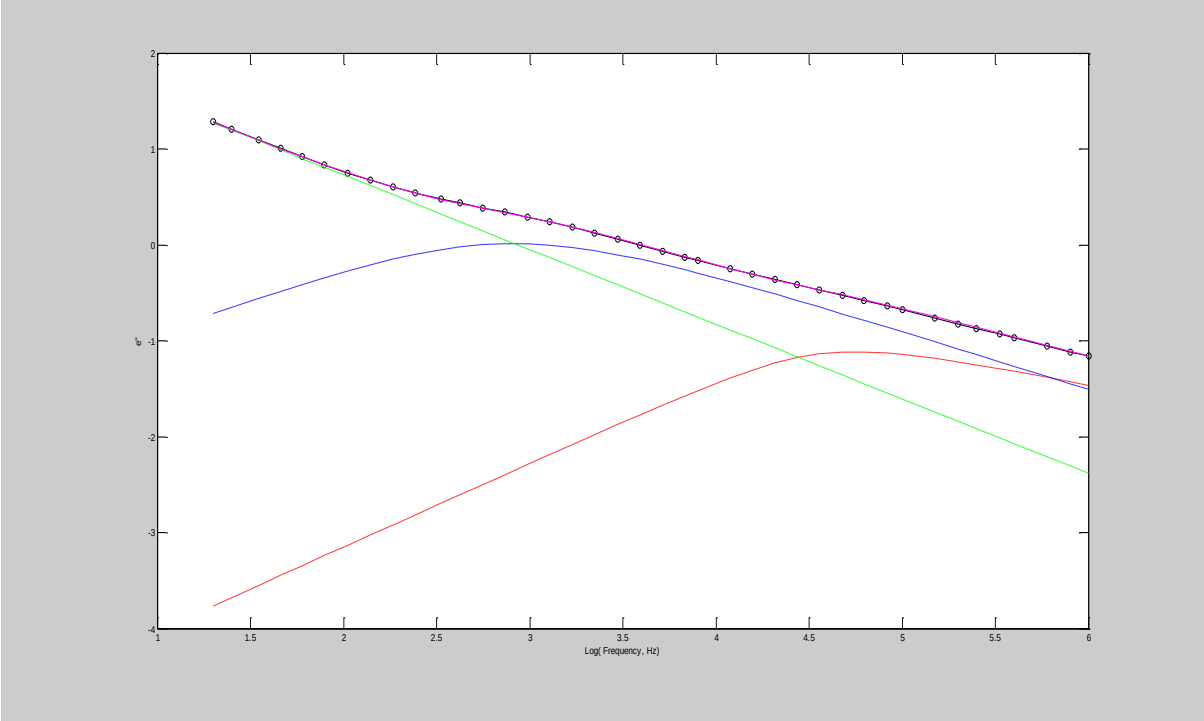

Figure S17 Fitted ε'' versus frequency for poly(1-ethyl-3-methyl-4-vinylimidazolium triflate) at 120°C.The black dotted line is the measured data. The pink solid line is the fitted data using HN equation. The blue dashed line is the fitted α-relaxation and the red dashed line is the fitted α'-relaxation. The green dashed line is the contribution of direct conductivity.

Principles of Dielectric Spectroscopy

Dielectric spectroscopy (sometimes called impedance spectroscopy), and also known as electrochemical impedance spectroscopy (EIS), measures the dielectric properties of a medium as a function of frequency. The concept of electrical impedance was first introduced by Oliver Heaviside in the 1880s and was soon afterward developed in terms of vector diagrams and complex numbers representation by A.E. Kennelly and C.P. Steinmertz. Since then the technique has gained in exposure and popularity, propelled by a series of scientific advancements in the field of electrochemistry, improvements in instrumentation performance and availability, and increased exposure to an ever-widening range of practical applications.

It is based on the interaction of an external field with the electric dipole moment of the material, often expressed by permittivity. It is also a useful method to characterize electrochemical systems. Use of this technique has increased tremendously in recent years and it is now being widely employed in probing bio-molecular interactions, fuel cell testing, and characterization of electrochemical cells.

Dielectric spectroscopy measures the impedance of a system over a range of frequencies, and therefore the frequency response of the system, including the energy storage and dissipation properties, is revealed. Often, data obtained by EIS is expressed graphically in a Bode plot or a Nyquist plot. Impedance is the opposition to the flow of alternating current (AC) in a complex system. A passive complex electrical system comprises both energy dissipater (resistor) and energy storage (capacitor) elements. If the system is purely resistive, then the opposition to AC or direct current (DC) is simply resistance.

There are a number of different dielectric responses, connected to the way a studied medium reacts to the applied field (**Figure S18**) Each dielectric response is centered around its characteristic frequency, which is the reciprocal of the characteristic time of the process. In general, dielectric mechanisms can be divided into relaxation and resonance processes. The most common, starting from high frequencies, are:

- Electronic polarization

This resonant process occurs in a neutral atom when the electric field displaces the electron density relative to the nucleus it surrounds. This displacement occurs due to the equilibrium between restoration and electric forces. Electronic polarization may be understood by assuming an atom as a point nucleus surrounded by spherical electron cloud of uniform charge density.

- Atomic polarization

Atomic polarization is observed when the nucleus of the atom reorients in response to the electric field. This is a resonant process. Atomic polarization is intrinsic to the nature of the atom and is a consequence of an applied field. Electronic polarization refers to the electron density and is a consequence of an applied field. Atomic polarization is usually small compared to electronic polarization.

- Dipole relaxation

This originates from permanent and induced dipoles aligning to an electric field. Their orientation polarization is disturbed by thermal noise (which misaligns the dipole vectors from the direction of the field), and the time needed for dipoles to relax is determined by the local viscosity. These two facts make dipole relaxation heavily dependent on temperature, pressure and chemical surrounding.

- Ionic relaxation

Ionic relaxation comprises ionic conductivity and interfacial and space charge relaxation. Ionic conductivity predominates at low frequencies and introduces only losses to the system. Interfacial relaxation occurs when charge carriers are trapped at interfaces of heterogeneous systems. A related effect is Maxwell-Wagner-Sillars polarization, where charge carriers blocked at inner dielectric boundary layers (on the mesoscopic scale) or external electrodes (on a macroscopic scale) lead to a separation of charges. The charges may be separated by a considerable distance and therefore make contributions to the dielectric loss that are orders of magnitude larger than the response due to molecular fluctuations.

- Dielectric relaxation

Dielectric relaxation as a whole is the result of the movement of dipoles (dipole relaxation) and electric charges (ionic relaxation) due to an applied alternating field, and is usually observed in the frequency range 10^2-10^{10} Hz. Relaxation mechanisms are relatively slow compared to resonant electronic transitions or molecular vibrations, which usually have frequencies above 10^{12}Hz.

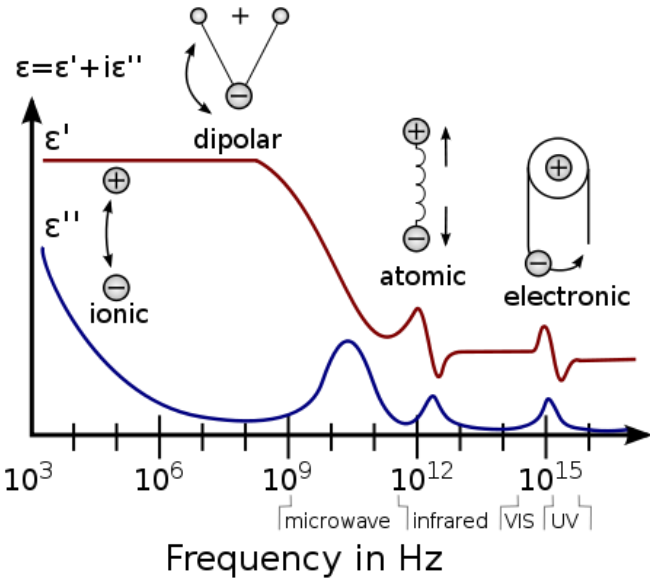

Figure S18 A dielectric permittivity spectrum over a wide range of frequencies. The real and imaginary parts of permittivity are shown, and various processes are depicted: ionic and dipolar relaxation, and atomic and electronic resonances at higher energies **http://www.usm.edu/polymer**